

https://dspace.org/

Biochemical and thermodynamic characterisation of ligand-binding to class alpha glutathione transferase A1-1

Sayed, Yasien

2010-07-02T11:51:44Z
http://hdl.handle.net/10539/8258

Downloaded from a DSpace repository. https://dspace.org/

BIOCHEMICAL AND THERMODYNAMIC CHARACTERISATION OF LIGAND-BINDING TO HUMAN CLASS ALPHA GLUTATHIONE TRANSFERASE A1-1

Yasien Sayed

A thesis submitted to the Faculty of Science, University of the Witwatersrand, Johannesburg, in fulfillment of the requirements for the degree of Doctor of Philosophy.

Johannesburg, April 2001.

DECLARATION

I declare that this thesis is my own, unaided work. It is being submitted for the degree of Doctor of Philosophy in the University of the Witwatersrand, Johannesburg. It has not been submitted before for any degree or examination in any other University.

Yasien Sayed

day of 2001.

This work is dedicated to those who have supported my choice of paths:

My parents: Sabera and Shamsudeen for all the support and encouragement over the years

My wife, Farhana, for her encouragement, understanding and endless patience

My daughter: Munawwarah, this is for you.

And Imam Zakariya Omar for always standing by me.

"Acquire knowledge, because he who acquires it in the way of the Lord performs an act of piety. He, who speaks of it, praises the Lord. He, who seeks it, adores the Lord. He, who dispenses instruction in it, bestows alms. He, who imparts it to its fitting objects, performs an act of devotion to Allah. Knowledge enables its possessor to distinguish what is forbidden from what is not. It lights the way to Heaven. It is our friend in the desert. Our companion in solitude, when bereft of friends. It guides us to happiness and it sustains us in misery. It is our ornament in the company of friends and it serves as armour against our enemies. With knowledge the creature of Allah rises to the heights of goodness and to a noble position. He associates with sovereigns in this world and attains the perfection of happiness in the next."

Prophet Muhammad (Peace be upon him)

PUBLICATION

Part of the results presented in this thesis have been published:

Sayed, Y., Wallace, L. A. and Dirr, H. W. (2000) The hydrophobic lock-and-key intersubunit motif of glutathione transferase A1-1: implications for catalysis, ligandin function and stability. *FEBS Lett*. **465**, 169-172

ABSTRACT

Phenylalanine 51 (F51) in the human class alpha GST forms part of a hydrophobic lock-and-key intersubunit motif at the dimer interface. Protein engineering techniques were used to replace the phenylalanine key with serine. The results indicated that the mutant protein is dimeric with a native-like core structure indicating that F51 at the dimer interface is not essential for dimerisation to occur. Replacing F51 with serine impacts on the catalytic and ligandin function suggesting that tertiary structural changes have occurred at/near the active and non-substrate ligand binding sites. The F51S mutant also displays an enhanced exposure of hydrophobic surface as well as ligandin function. The F51S mutant displays a diminished conformational stability when compared to the wild-type protein. The lock-and-key intersubunit motif, therefore, although not essential for dimerisation to occur does stabilise the quaternary structure at the dimer interface.

A unique structural feature of the class alpha GSTs is the C-terminal helix (residues 207-221). In this study, the role of F221 was assessed by deleting it from the C-terminal helix 9 of hGSTA1-1. The results showed that the deletion of F221 does not affect the secondary, tertiary and quaternary structure of the protein as observed using far-UV CD measurements, enzyme activity and conformational stability as probes, respectively. The wild-type protein binds ~ 1.7-fold more ANS than the F221del protein. Binding affinity studies indicated that although both proteins bind ANS with the same affinity, the wild-type protein binds ANS with a higher capacity than the F221del protein. ANS binding to the wild-type and F221del proteins in the presence of urea (0 - 5.5 M urea) indicated that F221 is required for stabilising helix 9 at the C-terminal of hGSTA1-1. Therefore, F221 is not required for catalysis nor does it impact on the conformational stability of the protein. F221 does, however, affect the ligandin function and is required for the stability of helix 9 at the C-terminus of hGSTA1-1.

ITC was used to dissect the binding energetics of glutathione (GSH) and glutathione sulfonate (GSO_3^-) to the wild-type and Y8F hGSTA1-1 proteins. The contribution of the tyrosyl hydroxyl group to the binding of GSH and GSO_3^- indicated that the Y8F mutant binds GSH tighter than the wild-type protein and the wild-type protein, in turn, binds GSO_3^- tighter than the Y8F mutant protein. The Y8F mutant displays a larger negative

ΔC_p than the wild-type protein when complexed with either GSH or GSO_3^-. This indicates the burial of a larger solvent-exposed hydrophobic surface area for the Y8F mutant than the wild-type protein. The burial of a large solvent-exposed hydrophobic surface area is related to the immobilisation of helix 9 onto domain I in the presence of active site ligands. The observation that the Y8F mutant displays burial of larger solvent-exposed hydrophobic surface area suggests that the tyrosyl hydroxyl group controls the dynamics of helix 9 at the C-terminal of hGSTA1-1. The $\Delta\Delta G$ values also suggest that the tyrosyl hydroxyl group stabilises the thiolate anion at the active site in the wild-type protein.

The binding energetics of non-substrate ligands (ANS and BSP) to the wild-type human class alpha GSTA1-1 were evaluated. The stoichiometry of the interaction between the wild-type protein and ANS indicated that one molecule of ANS binds per protein monomer. The binding interactions between ANS and the wild-type protein are enthalpically favourable indicating the possibility of hydrogen bond formation. ANS binding to the wild-type protein also resulted in the reduction of non-polar surface area exposed to solvent. It is proposed that the ANS binding site is the region adjacent to domain I that becomes buried when helix 9 is immobilised.

The binding of BSP to the wild-type protein involves a high and low affinity set of binding sites. The high affinity binding site binds one molecule of BSP per protein monomer whereas the low affinity site is capable of accommodating a minimum of ~ four BSP molecules. The binding energetics to the high affinity site is both enthalpically and entropically favourable with each term contributing favourably to the favourable Gibbs free energy of binding. Binding to the lower affinity site is not very favourable enthalpically and the major driving force behind the favourable Gibbs free energy of association is the entropic factor. This interaction, therefore, appears to be entropically driven.

ACKNOWLEDGEMENTS

My supervisor, Professor Heini Dirr for all his guidance, encouragement, and never-ending enthusiasm in this field. Thank you for the opportunity and privilege of working in your lab.

Dr. Louise Wallace for all her encouragement and very helpful discussions on the work presented here

Dr. Judith Hornby for helpful discussions on conformational stability and multi-state unfolding pathways of proteins

Thanks to Werner Streicher for help with the Y8F primer design and to Jiann-Kae Luo, Diane Barnwell and Manuel Fernandes for assistance with Molscript. All the members of the Protein Structure-Function Research Programme for very interesting and informative discussions.

Professor George I. Makhatadze and Dr. Marimar M. Lopez at Penn State University College of Medicine, USA for hosting and training me on the use of the isothermal titration calorimeter

AECI for the Post-Graduate Research Fellowship and Ms. Reinette Nel for all her help.
The Andrew Mellon Foundation and the University of the Witwatersrand for financial assistance

The National Research Foundation of South Africa

TABLE OF CONTENTS

	PAGE
DECLARATION	**ii**
DEDICATION	**iii**
PUBLICATION	**iv**
ABSTRACT	**v**
ACKNOWLEDGEMENTS	**vii**
ABBREVIATIONS	**xiv**
LIST OF FIGURES	**xvi**
LIST OF TABLES	**xix**
CHAPTER 1	
PROTEIN-BINDING AND THERMODYNAMICS	
1. Protein-binding	1
1.1 History revisited	1
1.1.1 Protein structural hierarchy	1
1.1.2 The protein folding problem	1
1.1.3 Thermodynamic versus kinetic hypotheses	2
1.2 Protein-binding versus protein folding	3
1.3 Molecular recognition in protein-binding	4
1.3.1 Hydrogen bonding	4
1.3.2 Hydrophobic interactions	5
1.3.3 Electrostatic interactions	6
1.4 Methods for determining protein-binding interactions	7
1.4.1 Computational methods	7
1.4.2 Calorimetry	8
1.4.3 Mass spectroscopy (MS)	9

1.4.4 Nuclear magnetic resonance spectroscopy (NMR) 9
1.4.5 Atomic force microscopy (AFM) 10
2. Thermodynamics of biomolecular interactions 11
2.1 What do the thermodynamic parameters mean? 11
2.1.1 Gibbs free energy of binding (ΔG^O) 12
2.1.2 Enthalpy of binding (ΔH^O) 13
2.1.3 Entropy of binding (ΔS^O) 13
2.1.4 Heat capacity (ΔC_p) 14

CHAPTER 2

GLUTATHIONE TRANSFERASES

2.1 Multifunctional supergene family of detoxification enzymes 16
2.1.1 Enzyme classification of glutathione transferases 17
2.1.2 Evolutionary relationship of the glutathione transferases 18
2.2 The three-dimensional structure of cytosolic glutathione transferases 18
2.2.1 The subunit structure 19
2.2.2 The subunit interface 21
2.2.3 The active site 23
2.2.3.1 The glutathione binding site (G-site) 26
2.2.3.2 The non-substrate hydrophobic binding site (H-site) 28
2.2.4 The non-substrate ligand binding site (L-site) 30
2.3 The catalytic mechanism 30
2.4 Conformational stability of glutathione transferases 32
2.5 Objectives 34

CHAPTER 3

EXPERIMENTAL PROCEDURES

3.1 Materials 36
3.2 Generation of F51S, F221del and Y8F hGSTA1-1 36
3.2.1 Mutagenic primer design for use with ExSite™ and QuikChange™ mutagenesis kits 36

3.2.2 PCR-based site-directed mutagenesis 37
3.3 Sequencing of mutant plasmid DNA 39
3.4 Over-expression and purification of the wild-type, F221del and Y8F hGSTA1-1 proteins 39
3.5 Over-expression and purification of F51S hGSTA1-1 40
3.6 Steady-state enzyme kinetic studies 41
3.6.1 The standard CDNB/GSH assay 41
3.6.2 Kinetic parameters (V_m, K_m) for the wild-type and F51S proteins 41
3.6.3 The peroxidase assay using cumene hydroperoxide 42
3.7 Spectral analysis of wild-type and mutant proteins 42
3.8 Determination of secondary structural content using far-UV circular dichroism 43
3.9 Determination of dissociation constants 43
3.10 Determination of Stern-Volmer (K_{sv}) constants using acrylamide quenching 44
3.11 Anisotropy studies 45
3.12 Urea-induced equilibrium unfolding studies 45
3.12.1 Reversibility studies 45
3.12.2 Protein-concentration dependence studies 45
3.12.3 Data analysis 46
3.13 The effect of reduced glutathione on the binding of ANS 47
3.14 The effect of urea on the binding of ANS to the wild-type and F221del proteins in the presence and absence of *p*-bromobenzylglutathione 47
3.15 Thermodynamic studies using isothermal titration calorimetry 48
3.15.1 Isothermal titration calorimetry (ITC) 48
3.15.1.1 Protein and ligand sample preparation 49
3.15.1.2 Dialysis procedure 49
3.15.1.3 Correction of protein concentration due to light scattering effects 50
3.15.2 Thermodynamics of ligand binding to the active site of

wild-type and Y8F hGSTA1-1 50
3.15.3 Thermodynamics of non-substrate ligand binding to wild-type hGSTA1-1 51
3.15.4 ITC data analysis 52
3.16 Data analysis and molecular graphics 53

CHAPTER 4
THE ROLE OF PHENYLALANINE 51 IN THE HYDROPHOBIC LOCK-AND-KEY INTERSUBUNIT MOTIF OF HUMAN GLUTATHIONE TRANSFERASE A1-1

4.1 The hydrophobic lock-and-key intersubunit motif of hGSTA1-1 54
4.2 Physicochemical properties of the wild-type and F51S proteins 55
4.2.1 Identification of the F51S mutant plasmid DNA 55
4.2.2 Over-expression and purification 55
4.2.3 Fluorescence spectral properties of wild-type and F51S hGSTA1-1 60
4.2.4 Far-UV circular dichroism of wild-type and F51S hGSTA1-1 60
4.2.5 Steady-state kinetic properties of the wild-type and F51S proteins 63
4.2.6 Dissociation constants for the non-substrate ligands ANS, BSP and *p*-bromobenzylglutathione 63
4.2.7 ANS binding to the wild-type and F51S proteins 63
4.2.8 The effect of glutathione on the binding of ANS 67
4.2.9 Acrylamide quenching of W20 at the domain-domain Interface 67
4.2.10 Steady-state anisotropy studies 67
4.3 Urea-induced equilibrium unfolding of wild-type and F51S proteins 67
4.3.1 Reversibility studies 67
4.3.2 Protein-concentration dependence of the unfolding transition 70
4.3.3 Analysis of the equilibrium unfolding transition and interpretation of $\Delta G(H_2O)$ and *m*-value 73

4.4 Discussion 76
4.5 Conclusion 78

CHAPTER 5
THE ROLE OF PHENYLALANINE 221 IN THE LIGANDIN FUNCTION OF HUMAN GLUTATHIONE TRANSFERASE A1-1

5.1 The C-terminal of helix 9 80
5.2 Physicochemical properties of the wild-type and F221del proteins 81
5.2.1 Identification of F221del mutant plasmid DNA 81
5.2.2 Over-expression and purification 84
5.2.2.1 Specific activity of the wild-type and F221del proteins using the CDNB-conjugation assay 84
5.2.2.2 Glutathione peroxidase activity of the wild-type and F221del proteins using cumene hydroperoxide 89
5.2.3 Fluorescence spectral properties of the wild-type and F221del proteins 89
5.2.4 Far-UV circular dichroism 89
5.2.5 ANS binding to the wild-type and F221del proteins 92
5.2.6 The dissociation constant for ANS 92
5.2.7 The effect of urea on the binding of ANS in the presence and absence of *p*-bromobenzylglutathione 95
5.2.7.1 ANS binding in the absence of *p*-bromobenzylglutathione 95
5.2.7.2 ANS binding in the presence of *p*-bromobenzylglutathione 98
5.3 Urea-induced equilibrium unfolding of the F221del mutant protein 98
5.3.1 Reversibility studies 98
5.3.2 Dependence of unfolding transition on protein-concentration 99
5.3.3 Analysis of the equilibrium unfolding transition and interpretation of the $\Delta G(H_2O)$ and *m*-value 99
5.4 Discussion 102
5.5 Conclusion 109

CHAPTER 6

THERMODYNAMICS OF LIGAND BINDING TO HUMAN GLUTATHIONE TRANSFERASE A1-1 USING ISOTHERMAL TITRATION CALORIMETRY

6. Glutathione and glutathione sulfonate binding to wild-type and Y8F hGSTA1-1 110

6.1 Role of Y8 in the catalytic mechanism of hGSTA1-1 110

6.1.1 Construction and identification of the Y8F mutant plasmid DNA 112

6.1.2 Over-expression and purification of theY8F mutant 112

6.2 Biochemical characterisation of Y8F hGSTA1-1 112

6.2.1 Fluorescence spectral properties of Y8F hGSTA1-1 112

6.2.2 Far-UV circular dichroism 116

6.2.3 Specific activity measurements using the CDNB-conjugation assay 116

6.2.4 Specific activity measurements using the cumene hydroperoxide assay 116

6.3 Thermodynamics of ligand binding to G-site of wild-type and Y8F hGSTA1-1 116

6.3.1 Glutathione (GSH) binding to wild-type and Y8F proteins 119

6.3.2 Glutathione sulfonate (GSO_3^-) binding to wild-type and Y8F proteins 124

6.4 Discussion 130

7. Non-substrate ligand binding to wild-type hGSTA1-1 146

7.1 Thermodynamics of ANS and BSP binding to wild-type hGSTA1-1 147

7.1.1 Energetics of ANS binding to wild-type hGSTA1-1 147

7.1.2 Energetics of BSP binding to wild-type hGSTA1-1 149

7.2 Discussion 155

7.3 Conclusion 162

CHAPTER 7

REFERENCES 164

ABBREVIATIONS

AEDANS	5-[[2-[(acetyl)amino)ethyl]amino]-naphthalene-1-sulfonic acid
ANS	8-anilino-1-naphthalene sulfonate
bp	base pairs
C_m	urea-induced midpoint of unfolding
CD	circular dichroism
CDNB	1-chloro-2,4-dinitrobenzene
ΔC_p	change in heat capacity
DSC	differential scanning calorimetry
EA	ethacrynic acid
EDTA	ethylenediaminetetra-acetic acid
F51S	replacement of wild-type phenylalanine (F) with serine (S) at position 51
F221del	deletion of phenylalanine (F) at position 221 from the wild-type protein
$\Delta G(H_2O)$	Gibbs free energy of unfolding in the absence of denaturant
G-site	glutathione binding site
GSH	reduced glutathione
GS-NBD	glutathione conjugate of 4-nitrobenzo-2-oxa-1,3-diazole
GSO_3^-	glutathione sulfonate
GST	glutathione transferase
ΔH^O	change in enthalpy
H-site	hydrophobic electrophilic binding site
hGSTA1-1	human class alpha glutathione transferase with two type one subunits
hGSTP1-1	human class pi glutathione transferase with two type one subunits
IPTG	isopropyl-thio-galactoside
ITC	isothermal titration calorimetry
K_a	association constant
K_d	dissociation constant
kDa	kilodalton
K_m	Michaelis-Menten constant
L-site	non-substrate ligand binding site
m-value	susceptibility of protein to denaturant i.e., co-operativity of unfolding transition

N_2	native folded dimer
NMR	nuclear magnetic resonance
PDB	protein data bank
PCR	polymerase chain reaction
rGSTA1-1	rat class alpha glutathione transferase with two type one subunits
rpm	revolutions per minute
SDS-PAGE	sodium dodecylsulfate-polyacrylamide gel electrophoresis
ΔS^O	change in entropy
SEC-HPLC	size exclusion high performance liquid chromatography
Sj26GST	26 kDa glutathione transferase from *Schistosoma japonicum*
U	unfolded monomer
V_m	maximum velocity
Y8F	replacement of wild-type tyrosine (Y) with phenylalanine (F) at position 8

The IUPAC-IUBMB one and three letter codes for amino acids are used

The numbering of amino aid residues in this work does not include the first methionine residue

Enzyme: Glutathione Transferase (EC 2.5.1.18)

LIST OF FIGURES

		PAGE
Figure 1.	Ribbon representation of human class alpha glutathione transferase A1-1 and sequence alignment of GSTs	22
Figure 2.	Ribbon representation of squid class sigma glutathione transferase GSTS1-1	24
Figure 3.	Backbone representations of representatives from the various GST gene classes showing the V-shaped cleft. The representations are viewed perpendicular to the two-fold axis	25
Figure 4	Schematic representation of the interactions between human GSTA1-1 and *S*-benzylglutathione	27
Figure 5.	Identification of F51S mutant plasmid DNA on 1% agarose gel	56
Figure 6.	cDNA sequencing results showing F51S mutation	57
Figure 7.	SDS-PAGE of purified F51S mutant protein	58
Figure 8.	SEC-HPLC of purified F51S mutant protein	59
Figure 9.	Spectral characterisation of the native and unfolded conformations of wild-type and F51S hGSTA1-1 proteins	61
Figure 10.	Far-UV circular dichroism spectra of the wild-type and F51S proteins	62
Figure 11.	Emission spectra of ANS binding to the wild-type and F51S proteins	66
Figure 12.	The effect of glutathione on the binding of ANS to the wild-type and F51S proteins	68
Figure 13.	Stern-Volmer plots for the quenching of tryptophan 20 fluorescence in the wild-type and F51S proteins	69
Figure 14.	Fluorescence and far-UV circular dichroism unfolding of the F51S mutant protein	71
Figure 15.	Protein-concentration dependence of the stability of the F51S mutant protein	72

Figure 16.	Urea-induced equilibrium unfolding of the wild-type and F51S proteins	74
Figure 17.	Ball-and-stick representation of the C-terminal environment in human GSTA1-1	82
Figure 18.	Space-filled representation of the environment of F221 at the C-terminus of helix 9 in human GSTA1-1	83
Figure 19.	Identification of F221del mutant plasmid DNA on a 1% agarose gel	85
Figure 20.	cDNA sequence results confirming the deletion of F221 in hGSTA1-1	86
Figure 21.	SDS-PAGE of the purified F221del mutant protein	87
Figure 22.	SEC-HPLC of the purified F221del mutant protein	88
Figure 23.	Spectral characterisation of the native and unfolded conformations of the wild-type and F221del proteins	90
Figure 24.	Far-UV circular dichroism spectra of wild-type and F221del proteins	91
Figure 25.	Emission spectra of ANS binding to wild-type and F221del proteins	93
Figure 26.	Determination of the dissociation constant for ANS using fluorescence enhancement techniques	94
Figure 27.	The effect of urea on ANS binding to the wild-type and F221del proteins in the absence and presence of *p*-bromobenzylglutathione	96
Figure 28.	Urea-induced equilibrium unfolding of wild-type and F221del proteins	97
Figure 29.	Protein-concentration dependence of stability of the F221del mutant protein	100
Figure 30.	Schematic diagram of helix 9 at the C-terminal end of various class alpha GST isoforms	107
Figure 31.	Identification of Y8F mutant plasmid DNA on a 1.2 % agarose gel	113

Figure 32.	cDNA sequencing results confirming the Y8F mutation	114
Figure 33.	Spectral analysis of Y8F mutant protein in the presence and absence of urea	115
Figure 34.	Far-UV circular dichroism spectrum of the Y8F mutant protein	117
Figure 35.	ITC titration profile of the binding of reduced glutathione to the wild-type protein	120
Figure 36.	ITC titration profile of the binding of reduced glutathione to the Y8F mutant protein	121
Figure 37.	The temperature-dependence of the enthalpy change upon binding of reduced glutathione to wild-type and Y8F proteins	125
Figure 38.	ITC titration profile of the binding of glutathione sulfonate to the wild-type hGSTA1-1 protein	127
Figure 39.	ITC titration profile of the binding of glutathione sulfonate to the Y8F mutant protein	128
Figure 40.	The temperature-dependence of the enthalpy change upon binding of glutathione sulfonate to the wild-type and Y8F proteins	131
Figure 41.	Representation of the active site structure of human GSTA1-1 indicating the position of water molecules	136
Figure 42.	ITC titration profile of the binding of ANS to the wild-type hGSTA1-1 protein	148
Figure 43.	The temperature-dependence of the enthalpy change upon binding of ANS to the wild-type protein	151
Figure 44.	ITC titration profile of the binding of BSP to the wild-type human GSTA1-1 protein	153
Figure 45.	The temperature-dependence of the enthalpy change upon binding of BSP to the wild-type hGSTA1-1 protein	156

LIST OF TABLES

		PAGE
Table 1.	Pdb accession codes for the various class alpha GSTs complexed with different ligands	20
Table 2.	Kinetic parameters for the wild-type and F51S hGSTA1-1	64
Table 3.	Binding affinities of non-substrate ligands for wild-type and F51S proteins	65
Table 4.	Specific activity of the wild-type and Y8F proteins using the CDNB-conjugation and cumene hydroperoxide enzyme assay systems	118
Table 5.	Energetics of the interaction between wild-type and Y8F proteins with reduced glutathione	123
Table 6.	Energetics of the interaction between wild-type and Y8F proteins with glutathione sulfonate	129
Table 7.	Heat capacity changes upon binding of reduced glutathione and glutathione sulfonate to wild-type and Y8F proteins	140
Table 8.	Energetics of the interaction between wild-type hGSTA1-1 and ANS	150
Table 9.	Energetics of the interaction between wild-type hGSTA1-1 and BSP	154
Table 10.	Heat capacity changes upon binding of ANS and BSP to wild-type hGSTA1-1	157

CHAPTER 1
PROTEIN-BINDING AND THERMODYNAMICS

1. Protein-binding

1.1 History revisited

The word protein is aptly named, being derived from the Greek word “proteios” which means “of the first rank”. Proteins play a central role in all biological processes. The complexity and diversity of these biological molecules as well as their roles in molecular recognition cannot be overstated. The central dogma of molecular biology, first formulated in the 1950s by Francis Crick, may be summarised as follows: DNA (deoxyribonucleic acid)→RNA (ribonucleic acid) →protein.

1.1.1 Protein structural hierarchy

A wealth of genetic information exists due to the progress made by the human genome project. However, it is the final product, proteins, which are ultimately of significance since these molecules are the “workhorses” of the cell. Linderstøm-Lang and Bernal (see Jaenicke and Rudolph, 1986) first identified the various levels of protein structural hierarchy. To date, there are four levels of protein organisation that are known. The primary structure refers to the linear sequence of covalently bonded amino acid residues in a polypeptide chain. The secondary structure refers to the arrangement of the polypeptide backbone into local structured regions such as α-helices and β-strands. The tertiary structure defines the folded, three-dimensional state. This state includes contributions by the amino acid side chains. Finally, the quaternary structure, which is only relevant to oligomeric or multi-subunit proteins, describes the assembly of subunits into dimers, trimers and higher order structures.

1.1.2 The protein folding problem

Nuclear DNA of all living organisms acts as the reservoir of genetic information, which is ultimately expressed as proteins by the cell. The amino acid sequence of a protein is determined by the base sequence of the DNA. Protein synthesis from the DNA blueprint occurs in two steps: transcription, i.e., the synthesis of a messenger RNA molecule which

possesses a structure that is complementary to the structure of the DNA molecule. Therefore, the genetic information is transferred to mRNA. After transporting the message to the cytosol, it is translated into protein. Proteins are synthesised on the ribosome, *in vivo*, and the nascent polypeptide chain is able to fold spontaneously into its final three-dimensional structure. Therefore, the amino acid sequence contains all the information required for the folding of a protein molecule into its correct three-dimensional structure in order for it to perform its biological function *in vivo* (Anfinsen, 1973). The protein folding problem addresses the question of how the information contained in the linear one-dimensional sequence is translated into the specific three-dimensional structure of a protein.

1.1.3 Thermodynamic versus kinetic hypotheses

The work of Anfinsen (1973) attempted to explain the principles governing the folding process of bovine pancreatic ribonuclease (RNase). He demonstrated that denatured RNase was able to refold to a native biologically active enzyme in the absence of any co-factors. This led to the formulation the thermodynamic hypothesis. This hypothesis states that the three-dimensional state of a protein represents the lowest Gibbs free energy state. The work on the refolding of RNase showed that the native state is thermodynamically stable and represents the state of lowest energy. This would represent the global minimum of free energy relative to all other states accessible on that time scale (Dill, 1990).

Levinthal calculated how long it would take for a protein to fold in the absence of any intermediates and if all conformations about the polypeptide backbone were sampled before the native state was reached. If one considered a polypeptide backbone of 100 residues, with two rotable bonds (ϕ and ψ), as well as three possible conformations about each rotable bond, there would be 3^{200} possible conformations of the backbone. Assuming that bond rotation occurs at a rate of 10^{13} sec^{-1}, then the time, t, required to sample each polypeptide conformation is $t = 3^{2n}/(2nX10^{13}) = 1.3X10^{80}$ sec, or $4X10^{72}$ years (Wetlaufer, 1973). This calculation suggested that protein folding was kinetically controlled because the time scale of folding does not allow for a search through all

possible conformations and consequently, the thermodynamically most stable state may not be reached. The existence of folding intermediates are thought to direct the folding process along a defined pathway (Privalov, 1996).

1.2 Protein-binding versus protein folding

Before a protein can be biologically active it must fold into a precise three-dimensional structure (Creighton, 1984). Although it is not yet understood how a given protein is able to assume its correct three-dimensional structure, it is clear that there are recurring protein structural motifs. This concept has helped to formulate some ideas on how proteins fold. Generally, the presence of a folded hydrophobic core in globular proteins is always enclosed by interacting secondary structural elements (Bowie *et al*., 1990; Dill, 1990). The number of unique protein folds is believed to be limited and this has provided some understanding in relating the biological function of a protein to a unique protein fold (Lesk and Chothia, 1980; Orengo *et al*., 1993; Murzin *et al*., 1995).

Apart from the very relevant aspect of protein folding, it is clear that proteins are extremely important biological macromolecules required for a variety of functions *in vivo*. The importance of protein-ligand, protein-DNA, hormone-receptor or antigen-antibody etc. interactions demonstrates the importance of these macromolecules in the immune response, gene expression and signal transduction cascades and their relevance cannot be ignored. Various laboratories have observed an overall similarity between protein-binding and protein folding (Janin *et al*., 1988; Janin and Chothia, 1990; Jones and Thornton, 1996). The fact that proteins are able to bind to one another in a highly specific manner is a very distinctive feature found in many biological processes. Therefore, there is great interest in trying to understand the forces that drive protein-protein interactions. Initially, it was believed that the forces stabilising the folded protein structure might also be the same forces responsible for protein-protein associations. Studies on the interactions that stabilise protein complexes have revealed that the extent of the role of the forces responsible for maintaining proteins in their folded native conformation may be different for stabilising protein complexes (Jones and Thornton, 1996; Tsai *et al*., 1997a, 1997b, 1997c; Xu *et al*., 1997b; Sheinerman *et al*., 2000).

Therefore, one of the most fundamental questions regarding protein associations is what is the nature of the forces responsible for stabilising protein binding interactions?

1.3 Molecular recognition in protein-binding

Mechanisms describing the folding of simple monomeric proteins have been studied quite extensively (Oliveberg and Fersht, 1996; Shastry *et al*, 1994; Houry *et al*, 1996; Jackson, 1998). These studies have provided valuable information on the role of intramolecular forces in folding and stabilising the secondary and quaternary structure of monomeric protein systems. The models describing simple monomeric systems, however, are not adequate in addressing the role of intermolecular interactions required for the stabilisation of oligomeric protein systems.

Dimeric proteins provide the simplest model for investigating the role of interactions required for the stabilisation of protein complexes (e.g., subunit-subunit, domain-domain interactions, etc). Recently, the mechanism of folding of the homodimeric class alpha glutathione transferase was studied. This investigation highlighted the importance of hydrophobic and polar interactions required for subunit stabilisation as well as subunit association (Wallace and Dirr, 1999). Conformational stability studies have also been performed on the classes pi, mu and sigma GSTs as well as GST *from Schistosoma japonicum* (Dirr and Reinemer, 1991; Erhardt and Dirr, 1995; Hornby *et al*., 2000; Stevens *et al*., 1998; Kaplan *et al*., 1997).

Unfolding/refolding studies have also been performed on a number of other dimeric proteins (Blond and Goldberg, 1986; Gloss and Matthews, 1998; Gokhale *et al*., 1999). The oligomeric nature of many proteins plays an essential role in determining the unique biological functions of proteins *in vivo* and it is important that we understand the role of interactions required for stabilising protein complexes.

1.3.1 Hydrogen bonding

Hydrogen bonds (D-H---A) are non-covalent interactions that are formed between a donor (D-H) and an acceptor atom (A) that contains a lone electron pair. In proteins, the

polar amino acid side chains and the peptide backbone act as donor and acceptor groups. Hydrogen bonds involve permanent dipoles and are essentially dipole-dipole interactions. The strength of a hydrogen bond is dependent on the geometry of the interaction (Murphy, 1995). Many studies have shown that hydrogen bonding contributes favourably to the stability of proteins (Marqusee and Sauer, 1994; Makhatadze and Privalov, 1995; Byrne *et al*., 1995; Haberman and Murphy, 1996). Experiments on the role of hydrogen bonds at protein interfaces have revealed that there are 8 to 13 hydrogen bonds and salt bridges per binding interface that has only 1600 $Å^2$ of buried surface area on average (Janin and Chothia, 1990). Overall, it appears that electrostatic interactions play a more favourable role in binding than in folding. This may, therefore, explain the high density of hydrogen bonds and electrostatic interactions found at interfaces than in protein cores (Xu *et al*., 1997b). An example of the role of hydrogen bonds was observed in the chaperone PapD which makes extensive use of hydrogen bonds to the peptide backbone (Kuehn, 1993).

1.3.2 Hydrophobic interactions

Kauzmann (1959) was the first to state the importance of the hydrophobic interaction in protein folding (see Dill, 1990). Today, it is widely accepted that hydrophobic interactions stabilise globular protein structures and are also the major driving force for protein folding (for a review see Rose *et al*., 1985; Dill, 1990). Examination of protein-protein complexes illustrates that the arrangements of secondary structural elements in protein monomers also occur at the interfaces of proteins (Tsai *et al*., 1997c). Therefore, one would expect the hydrophobic effect to play a dominant role in protein-protein interactions as well. However, a detailed study on the role of hydrophobic interactions at protein-protein interfaces has shown that the hydrophobic effect is not as dominant in protein-binding as it is in folding (Tsai *et al*., 1997b). A study by Jones and Thornton (1996), in which they analysed the average hydrophobicities of protein-protein interfaces and compared these with the hydrophobicities present in protein cores and surfaces indicated that the average hydrophobicity of the protein core is positive whereas the average hydrophobicity of the protein surfaces were negative. Homodimers were found to be the only class of protein complexes that possess interfaces with a positive mean

hydrophobicity. Enzyme-inhibitor complexes have mean hydrophobicities close to zero and antigen-antibody complexes have mean residue hydrophobicities that are indistinguishable from that of a typical protein surface.

It appears that the residue composition of most protein-protein interfaces is more similar to protein surfaces than to that of a protein core. Tsai *et al.* (1997c) have found that interfaces are enriched with both charged and polar residues when compared to protein cores. Hydrophobic residues tend to be scattered over the entire surface and form small patches that are interspersed with charged and polar residues. Overall, it appears that protein interfaces tend to reflect the composition of protein surfaces rather than the interiors of proteins, although they are somewhat enriched in hydrophobic residues.

1.3.3 Electrostatic interactions

Electrostatic interactions occur between charges on protein groups. These charges are present at the amino- and carboxy-termini and on many ionisable side chains (Lys, Arg, His, Glu and Asp). Electrostatic interactions are strongest when the charges are located in the protein interior since it has the lowest dielectric medium (Murphy, 1995). Recent studies have revealed the presence of a significant population of charged and polar residues on protein-protein interfaces. The interaction of ion pairs, by means of hydrogen bonding, buried in the interior of proteins ensures that the thermodynamic requirements are satisfied.

Protein surfaces are quite polar and, therefore, it is not surprising that protein interfaces are polar as well. Complex formation results in the burial of a significant number of charges and polar residues. It appears that the interfaces may have evolved to be non-polar and to be similar to the interiors of individual monomers. The role of electrostatic interactions in protein folding and protein-binding has been evaluated. Hydrophilic pairs refer to the strong electrostatic interactions observed in salt-bridges, hydrogen bonds, polar-polar interactions etc. The results of a study by Xu *et al*. (1997a) indicated that electrostatic interactions play an important role in stabilising protein complexes. The contribution of electrostatic interactions to protein-binding may originate from a

generally more favourable, or less unfavourable, electrostatic free energy for transferring a hydrophilic pair from the protein surface in the folded but unbound state to the complex interface in the bound state, as compared to the change from the unfolded to the folded state. The fact that a salt bridge stabilises an antigen-antibody complex supports this view (Slagle *et al*., 1994). Electrostatic interactions have been found to destabilise the folded conformation of proteins. The reason for salt bridges destabilising the folded protein structure may be related to a desolvation cost. The removal of two ions from water, a high dielectric medium, to form a salt bridge in a low dielectric medium is unfavourable, since the loss of solvation energy cannot be fully compensated by the Coulombic attraction between the ion pair (Honig *et al*., 1989). Very few salt bridges have been observed buried in the interiors of proteins. Calculations have shown that most salt bridges destabilise proteins due to incomplete Coulombic compensation of desolvation effects. Therefore, due to desolvation effects, electrostatic interactions are usually unfavourable in protein folding. In a study by Xu *et al*. (1997a), they found that electrostatic interactions play a more favourable role in protein binding than in folding. Therefore, it is quite evident that we have to differentiate between the properties of the protein-binding interface and the protein core and more importantly, that the conclusions arrived at from protein folding studies may not apply to protein-binding.

1.4 Methods for determining protein-binding interactions

1.4.1 Computational methods

Computer-based analysis of molecular interactions has become more feasible and possible due to the increasing amount of molecular biological data available. Currently, most of the computer-based molecular docking studies have focussed on one of the docking partners being a protein molecule. This is because of the presence of the relatively large number of known protein structures available. The reason is also because proteins are known to bind other proteins, DNA, RNA, as well as ligands. Most algorithms approach the protein-protein docking problem assuming the “rigid body” assumption. This type of association assumes that for a reversible association, the structures of the proteins do not change significantly upon complex formation. Rigid body methods, however, have not been very successful in finding binding modes of

proteins to a high degree as well as determining the free energy of association accurately. The rigid docking methods are currently employed on protein conformations taken from the desired complex. This is unrealistic because it excludes the induced fit phenomenon that protein structures experience during a binding process. A more realistic and accurate test would be to start with the unbound structures of both molecular docking partners (Lehgauer and Rarey, 1996). Therefore, the computer-based docking approach would be more reliable if the structural flexibility of proteins is incorporated into the docking method approach. Although these computer-based algorithms have to be refined a great deal more, the technology for biomolecular docking is an important component of rational drug design.

1.4.2 Calorimetry

It is widely accepted that both thermodynamic and structural information is required to understand the complex relationships that exist between structure, energetics and biological function. Calorimetric studies are gradually replacing the use of van't Hoff analyses of equilibrium data as a means of evaluating the thermodynamics of biomolecules and related systems. The two major systems in use today are differential scanning calorimetry (DSC) and isothermal titration calorimetry (ITC). With DSC, one measures the excess heat capacity of a macromolecule-containing solution as a function of temperature. This is measured relative to a control buffer solution. Integration of the excess heat capacity versus temperature yields the transition enthalpy. A comparison of the calorimetrically determined enthalpy with the corresponding van't Hoff enthalpy, determined from the shape of the DSC curve, allows one to assess whether the transition occurs as a two-state or multi-state process.

The most suitable technique for studying binding interactions is with the use of isothermal titration calorimetry (ITC). Isothermal titration calorimetry (ITC) is the most rigorous method available that allows the characterisation of protein-binding interactions. Because heat is a universal property of most binding interactions, ITC is capable of directly measuring the intrinsic heat absorbed or evolved during any reaction. ITC is directly applicable to a variety of biomolecular interactions that include proteins, nucleic

acids, carbohydrates, lipids, small organic molecules, metals, ions and protons (Doyle, 1999). In a typical ITC experiment, small aliquots of a titrant solution are injected into a titrate solution and the heat absorbed or evolved is measured. Careful selection of the reactant conditions yields a curve that is analysed to obtain the stoichiometry (N), the equilibrium binding affinity constant (K_a), the binding enthalpy (ΔH^O), binding entropy (ΔS^O) as well as the Gibbs free energy of binding (ΔG^O). The heat capacity change (ΔC_p) is obtained from the temperature dependence of the binding enthalpy of the reaction on temperature. Therefore, ITC provides a detailed thermodynamic profile of molecular associations.

1.4.3 Mass spectroscopy (MS)

Using defined conditions, protein complexes may be observed to remain intact during matrix-assisted laser desorption ionisation-time of flight mass spectroscopy (MALDI-TOF-MS). This technique has been used successfully to probe protein-protein interactions. MALDI-TOF has been used to identify peptide ligands (Kelly *et al*., 1996). MS has also been used to screen combinatorial libraries as well as peptide digests for specific binding sequences because the accurate masses obtained allow for a detailed if not completely unambiguous identification of the ligand (Zhao *et al*., 1996).

1.4.4 Nuclear magnetic resonance spectroscopy (NMR)

Proteins perform a variety of functions such as ligand binding and enzymatic reactions. While carrying out these functions they usually undergo conformational changes and are, therefore, very dynamic molecules. The dynamic nature of proteins can be exploited to obtain information on the location and energetics of the conformational changes occurring in protein molecules. Nuclear magnetic resonance (NMR) spectroscopy is a powerful tool that enables one to monitor the dynamic behaviour of macromolecules in solution. Various studies on the target binding sites of protein molecules have been shown that these sites are flexible. Using NMR spectroscopy, the flexible residues in the binding site of protein-protein interactions can be identified (Duggan *et al*., 1999; Crump *et al*., 1999).

1.4.5 Atomic force microscopy (AFM)

One of the most interesting and exciting areas of biophysics is the use of force measurements on molecules in order to observe the effects of stress on molecular interactions. Various studies have already shown that force may be used as a structural probe in ligand-receptor studies (Florin *et al*., 1994; Moy *et al*., 1994). The use of atomic force microscopy (AFM) has been performed successfully on the dissociation or unbinding of biotin to avidin or streptavidin. The authors were able to explore the rupture pathway and obtain the rupture force for the interaction between biotin and avidin or streptavidin (Grubm**ü**ller *et al*., 1996). AFM allows the measurement of biologically relevant forces from a few femtonewtons (10^{-15} N) to many nanonewtons (10^{-9} N). There are essentially two types of biologically relevant forces: entropic and elastic (bonding).

An example of an entropic force is a free DNA molecule in solution. The DNA molecule is able to adopt a random-coil configuration, thereby maximising its conformational entropy. When the DNA molecule is stretched so that it is at its full extension, its molecular entropy would, therefore, be reduced because there is only one configuration left. This conformation is similar to a straight polymer joining the two ends of the DNA molecule. In order for the stretched DNA molecule to reach that conformation, a force has to be applied and work has to be performed against the entropy. The force required to achieve this conformational state is ~ 4 pN. Therefore, entropic forces are described as being weak forces. This force is similar to the ones exerted by molecular motors such as myosin on actin (Finer *et al*., 1994) and the force required to stretch a DNA molecule to its contour length (Smith *et al*., 1992; Bensimon, 1996).

Elastic or bonding forces are described as being much stronger because they involve the breaking and rearrangement of many van der Waals interactions, hydrogen bonds, electrostatic interactions as well as the stretching of covalent bonds. The elastic forces are reported to be in the range of ~ 160 pN. These have been reported to be the forces required for breaking receptor-ligand interactions (Dammer *et al*., 1995).

2. Thermodynamics of biomolecular interactions

2.1 What do the thermodynamic parameters mean?

When performing thermodynamic measurements or calculations it is essential to know what the independent variables are. The independent parameters of an ITC experiment include the stoichiometry of the interaction (N), equilibrium affinity binding constant (K_a), and the enthalpy of the binding interaction (ΔH^O). The dependent parameters are the Gibbs free energy (ΔG^O) and the entropy (ΔS^O) of the binding interaction. This information enables us to understand which thermodynamic property provides the criterion for a spontaneous chemical reaction. For example, if temperature (T) and pressure (P) are independent variables, then it is the Gibbs free energy, G, which provides the criterion $(dG)_{T,P} \leq 0$ of spontaneous chemical change. Therefore, a system can move from a state of high Gibbs free energy to a state of lower Gibbs free energy at a particular temperature and pressure. At equilibrium, dG for any infinitesimal change is equal to zero because G has its minimum value. If the pH is maintained at a particular value, a different equilibrium is obtained than if the pH is not controlled or if the pH is changed to a different value. Under these conditions, $(dG)_{T,P} \leq 0$ is not the criterion for spontaneous chemical change. In order to find the criterion at a specified pH, it is necessary to define a new thermodynamic property, G′, that has its minimum value at equilibrium at a specified pH. When the pH is introduced as an independent variable, there are new thermodynamic properties, new symbols, names and different numerical values. For example, the standard thermodynamic properties calculated from K′ and its temperature coefficient is represented as $\Delta G'^O$, $\Delta H'^O$ and $\Delta S'^O$. These thermodynamic parameters will be distinguished from the standard reaction properties ΔG^O, ΔH^O and ΔS^O, calculated from K and its temperature coefficient. Also, the difference between $\Delta G^{O\prime}$ and $\Delta G'^O$ is not trivial one. The point is that the Gibbs energy is not a function of pH because it is a function only of T and P. It is important to associate the prime with the G in G′ to represent the transformed thermodynamic property that is a function of T, P and pH.

Many biochemical reactants are mixtures of species at pH 7, but even if they are not, $\Delta G'^O$ is different from ΔG^O for a species if it contains hydrogen. Therefore, it is important for biochemists to understand these basic concepts because it affects the way biochemical

equations are written and the nomenclature for reactants (Alberty, 1994). According to Doyle (1999), there is still a lot of variability in the nomenclature used to report ligand-binding thermodynamic data. The precise physical meaning of the thermodynamic parameters can be understood only if they are defined explicitly, including the solution conditions under which they were measured. The nomenclature used in this work (Chapter 6) is according to that used by Wiseman *et al*. (1989) and Baker and Murphy (1998).

The standard Gibbs free energy (ΔG^O) of a binding process is related to the equilibrium binding constant (K_a) by the equation: $\Delta G^O = -RT\ln K_a$, where R is the universal gas constant (8.314 J/mol/K) and T is the absolute temperature. The equation relating the enthalpy (ΔH^O) and entropy (ΔS^O) changes to the Gibbs free energy change is expressed in the equation: $\Delta G^O = \Delta H^O - T\Delta S^O$. The superscript symbol (^{O}) indicates that the standard state concentration units are in molarity.

2.1.1 Gibbs free energy of binding (ΔG^O)

The Gibbs free energy change is the most important quantity in the thermodynamic description of a binding reaction. This parameter determines the binding affinity of a ligand or, in general, the stability of any biological process. According to Luque and Freire (1998a), the Gibbs free energy of binding can be separated into different terms and then written as the sum of those contributions. The decomposition can be expressed as follows: $\Delta G = \Delta G_{gen} + \Delta G_{ion} + \Delta G_{tr} + \Delta G_{other}$ where ΔG_{gen} represents the contributions due to secondary and tertiary structure (van der Waals interactions, hydrogen bonding, hydration as well as conformational entropy), ΔG_{ion} the contributions due to electrostatic and ionisation effects and ΔG_{tr} represents the contributions due to the change in the translational degrees of freedom. The contributions inherent in specific systems that require individual consideration are represented as ΔG_{other} (Luque and Freire, 1998a). Although the ΔG^O is able to describe the affinity of a particular interaction, it may also be insensitive to subtle changes in molecular details of an interaction in terms of enthalpy and entropy. That is, the ΔG^O remains unchanged due to enthalpic and entropic

compensations. Therefore, enthalpy and or entropy changes may be more sensitive reporters of molecular interactions (Bhatnagar *et al*., 1995).

2.1.2 Enthalpy of binding (ΔH^O)

Contributions to the enthalpic term are primarily from the loss of protein-solvent hydrogen bonds and van der Waals contacts. The formation of protein-ligand hydrogen bonds, salt-bridges and van der Waals contacts as well as the change in solvent-solvent interactions near protein surfaces contribute toward the binding enthalpy of a reaction. The breaking of bonds will be endothermic (positive ΔH^O) whereas the negative ΔH^O refers to the formation of hydrogen bonds and van der Waals interactions (Sigurskjold *et al*., 1991).

2.1.3 Entropy of binding (ΔS^O)

Entropy may be viewed as the amount of freedom a system possesses to explore available conformational space. According to Brady and Sharp (1997), the entropy of protein binding interactions may be divided into solvent (ΔS^{solv}) and macromolecular (ΔS^{molc}) contributions. The macromolecular contributions (ΔS^{molc}) may be further divided into the intramolecular conformational (ΔS^{conf}), unconstrained rotational (ΔS^{rot}) and translational (ΔS^{trans}) entropy. In a protein-ligand complex, ΔS^{res}, describes the residual entropy resulting from constrained intermolecular rotational and translational motions. The conformational entropy (ΔS^{conf}) in turn is further subdivided into the contributions made by backbone (ΔS^{back}) and side chains (ΔS^{side}).

Studies on model compounds show that the entropy of solvation is negative for most nonpolar, polar and ionic solutes at room and physiological temperatures. This implies that the burial of groups in protein-binding and folding results in the release of water and this generally results in ΔS^{solv} being positive (Habermann and Murphy, 1996). During binding interactions of charged molecules (e.g., protein-nucleic acid interactions), additional entropic contributions arise from the ordering of water dipoles by means of

long range interactions as well as the arrangement of the ionic environment (Sharp, 1995).

Protein-binding may be separated from protein folding by considering the entropic loss that occurs due to the reduction in translational and rotational freedom when two molecules bind to one another. According to Brady and Sharp (1997), the net loss of "association" entropy may be calculated as follows: $\Delta S^{ass} = S^{res} - S^{trans} - S^{rot}$.

2.1.4 Heat capacity (ΔC_p)

Heat capacity is a fundamental thermodynamic parameter of biologically important molecules that include proteins, peptides and amino acids. Heat capacity data for amino acids, peptides and some protein molecules have been compiled (Makhatadze, 1998). The heat capacity at constant pressure is defined as the temperature derivative of one of the basic thermodynamic parameters that describe the state of a macroscopic system, namely, the enthalpy (Makhatadze and Privalov, 1990; Privalov and Makhatadze, 1990). Edsall (1935) was among the first to draw attention to the large changes in heat capacity at constant pressure when non-polar groups interact with water (see Connelly and Thompson, 1992). In protein-binding processes, a large number of non-polar groups of ligands and/or of the protein-binding site are removed from contact with solvent and become buried in the interior of the protein-ligand complex. This was the observation that led to the idea that hydrophobic interactions play a major role in determining the stability of protein-ligand complexes. Hydrophobic interactions may be considered as two processes: the removal of non-polar groups from water and the packing of these groups within the protein-ligand complex. The heat capacity changes that are observed in protein unfolding studies have been correlated to the changes in solvent-accessible surface area. Spolar *et al*. (1989) and Livingstone *et al*. (1991) have indicated that the heat capacity change for unfolding proteins is directly proportional to the difference in solvent-accessible non-polar surface area between native and denatured states. Experiments have shown that the transfer of non-polar solutes from an aqueous environment to a non-polar solvent is characterised by a large negative change in heat capacity (Nozaki and Tanford, 1971).

Finally, it is important to realise one should interpret thermodynamic data with the use of additional experimental evidence, such as structural data. A combination of various different types of experiments will provide insights into the nature of the various interactions involved, for example, conformational changes, changes in hydration of the protein or ligand and if proton transfers are coupled to the primary binding event (Baker and Murphy, 1996).

CHAPTER 2
GLUTATHIONE TRANSFERASES

2.1 Multi-functional supergene family of detoxification enzymes

The cytosolic glutathione transferases (GSTs, EC 2.5.1.18) represent a supergene family of multi-functional detoxification enzymes. The GSTs are found in a variety of organisms that include vertebrates, plants, insects, yeasts as well as aerobic bacteria. The GSTs are considered to play a very important role in the cellular defence against electrophilic chemical species of endogenous and xenobiotic origins. The GSTs were first discovered in rat liver cytosol when measuring the enzyme-catalysed conjugation of aryl halides with glutathione (Booth *et al*., 1961; Combes and Stakelum, 1961). Initial studies on the GSTs using a variety of electrophilic substrates indicated the existence of several enzymes with differing substrate specificities (Boyland and Chasseaud, 1967). It was only later, with the introduction of improved purification protocols, that the various isoenzymes catalysing the same reaction were identified (Habig *et al*., 1974b; Askelöf *et al*., 1975; Mannervik, 1985).

The GSTs function in the Phase II detoxification (Jakoby and Ziegler, 1990) of a large number of endogenous and toxic xenobiotic substances. The GSTs catalyse the nucleophilic addition of the thiol of reduced glutathione (GSH) to a variety of compounds such as alkyl- and aryl halides, lactones, epoxides, quinones, esters and activated alkenes (Mannervik and Danielson, 1988a, 1988b). The resultant glutathione conjugates (i.e., glutathionyl-*S*-conjugates) are rendered more water-soluble thus allowing their eventual elimination via the mercapturate pathway (Boyland and Chasseaud, 1969; Wilce and Parker, 1994).

The GSTs are also capable of selenium-independent peroxidase activity using organic peroxides as substrates (Lawrence and Burk, 1976; Stenberg *et al*., 1991). The role of the physiological tripeptide glutathione (GSH) in the isomerisation of 3-ketosteroids (Benson *et al*., 1977) and Δ^5-androstene-3, 17-dione (Benson *et al*., 1977; Pettersson and

Mannervik, 2001) as well as the biosynthesis of peptide leukotrines (Tsuchida *et al*., 1987) have also been demonstrated.

Glutathione transferases also function as ligand-binding proteins ("ligandins") (Litwack *et al*., 1971) and thereby facilitate the intracellular transport and storage of a variety of hydrophobic non-substrate compounds including heme, bilirubin, bile acid, steroids, hormones metabolites and drugs (Mannervik and Guthenberg, 1981; Mannervik, 1985; Listowsky *et al*., 1988; Danger *et al*., 1992).

As a consequence of their catalytic functions, GSTs have been implicated in the development of resistance of tumours towards various alkylating, electrophilic anti-cancer drugs (Coles and Ketterer, 1990; Waxman, 1990; Tsuchida and Sato, 1992; Hayes and Pulford, 1995).

2.1.1 Enzyme classification of glutathione transferases

The soluble glutathione transferases can be divided into distinct classes. GST enzyme classification was originally based on structural and functional properties (Mannervik *et al*., 1985) but recently primary structures have been used to classify the GST family. Presently, the mammalian GSTs are grouped into nine species-independent gene classes: alpha, mu, pi (Mannervik *et al*., 1985), sigma (Buetler and Eaton, 1992), theta (Meyer *et al*., 1991), kappa (Pemble *et al*., 1996), zeta (Board *et al*., 1997), beta (Rossjohn *et al*., 1998) and omega (Board *et al*., 2000).

Another GST class is represented by the membrane-bound GST first identified by Morgenstern *et al* (1979). This GST is an abundant protein in the endoplasmic reticulum and the outer mitochondrial membrane. This form of GST also appears to act as a detoxification enzyme and is active with both endogenous and xenobiotic electrophiles, including sulfhydryl-modifying agents (Morgenstern *et al*., 1983). In addition to the cytosolic and membrane-bound GSTs, a plasmid-borne GST has been identified in clinical isolates of bacteria (Arca *et al*., 1988; Arca *et al*., 1990a, 1990b). This form of GST is a metalloprotein and it is thought to be involved in bacterial resistance to

fosfomycin. This GST has no known GST equivalent in human tissues, but it is structurally related to another glutathione-linked enzyme, glyoxalase I (Cameron *et al*., 1997; Bernat *et al*., 1997).

2.1.2 Evolutionary relationship of the glutathione transferases

The various isoenzymes of the cytosolic GSTs are thought to have evolved through a divergent pathway (Armstrong, 1997). A comparison of the cDNA and gene sequences of GSTs from the class alpha/mu/pi with that of the class sigma/theta GSTs suggest that the alpha, mu and pi class GSTs originated from the duplication of the theta gene (Pemble and Taylor, 1992; Pemble *et al*., 1996; Armstrong, 1997). The existence of a highly conserved 3′ non-coding region between the class mu and theta genes suggests that the class mu diverged from the class theta precursor before the alpha and pi gene. The kappa class of enzymes encodes the mitochondrial enzyme and is thought to be the progenitor of the theta class (Pemble *et al*., 1996). The class sigma GST is thought to have diverged from the theta or an early alpha/mu/pi precursor for the purpose of production of the *S*-crystallins (refractory proteins) in the lens of the cephalopod eye (Tomarev *et al*., 1993).

2.2 The three-dimensional structure of cytosolic glutathione transferases

Crystal structure data suggests that although there is low sequence identity between the gene classes, the overall protein fold is remarkably alike. All cytosolic GSTs have a dimeric quaternary structure (M_r ~ 50 kDa) and they exist as either stable homo- or heterodimeric structures. The cytosolic GSTs are roughly globular proteins with dimensions of ~ 62 Å X 51 Å X 46 Å. Only the class alpha and mu isoenzymes exist in the heterodimeric form. This is because of the expression of multiple genes and intraclass subunit hybridisation.

Three-dimensional structures from representatives for the various cytosolic GSTs have been determined. The structures are: class alpha (Sinning *et al*., 1993; Cameron *et al*., 1995), mu (Ji *et al*., 1992; Raghunathan *et al*, 1994), pi (Reinemer *et al*., 1991; 1992; Dirr *et al*., 1994a; Garcia-Sáez *et al*., 1994; Oakley *et al*., 1997a, 1997b), sigma (Ji *et al*., 1995), theta (Wilce *et al*., 1995; Reinemer *et al*., 1996), zeta (Board *et al*., 1997), beta

(Rossjohn *et al*., 1998) and omega (Board *et al*., 2000). The three-dimensional structure from the parasitic helminth, *Schistosoma japonicum* GST, has also been solved (Lim *et al*., 1994; McTigue *et al*., 1995).

The soluble GSTs can be divided into various classes based on sequence similarities that also reflect the evolutionary branches from an ancestral protein (Mannervik *et al*., 1985). The nomenclature of the glutathione transferases is based on the Greek letters: Alpha, Mu, Pi, Sigma, Theta, Kappa and Zeta and is abbreviated A, M, P, S, T, K and Z, respectively. The subunits are numbered using Arabic numerals because any given gene class may contain one or several protein sequences. For example, the gene for the class alpha subunit 1 is written as GSTA1. The name of the functional dimeric enzyme also reflects its subunit content. Therefore, the homodimeric class alpha enzyme that is composed of two copies of subunits 1 is termed GSTA1-1. Likewise, the heterodimeric class alpha enzyme that is composed of subunits 1 and 2 is referred to as GSTA1-2. The organism from which the enzyme was isolated is represented by lower case letters and is included in the nomenclature. The class alpha GST isolated from a human is, therefore, designated by h. Thus, a human class alpha homodimer that is composed of two type 1 subunits is written as hGSTA1-1. Nomenclature corresponding to allelic variants has also been specified (Mannervik *et al*., 1992).

2.2.1 The subunit structure

Crystal structures of the class alpha enzymes are available from the Brookhaven Protein Data Bank. The accession codes for the various human class alpha structures are shown in Table 1. Recently, crystal structures of a double mutant of the rat GSTA1-1 (W20F/F219Y) and a single mutant (W20F) both in complex with glutathione sulfonate have been solved (Adman *et al*., 2001).

The homodimeric class alpha GSTA1-1 is composed of 221 amino acid residues per subunit. Each subunit is composed of two spatially distinct domains. The first domain (81 residues) is an α/β structure composed of a mixed β-sheet of four strands (β1 to β4) and three α-helices with a folding topology corresponding to βαβαββα. The overall folding

Table 1. The Brookhaven Protein Data Bank (pdb) accession codes for crystal structures of the various class alpha GSTs.

pdb code	GSTA1-1	Ligand
1gsd	human	apo-enzyme
1gsf	human	ethacrynic acid
1gse	human	ethacrynic acid-glutathione conjugate
1guh	human	*S*-benzylglutathione
1f3a	murine	reduced glutathione
1f3b	murine	glutathione conjugate of benzo(A)pyrine epoxide
1ev4	rat	glutathione sulfonate
1ev9	rat	glutathione sulfonate

topology of this domain is closely related to the fold observed in the bacteriophage T4 glutaredoxin (Eklund *et al*., 1992). Similar folds have also been found in the *E.coli*

thioredoxin (Holmgren *et al*., 1975) and glutathione peroxidase (Epp *et al*., 1983). The larger C-terminal domain is an all α-helical domain (140 residues) that is composed of six amphipathic alpha helices. The class alpha GST has a unique helix 9 that is wedged between the two domains between alpha helices 2 and 4, and is positioned above the loop connecting β1 and α1 (Sinning *et al*., 1993). Helix 9 is formed by 15 residues at the C-terminus segment of the polypeptide chain.

2.2.2 The subunit interface

Cytosolic GSTs are dimeric proteins. The dimer is formed by an almost perfect 2-fold axis running through an extensive interface (Figure 1A). Dimer formation decreases the solvent accessible surface area so that ~ 14% of the initial water accessible surface area becomes buried at the subunit interface (Sinning *et al*., 1993; Dirr *et al*., 1994a). The interface measures ~ 25 Å X 35 Å. At either end of the dimeric structure there is a high density of side chain interactions that is lowered in the middle of the molecule closer to the 2-fold axis. At a height of ~ 25 Å the monomers separate to form a solvent accessible V-shaped cleft (Sinning *et al*., 1993). At the ends of the interface, all the side chain interactions appear to be predominantly hydrophobic. These interactions are mainly between domain I (alpha helix 2) of one subunit and domain II (alpha helices 3 and 4) of the other subunit.

The human GSTA1-1 crystal structure (1guh) was also examined using the SPIN-PP (Surface Properties of Interfaces-Protein Protein Interfaces) database. The results indicated that there are five critical residues that that are buried at the subunit interface after complex formation. The residues (from subunit A and subunit B) are M50, F51, I85, A89 and M93 (our numbering). A comparison of the above residues indicates that F51 is the residue that is buried the most (100%) upon dimer formation. A89 (98%) and M93 (93%) are also buried to a large extent. The residue preceding F51 in the linear amino acid sequence, M50, is also regarded as a critical residue because 83% of area becoming

A.

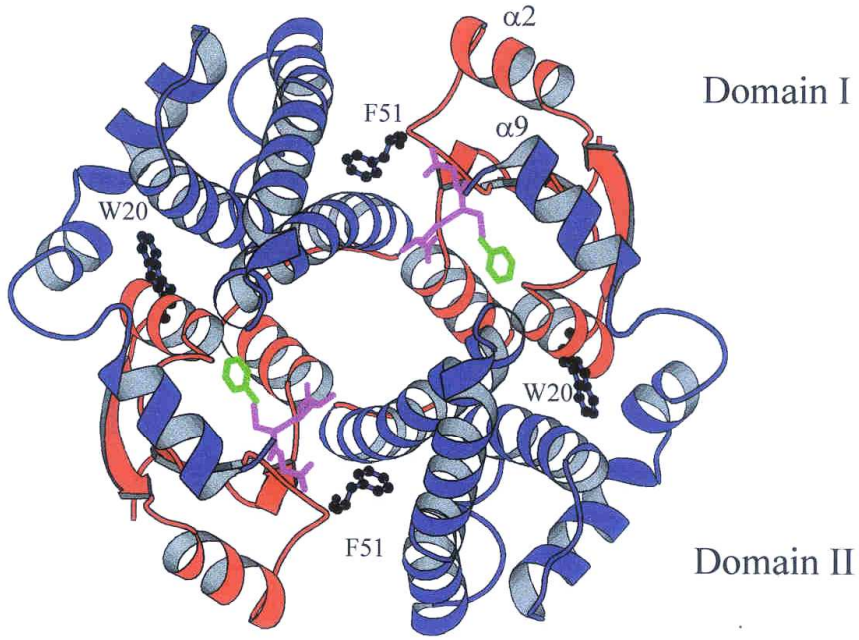

B.

```
          39                                                  57
Alpha     DLDKLRNDGY-------LMFQQVPMV
Mu        APDYDRSQWLNEKFKLGLDFPNLPYL
Pi        PPLKPSCL-----------FRQLPKF
Sj26GST   KWRNKKFELG-------LEFPNLPYY
Sigma     --DWPNLKAT-------MYSNAMPVL
Theta     EHLKPEFLKI-------NPQHTIPTL
            α2                                                β3
```

Figure 1. (A) Ribbon representation of human class alpha GSTA1-1 viewed down the two-fold axis. The location of F51 and W20 are represented as ball-and-sticks. The active site ligand (*S*-benzylglutathione) is shown in bold. The region occupied by the GSH moiety (violet) is referred to as the G-site and the region occupied by *S*-benzyl (green) is referred to as the H-site. (B) The sequence alignment of topologically equivalent residues from representatives of the various gene classes for which crystal structures are known. The residue numbering shown above the sequences is for the hGSTA1-1. The boxed-in residues refer to the conserved phenylalanine residues in class alpha/mu/pi/Sj26 GSTs as well as the topologically equivalent residues in classes sigma and theta. The underlined residues in hGSTA1-1 are located in the secondary structural elements, where α refers to α-helix and β refers to β-srand.

buried after subunit complex formation. Therefore, it is quite conceivable that F51 together with M50 contributes towards subunit stabilisation at the dimer interface.

Examination of the structural features at the subunit interfaces of the various gene classes reveals the existence of two major types of interfaces: the alpha/mu/pi/Sj26GST type and the sigma/theta type (Figure 2). The subunit interfaces of the former group have a curved topography and are hydrophobic with few polar interactions. In the hGSTA1-1 crystal structure, two residues, M50-F51, on the loop between α2-β3 in domain I, are wedged between the α4/α5 helices, and residues from the edge strand of β4 of domain I interact with α3. There is a conserved hydrophobic interaction formed by the side chain of a phenylalanine residue (F51 in alpha; F56 in mu; F46 in pi and F51 in Sj26GST) (Figure 1B) that protrudes from a loop in domain I of one monomer into a hydrophobic pocket between α-helices 4 and 5 of domain II of the other monomer (Figure 1A). This lock-and-key motif physically anchors the two subunits together at either ends of the interface.

A recent study involving the replacement of F51 with serine in the hGSTA1-1 protein indicated that the mutation impacted negatively on the catalytic functioning and conformational stability of the protein and that the ligandin function (i.e., ANS binding) was enhanced (Sayed *et al*., 2000). In contrast, the lock-and-key type interaction is absent in the class sigma/theta enzymes (Figure 2). This results in a dimer interface that is flat and more hydrophilic with an extensive network of polar interactions (Wilce and Parker. 1994; Ji *et al*., 1995).

2.2.3 The active site

Crystal structure data has verified that the dimer contains two active sites, one at each end of the V-shaped crevice (see Figure 3) spanning the dimer interface (Sinning *et al*., 1993). The two active sites also behave independently of one other (Danielson and Mannervik, 1985). Each site can be separated into two distinct functional regions: a hydrophilic G-site for binding the physiological tripeptide glutathione (GSH) and an adjacent hydrophobic H-site for binding structurally diverse electrophilic substrates (see Figure 1A). A fully functional active site is formed by structural elements from both

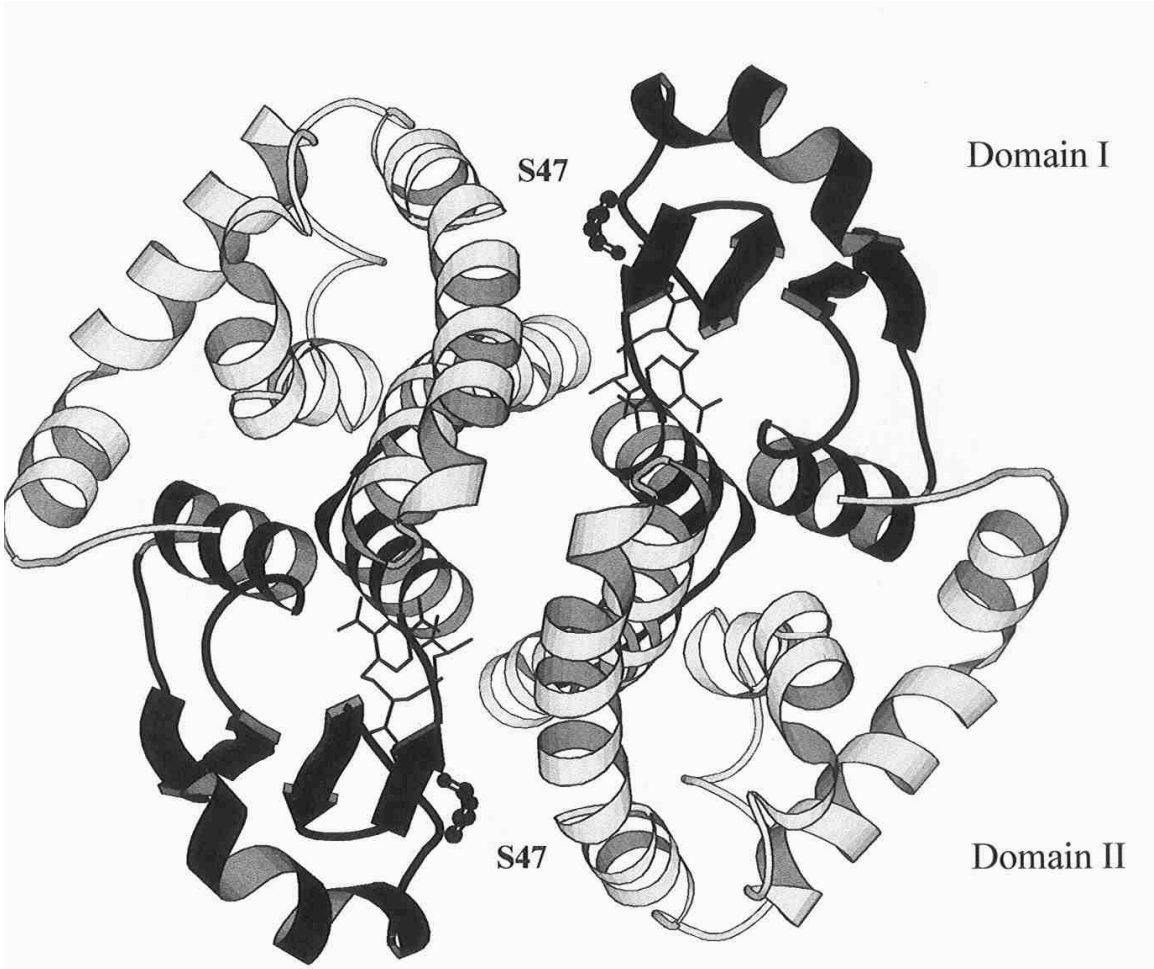

Figure 2. Ribbon representation of the squid class sigma GSTS1-1 viewed down the two-fold axis. The location of the topologically equivalent residue, S47, at the subunit interface is represented as ball-and-sticks. The active site ligands, 1-(*S*-glutathionyl)-2,4-dinitrobenzene, are shown as sticks.

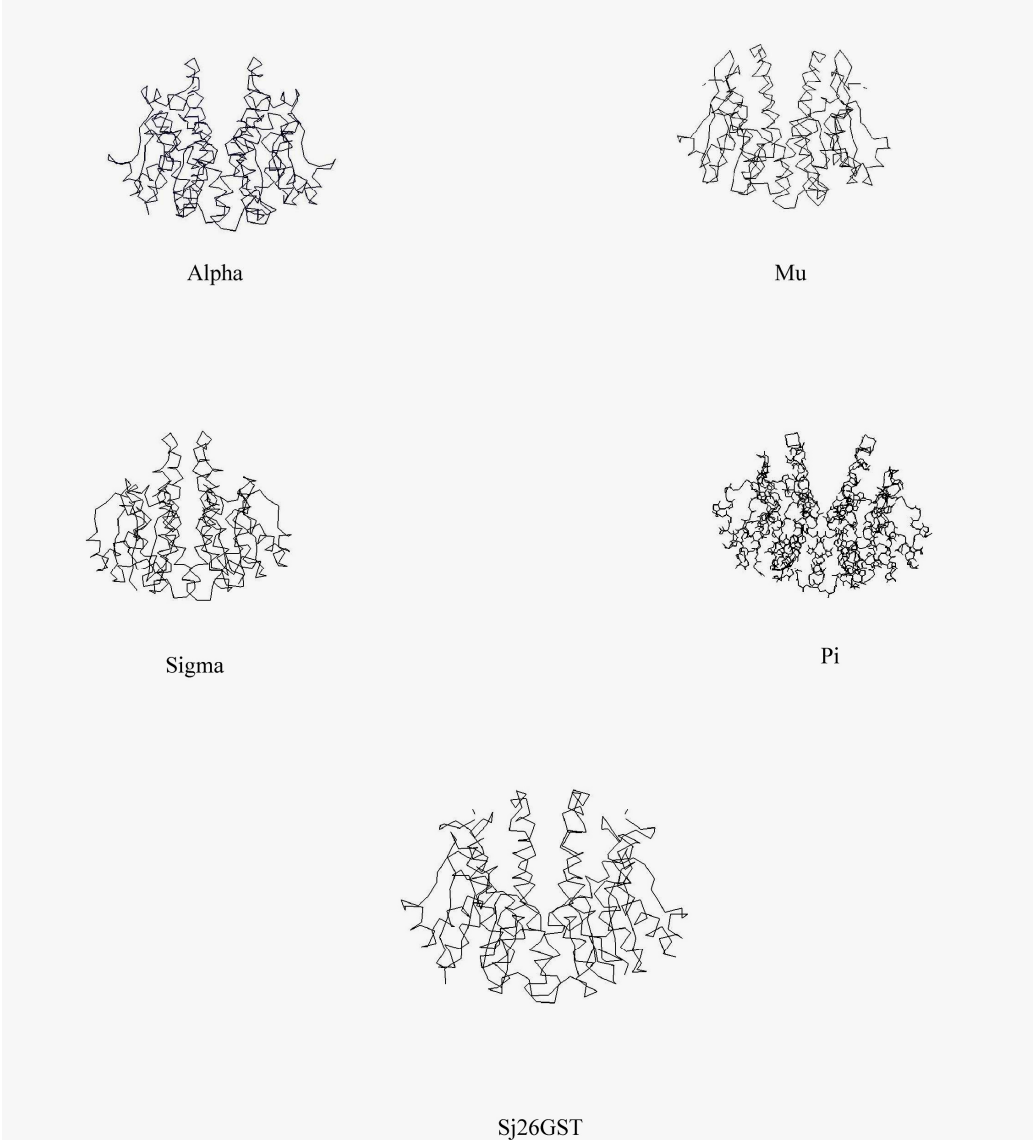

Figure 3. The backbone representation of representatives from the various GST gene classes for which crystal structures are known. The structures are viewed perpendicular to the two-fold axis to show the V-shaped cleft at the dimer interface. The figures were generated using Swiss-pdb viewer.

subunits of the dimer, with the conserved core of domain I providing the major structural framework (Dirr *et al*., 1994b).

2.2.3.1 The glutathione binding site (G-site)

Crystallographic data of hGSTA1-1 in complex with *S*-benzylglutathione allows for the description of the G-site as well as the neighbouring H-site (Figure 1A) (Sinning *et al*., 1993). The G-site is highly specific for glutathione (GSH) and the molecular recognition of GSH (γ-Glu-Cys-Gly) involves a network of specific polar interactions between the tripeptide and domain I of one subunit and either no (class theta), one (class sigma/pi/mu/Sj26GST) or two (class alpha) amino acid residues from domain II of the other subunit (Dirr *et al*., 1994b).

In the crystal structure of the hGSTA1-1, most of the interactions between GSH and the enzyme come from domain I (Figure 4). Salt links (Asp100 and Arg130) are also formed at each end of the tripeptide (GSH) with residues from domain II of the two-fold related monomer. Most of the polar atoms in GSH are involved in hydrogen bonds or salt links. The tripeptide binds the G-site in an extended conformation with the γ-glutamyl moiety pointing downward towards the dimer interface. The γ-glutamyl moiety interacts with the enzyme in a similar manner for all gene classes although there are differences in the specific interactions (Dirr *et al*., 1994a; Ji *et al*., 1995). For example, in the human class alpha GST, the carboxylate of the γ-glutamyl side-chain hydrogen bonds to the peptide nitrogen and the hydroxyl of Thr67 and to a solvent molecule. The cysteinyl sulfur atom forms two close contacts to (1) the tyrosyl hydroxyl group (Y8) and to (2) the N^{ε} of Arg14. The Y8 hydroxyl group also forms a hydrogen bond to the peptide nitrogen of Arg14 and the Arg15 side-chain in turn salt links to Glu104 (Figure 4) (Sinning *et al*., 1993). The interactions between the cysteinyl and glycine residues of GSH are more variable between the gene classes. (Ji *et al*., 1992; Lim *et al*., 1994; Ji *et al*., 1995). The removal of the glycyl moiety from the tripeptide resulted in a greater affinity of the electrophilic substrate suggesting that this moiety may influence the topology of the active site and also assist in the binding of the second substrate of the enzyme (Widersten *et al*., 1996).

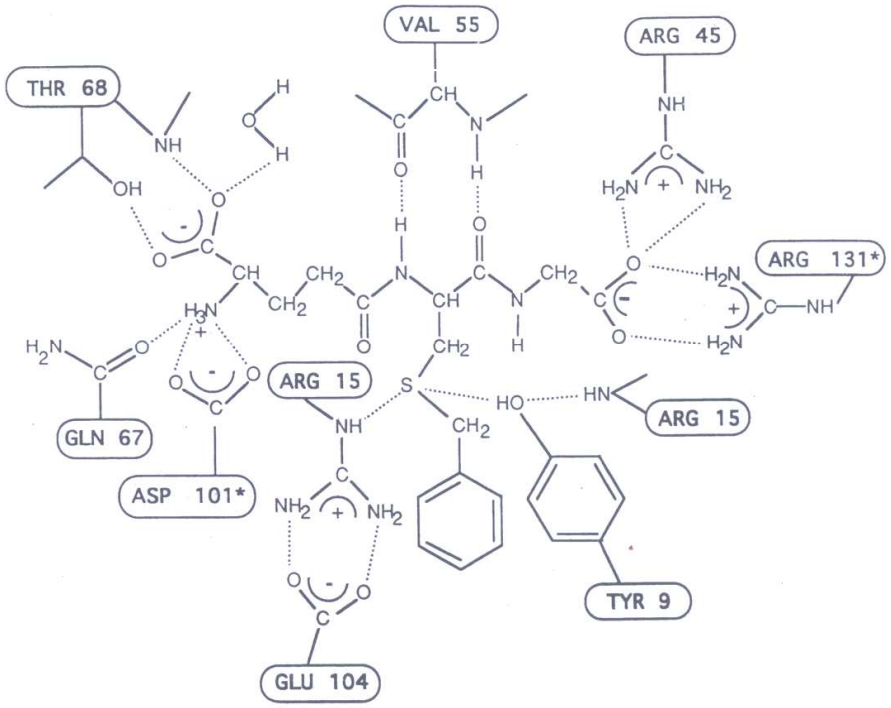

Figure 4. A schematic representation of the residues of hGSTA1-1 that interact via hydrogen bonds and salt linkages with the ligand, *S*-benzylglutathione. The two residues marked with an asterisk are from the two-fold related molecule. The numbering shown in the schematic does not include methionine 1. Adapted from Sinning *et al.*, 1993.

2.2.3.2 The non-substrate hydrophobic binding site (H-site)

The presence of the substrate-product analogues *S*-hexylglutathione (Reinemer *et al*., 1992, 1996;), *S*-benzylglutathione (Sinning *et al*., 1993), and *S*-(-p-nitrobenzyl)glutathione (Garcia-Sáez *et al*., 1994) has helped in the identification of the hydrophobic, electrophilic substrate binding site. The co-crystallisation of the transition state analogues (*S*-2,4-dinitrophenyl)glutathione (Ji *et al.*, 1993, 1995) as well as the enzyme in the presence of ethacrynic acid (EA) or glutathione-ethacrynic acid (GS-EA) conjugate (Cameron *et al*., 1995; Oakley *et al*., 1997b), has also been helpful in the identification of the H-site. In the crystal structure, the glutathione always binds in an extended conformation and the moiety that is covalently attached to the sulfur atom is located in the H-site (Figure 1A).

Recently, a murine class alpha GST was co-crystallised in the presence of a carcinogenic metabolite, [(+)-*anti*-BPDE] (Gu *et al*., 2000). The results indicated the existence of very important structural differences in the H-site between the murine and human class alpha GSTs. The presence of the guanidino group of R216 is important in orientating and positioning the carcinogenic metabolite in the H-site. The absence of R216 in the human class alpha GST may explain the inability of hGSTA1-1 to accommodate the bulky substrate in the narrow H-site as well as the low catalytic efficiency of hGSTA1-1 toward (+)-*anti*-BPDE (Gu *et al*., 2000).

Although differences in structure of the H-site between gene classes do exist, there are clusters of hydrophobic side-chains that result in the formation of a highly hydrophobic surface that is exposed to solvent in the absence of H-site substrates. The differences in topology allow the H-site to accommodate a variety of hydrophobic electrophilic substrates of different size and polarity (Dirr *et al*., 1994b). In the hGSTA1-1 structure, the H-site is composed of hydrophobic residues, F9, R14, M207, A215, A218, F219 and F221, among which four are located in the C-terminal helix. The C-terminal region of the hGSTA1-1 protein has been shown to be an important part of the H-site (Board and Mannervik, 1991; Hoesch and Boyer, 1989; Sinning *et al*., 1993; Cameron *et al*., 1995). The C-terminus of the hGSTA1-1 protein contains a unique helix, helix 9, that is

crystallographically “invisible” in the apo-form of the protein (Sinning *et al*., 1993; Cameron *et al*., 1995). Helix9, however, becomes immobilised over the H-site when the active site is occupied by an active site ligand.

Helix 9 is a structural determinant for specificity toward hydrophobic electrophiles (Board and Mannervik, 1991). Helix 9 becomes immobilised over domain I and provides a highly hydrophobic environment for the electrophilic binding pocket. The localisation of helix 9 over the H-site effectively restricts accessibility of the H-site from bulk solvent. The dynamic behaviour of helix 9 is clear from crystallographic (Sinning *et al*., 1993, Cameron *et al*., 1995) and NMR (Lian, 1998) data. A recent study by Dirr and Wallace (1999) indicated that helix 9 stability is enhanced by the presence of ligands at the active site. The authors also showed that the order of the ligand-induced stabilisation of helix 9 at the C-terminus of hGSTA1-1 increases from H-site occupation, to G-site occupation, to the combined occupation of the H- and G-sites. It appears that the C-terminus helix 9 does not affect the overall conformational stability of the protein but that it is required for the catalytic and ligandin function of the human class alpha GST (Dirr and Wallace, 1999).

Recently, the crystal structure of a double mutant (W20F/F219Y) of the rat GSTA1-1 complexed with glutathione sulfonate was solved. The crystal structure showed that helix 9 is ordered as a helix but that it was not located at its expected position (Adman *et al*., 2001). The fact that an ordered helix was observed suggested that is was the localisation of the mobile helix rather than a helix-coil transition that was required for a completed active site in the rat GSTA1-1. The first kinetics refolding model for the GST superfamily proposed that the human class alpha GSTA1-1 folds very rapidly (millisecond time scale) to form structured but loosely packed monomers with exposed hydrophobic cores. The events that follow are subunit association and domain docking. The final slow step in the formation of the fully active folded dimer involves the localisation of the C-terminal helix 9 of hGSTA1-1 (Wallace and Dirr, 1999).

2.2.4 The non-substrate ligand binding site (L-site)

Dimerisation of the individual subunits of GSTs result in the formation of a V-shaped cleft at the dimer interface (see Figure 3). The cleft is a feature common to all GSTs. GSTs possess a wide range of specificities and affinities for various anionic ligands due to differences in the cleft topography (Danielson and Mannervik, 1985). The GSTs also bind large lipophilic molecules leading to the suggestion that they are involved in storage and transport of these molecules in the aqueous phase of the cell (Litwack *et al*., 1971; Habig *et al*., 1974a; Tipping and Ketterer, 1981; Caccuri *et al*., 1990). The "ligandin" function of GSTs was observed in very early work when GSTs were observed to bind ligands such as hemin, bilirubin, bile salts, steroids, thyroid hormones, fatty acids and drugs (Ketterer *et al*., 1987). Ligand binding is characterised by non-competitive inhibition towards the substrate CDNB (Ketley *et al*., 1975; Mannervik and Danielson, 1988a, 1988b). The location of a possible ligand-binding site has been supported by crystal structure data that shows the binding of ligands at the dimer interface (McTigue *et al*., 1995; Ji *et al*., 1996). Other laboratories have also suggested that the L-site in human class GST is located at a buffer binding site (Ji *et al*., 1997; Prade *et al*., 1997). In mammalian GSTs, the V-shaped cleft at the dimer interface was proposed as the L-site for the binding of ANS, BSP as well as aflatoxin B1 (Sluis-Cremer *et al*., 1996; Sluis-Cremer *et al*., 1998). Recently, crystal structure data of a variety of non-substrate ligands (sulfasalazine, *S*-nonylglutathione, cibacron blue and BSP) complexed to human class pi GST indicated that the L-site is located in the electrophile binding site (H-site) (Oakley *et al*., 1999). Therefore, the exact location/s as well as the number of L-sites is not yet clear. ITC data obtained from the binding of ANS to the wild-type hGSTA1-1 protein shows that one molecule of ANS binds per subunit (see Chapter 6). Also, ITC data of BSP binding to the wild-type protein indicates that there are two sets of binding sites corresponding to a higher and a lower affinity binding site (see Chapter 6). The exact locations, however, of the binding sites for ANS and BSP are still not clear.

2.3 The catalytic mechanism

The systematic name of GSTs is "RX: glutathione transferase" (EC 2.5.1.18) and the Enzyme Commission has recommended the trivial name "glutathione transferase"

without a prefix. The abbreviation GST is, however, adequate. The commonly used "glutathione *S*-transferase" is a misnomer since the sulfur atom is not transferred, but the R-substituent, or the glutathionyl group (GS^-) (Johansson and Mannervik, 2001).

The glutathione transferases catalyse the reaction that involves the nucleophilic addition of reduced glutathione (GSH) to a variety of electrophilic compounds. The catalytic mechanism of the GSTs may be described as a sequential catalytic mechanism involving a ternary complex of enzyme, reduced GSH and the electrophilic substrate. The class alpha GST has a tyrosyl hydroxyl group that acts as a hydrogen bond donor to the sulfur atom of GSH thereby lowering the pK_a of the thiol group so that it is predominantly ionised (GS^-) at physiological pH (Liu *et al*., 1992; Kolm *et al*., 1992; Wang *et al*., 1992; Armstrong, 1997). The sequential mechanism referred to above may be represented as follows:

$$E + GSH \Leftrightarrow E{\bullet}GS^- + H^+ \Leftrightarrow E{\bullet}GS^-{\bullet}\overset{R\text{-}X}{} \Leftrightarrow E{\bullet}GSR{\bullet}X^- \Leftrightarrow E + GSR + X^-$$

where E is GST, R-X is the hydrophobic electrophilic substrate, GSH is the reduced glutathione and GS^- is the highly reactive thiolate anion. Due to the high GSH concentration in the cell (1-10 mM GSH) it is possible that reduced GSH is complexed to the enzyme first (Dirr *et al*., 1994b).

The class alpha GST also involves the participation of Arg14 into the inner co-ordination sphere of the sulfur atom of GSH. It has been proposed that in the class alpha GSTs, the reactive species in the binary complex most likely involves the thiolate anion which can accept a hydrogen bond from the tyrosyl hydroxyl group and may also obtain additional stabilisation energy from the positive charge of Arg14 (Armstrong, 1997). This can be represented as follows: E-O-H ----- $^-$SG, where E-O-H represents the enzyme (GSTA1-1) tyrosyl hydroxyl group.

The role of the active site tyrosyl hydroxyl group (alpha/mu/pi/sigma/Sj26GST) in the catalytic mechanism remains a matter of dispute. The question asked is whether the

hydroxyl group acts as a hydrogen bond donor (electrophilic participant) or hydrogen bond acceptor (general base). The dispute, therefore, arises over the position of the protons in the active site. The arguments in favour of the active site tyrosyl hydroxyl group acting as a base (Atkins *et al*., 1993; Dietze *et al*., 1996a, 1996b; Karshikoff *et al*., 1993; Meyer *et al*., 1993) are based on the observation that the class alpha enzyme has a tyrosyl hydroxyl group with a very low pK_a ~ 8.5. However, it is reasoned that far less than 50% of the tyrosyl hydroxyl groups will be ionised at physiological pH, suggesting that the scenario of the tyrosyl hydroxyl group acting as a general base may be a minor pathway (Armstrong, 1997). A study showed that when all fourteen tyrosyl residues were replaced with 3-fluorotyrosine, the hydroxyl group of the tyrosyl residue stabilises the thiolate anion of bound GSH prior to nucleophilic attack, therefore, arguing against the general base catalytic model (Parsons and Armstrong, 1996). Also, the fact that the anionic analogues of glutathione (γ-L-Glu-L-AspGly and glutathione sulfonate) bind the enzyme more tightly than does GSH also argues against a significant ionisation of the active site tyrosyl hydroxyl group at the active site (Graminski *et al*., 1989a).

2.4 Conformational stability of glutathione transferases

Conformational stability studies performed on the class alpha (Wallace *et al*., 1998b), pi (Dirr and Reinemer, 1991; Erhardt and Dirr, 1995) and Sj26GST (Kaplan *et al*., 1997) enzymes indicate that equilibrium unfolding and dissociation is consistent with a highly co-operative two-state transition involving the native dimer and the unfolded monomer. The stabilisation energy of the native structure is ~ 25 kcal/mol. The class mu (Hornby *et al*., 2000), sigma (Stevens *et al*., 1998) and beta (from *Proteus mirabilis*) (Sacchetta *et al*., 1993) enzymes, however, display a multi-step equilibrium pathway with the class mu enzymes displaying an enhanced conformational stability when compared to the class sigma and beta enzymes. The greater stability observed in the class alpha/mu/pi/Sj26GST when compared to the class sigma enzyme is attributed to the differences observed at the dimer interface.

The lack of the hydrophobic interaction at the subunit interface of the class sigma GST is compensated for by an increase in electrostatic interactions. A conserved intermolecular

contact found in the middle on the dimer interface is formed due to the stacking of symmetrically equivalent arginine guanidino groups (Arg69, alpha; Arg77, mu; Arg68, pi; Arg72, Sj26GST and Arg68, sigma). The charges on the guanidino groups are mitigated by nearby acidic residues. This type of interface is not observed in the class theta enzymes (Wilce *et al*., 1995).

The class mu and sigma enzymes yield molten globule-like inactive monomeric intermediates that indicate that the extent of subunit stabilisation by quaternary interactions is less for these two classes. Quaternary interactions appear to be more important for the class alpha/pi/Sj26GST enzymes because no stable monomeric intermediates are observed. Therefore, it appears that the more ancient GSTs have more stable subunits than the more recent GSTs and that functionality of the protein dimer is most likely the major evolutionary pressure rather than enhancing subunit stability.

Stopped-flow kinetic studies of the wild-type hGSTA1-1 have indicated the existence of a three-state kinetic unfolding mechanism in which the only the unfolded monomer and folded dimer are significantly populated at equilibrium (Wallace *et al*., 1998b). The presence of structured monomers possessing native-like secondary structures was observed in the kinetic refolding study (Wallace and Dirr, 1999). The class sigma appears to unfold via an unfolding mechanism that includes the presence of both a thermodynamically stable dimers and thermodynamically stable monomeric intermediate species (Stevens *et al*., 1998).

The interactions at the subunit interface, therefore, play an important role in stabilising the subunit tertiary structure for all the GST classes. The cytosolic GSTs have distinct quaternary structures and molecular recognition at the subunit interface is class specific; i.e., dimerisation will only occur between subunits from the same gene class. Also, the dimeric structures are required to maintain catalytically functional conformations of the individual subunits and the non-substrate ligand-binding site at the dimer interface.

2.5 Objectives

The main goal behind protein studies is to understand the complex relationship between the structure of a protein and its biological function *in vivo*. Crystal structure data has provided us with a wealth of information that has aided in our understanding of the folding and assembly of many proteins. Structural data of the class alpha/mu/pi/Sj26GST all indicate the presence of a conserved phenylalanine residue (F51 in alpha; F56 in mu; F47 in pi and F51 in Sj26GST) at the subunit interface. Replacing the lock residue (F51) with serine assessed the role of this residue in the lock-and-key type interaction at the subunit interface.

The binding of ligands to proteins is of central importance to biology. GSTs were initially described as "ligandins" because they displayed impressive binding activity towards a wide variety of ligands. A deletion mutant (F221del) was constructed using protein engineering techniques. Biochemical characterisation was performed to assess the role of F221 in the ligandin function and its possible role in the flexibility of a unique C-terminal helix 9 of hGSTA1-1.

The nature of the interactions of a substrate molecule and (a) specific residue/s located at the active site of an enzyme is essential in understanding the mechanism of enzyme action. Isothermal titration calorimetry (ITC) was used to dissect the binding energetics of the physiological tripeptide glutathione (GSH) as well as the inhibitor, glutathione sulfonate (GSO_3^-), to the wild-type and Y8F hGSTA1-1 proteins. In this way, a complete thermodynamic profile was obtained that could explain the contribution of the tyrosyl hydroxyl group to the binding of G-site ligands. The role of the tyrosyl hydroxyl in modulating the conformational dynamics of helix 9 is also addressed.

Very little is known about the ligandin function of GSTs, whereas an abundance of information is available regarding the catalytic functions of GSTs. The location as well as the number of non-substrate ligand-binding sites (L-sites) is still under investigation. In order to enhance our understanding of the ligandin function of the class alpha GST,

isothermal titration calorimetry was used to obtain a thermodynamic profile of the binding energetics of the non-substrate ligands, ANS and BSP, to wild-type hGSTA1-1.

Chapter 3

EXPERIMENTAL PROCEDURES

3.1 Materials

8-anilino-1-naphthalenesulfonic acid (ANS), sulfobromophthalene (BSP), *tris*-(carboxyethyl)-phosphine (TCEP) and CDNB were purchased from Sigma. Reduced glutathione (GSH), glutathione sulfonate (GSO_3^-) and glutathione reductase were from Boehringer Mannheim. Ultrapure urea was purchased from ICN Biomedicals, Inc. *S*-hexylglutathione was prepared in our laboratory according to the method of Vince *et al* (1971). The diagnostic restriction enzymes, *Eco*R V, *Bgl* II and *Hind* III, were from Amersham Life Science International. The ExSite™ and QuikChange™ mutagenesis kits were purchased from Stratagene. The plasmid, pKHA1, was a generous gift from Prof. B. Mannervik (Stenberg *et al*., 1992). All other reagents were of an analytical grade.

3.2 Generation of F51S, F221del and Y8F hGSTA1-1

All the oligonucleotide primers were designed using the computer software package, Gene Runner, v3.04. The cDNA sequence contained in the pKHA1 plasmid codes for the human glutathione transferase from human hepatoma HepG2 cells (Stenberg *et al*., 1992). Primer design was according to the manufacturers instructions. The primers were designed using the wild-type nucleotide sequence as the template.

3.2.1 Mutagenic primer design for use with the ExSite™ and QuikChange™ mutagenesis kits

The F51S and F221del mutants were generated using the ExSite™ PCR-Based Site Directed Mutagenesis Kit. The mutagenic primers that were used to construct the F51S and F221del mutants were:

F51S FWD PRIMER 5′GGA TAT CTG ATG **TCC** CAG CAA GTG CCA ATG 3′ and F51S REV PRIMER 5′ATC ATT TCT TAA CTT GTC CAA ATC 3′ and

F221STOP FWD 5′GG AAG ATC TTC AGG **TAA** TAA TAA CGC AGT CAT GG 3′ and F221STOP REV 5′ TTG CTT CTT CTA AAG ATT TCT CAT CCA TGG G 3′, respectively. The underlined nucleotide sequences represent the translationally silent mutations that also code for the diagnostic restriction sites, *Eco*R V and *Bgl* II, for the

F51S and F221del mutations, respectively. The codons in bold print represent the F51S and F221del mutations, respectively.

The QuikChange™ Site-Directed Mutagenesis Kit was used to generate the Y8F mutant. The mutagenic oligonucleotides were: Y8F TOP 5′AAG CCC AAG CTT CAC **TTC** TTC AAT GCA CGG GGC 3′ and Y8F BOTTOM 5′GCC CCG TGC ATT GAA **GAA** GTG AAG CTT GGG CTT 3′. The underlined nucleotide sequence represents the translationally silent mutation as well as the *Hind* III diagnostic restriction site. The bold letters represent the Y8F mutation.

3.2.2 PCR-based site-directed mutagenesis

The ExSite™ kit was used to introduce either the F51S or F221del mutation directly into the intact, double-stranded DNA, pKHA1 plasmid encoding the hGSTA1-1. The PCR reaction was carried out as detailed in the manufacturers instruction manual. Briefly, the PCR reaction mixture contained 0.5 pmol double-stranded plasmid DNA (pKHA1), 1X mutagenesis buffer, 15 pmol of each mutagenic oligonucleotide primer, 1 mM of each dNTP made up to a final volume of 24 µl in sterile deionized, distilled water. The mutagenesis buffer is composed of 200 mM Tris-HCl (pH 8.75), 100 mM KCl, 100 mM $(NH_4)_2SO_4$, 20 mM $MgSO_4$, 1% (v/v) Triton® X-100 and 1 mg/ml bovine serum albumin (BSA). After performing a 10 minute hot start at 94°C, 1 µl of ExSite DNA polymerase blend (5 U/µl) was added to the PCR reaction tube. The PCR reaction conditions that generated a PCR product for the F51S and F221del mutants were: 12 cycles consisting of (1) melting temperature at 94°C for 100 seconds, (2) annealing temperature at 55°C for 160 seconds and (3) extension temperature at 72°C for 240 seconds. A final extension at 72°C for 10 minutes was performed before analysing the PCR product on a 1% agarose gel containing ethidium bromide. The linearised PCR reaction products were digested with *Dpn* I (10 U/µl) to digest parental template DNA. *Pfu* DNA polymerase (4 U/µl) was used to remove extended bases at the 3′ ends of the PCR product. After ligating the PCR product, it was transformed into supercompetent Epicurian Coli XL1-Blue cells.

The QuikChange kit makes use of supercoiled, double-stranded DNA, two oligonucleotide primers containing the desired mutation and a thermal cycler. Each oligonucleotide primer is complementary to opposite strands of the plasmid and extension is achieved using *Pfu* DNA polymerase during temperature cycling. In order to generate the Y8F mutant, three reactions were set up that contained 5, 15 and 40 ng of template DNA per reaction. In addition, the reaction mixture also contained 125 ng of each oligonucleotide primer, 2.5 mM of each dNTP, 1 X reaction buffer. The mixture was made up to a final volume of 50 µl deionized, distilled water. *Pfu* DNA polymerase (2.5 U) was also added. The reaction buffer is composed of 100 mM KCl, 60 mM $(NH_4)_2SO_4$, 200 mM Tris-HCl (pH 8.0), 20 mM $MgCl_2$, 1% Triton® X-100 and 100 µg/ml nuclease-free bovine serum albumin (BSA). The thermal cycling parameters used were: 1 cycle at 95^OC for 30 seconds followed by 15 cycles at 95^OC for 30 seconds, 65^OC for 60 seconds and 68^OC for 8 minutes. In order to assess the success of each reaction, an aliquot from each reaction mixture was electrophoresed on a 1% agarose gel containing ethidium bromide. Each reaction indicated the presence of the desired product, and was, therefore, used in the subsequent procedures. *Dpn* I (10 U/µl) was added to each reaction tube to a final concentration of 10 U/µl. The reaction mixture containing *Dpn* I was allowed to incubate at 37^OC for two hours following which it was left at 20^OC for one hour. This step represented a slight modification of the suppliers instructions. The *Dpn* I-treated DNA from each reaction mixture was transformed into supercompetent Epicurian Coli XL1-Blue cells.

The transformed cells were screened for the presence of the desired mutation using restriction enzyme digestion analysis. After randomly selecting possible mutant containing colonies (for F51S, F221del and Y8F), an overnight culture was grown in 5 ml of LB media at 37^OC supplemented with the appropriate antibiotic (final concentration of 100 µg/ml ampicillin) selectable marker. The supernatant was discarded after pelleting ~ 3 ml of the overnight culture at 14 000 rpm for 1 minute. The pellet was resuspended in 100 µl of ice cold Solution I (25 mM Tris-HCl, pH 8.0, 10 mM EDTA and 50 mM glucose). A further 200 µl of ice-cold Solution II (0.2 M NaOH and 1% SDS) was added to the mixture and then inverted several times. The denatured DNA was then treated with

150 µl of ice-cold Solution III (5 M potassium acetate) and the mixture was allowed to incubate on ice for 15 to 20 minutes. After centrifuging at 14 000 rpm for 20 minutes at 4°C, the supernatant was carefully removed and placed into a clean, sterile tube. An equal volume of room temperature isopropanol was added and inverting the tube several times mixed the contents. The mixture was centrifuged for a further 30 minutes at 14 000 rpm. The supernatant was discarded and the pellet was washed with 100 µl of 99% ethanol. After briefly centrifuging for 2 minutes at 14 000 rpm, the ethanol was carefully removed taking care not to dislodge the pellet (DNA). The pellet was left to air-dry for ~ 5 minutes before resuspending it in 15 µl of sterile, Milli-Q water. To allow complete resuspension to take place, the DNA solution was incubated at 37°C for 1 hour or at 4°C overnight. The plasmid DNA was digested overnight with the appropriate diagnostic restriction enzyme. The products were electrophoresed on a 1% (F51S and F221del mutants) or 1.2 % (Y8F mutant) agarose gel containing ethidium bromide.

3.3 Sequencing of mutant plasmid DNA

All mutant plasmid DNA were sequenced using an ABI Prism 310 Genetic Analyser from PE Biosystems (CA, USA). DNA sequencing reactions were set up as recommended by the supplier. Briefly, the reaction mixture contained 500 ng mutant plasmid DNA (F51S, F221del or Y8F) and 3.2 pmol of sequencing primer made up to a final volume of 12 µl with sterile Milli-Q water.

3.4 Over-expression and purification of the wild-type, F221del and Y8F hGSTA1-1 proteins

The wild-type pKHA1 and mutant plasmids (F221del and Y8F) were transformed into *E.coli* BL21 DE3 cells containing the pLysS plasmid. Over-expression of the above-mentioned proteins was always initiated by inoculating a single colony into 100 ml of LB media supplemented with 100 µg/ml of ampicillin and chloramphenicol. All protein over-expression studies were performed at 37°C. The wild-type and mutant proteins were purified using *S*-hexylglutathione affinity chromatography as described previously (Stenberg *et al.*, 1992). The bound protein was eluted from the affinity column using 50 mM glycine-NaOH, pH 10 (Cameron *et al.*, 1995). In this way, the protein could be

purified in the apo-form (i.e., in the ligand-free enzyme form). All recombinant hGSTA1-1 proteins were stored in 20 mM sodium phosphate buffer, pH 6.5 containing 0.1 M NaCl, 1 mM EDTA and 0.02% sodium azide.

3.5 Over-expression and purification of F51S hGSTA1-1

The F51S and wild-type proteins were purified from BL21 DE3 cells using CM-Sephadex cation exchange chromatography. The over-expression procedure was identical to that described above except that the pellet containing the whole cell extract was resuspended in start buffer (10 mM sodium phosphate, pH 7.45, 1 mM EDTA and 0.02% sodium azide). The resuspended cells were placed at -70°C for two hours to promote cell lysis. After a brief sonication step, the cells were centrifuged at 14000 rpm for 20 minutes at 4°C. The cytosol was then carefully added to the bed of a CM-Sephadex column pre-equilibrated with start buffer. After washing the column with a minimum volume of 2 litres of start buffer, the protein was eluted using a salt gradient of 0-0.3 M NaCl (200 ml final volume) prepared in start buffer. The absorbance was measured at 280 nm and fractions were run on a SDS-PAGE gel in order to assess the purity of the protein fractions. Only the fractions containing pure protein were pooled.

The purity and homogeneity of all proteins samples were assessed using SDS-PAGE (Laemmli, 1970) and SEC-HPLC. The wild-type and mutant proteins all appeared as a single band on a 15% polyacrylamide gel with a molecular mass of 27 kDa. The proteins eluted as a single symmetrical peak with a dimeric molecular mass of 55 kDa when using SEC-HPLC.

The protein concentration was determined spectrophotometrically using the molar extinction coefficient (ε) at 280 nm according to the method as described by Perkins, (1986). The molar extinction coefficient was calculated as follows:
ε (M^{-1} cm^{-1}) = 5550(# Trp residues) + 1340(# Tyr residues) + 150(# Cys residues). The wild-type, F51S and F221del proteins contain 2 tryptophan, 20 tyrosine and 2 cysteine residues per dimer. The dimeric protein concentrations were, therefore, estimated using a molar extinction coefficient of 38 200 M^{-1} cm^{-1} at 280 nm for the wild-type, F51S and

F221del proteins. Similarly, a molar extinction coefficient of 35 520 M^{-1} cm^{-1} was used for the Y8F hGSTA1-1 protein.

3.6 Steady-state enzyme kinetic studies

3.6.1 The standard CDNB/GSH assay

Steady-state enzyme kinetic studies for the wild-type and mutant enzymes were measured spectrophotometrically at 340 nm in assay buffer (0.1 M potassium phosphate buffer, pH 6.5, containing 1 mM EDTA and 0.02% sodium azide) (Habig and Jakoby, 1981). The standard assay was performed using final concentrations of 1 mM reduced glutathione (GSH) and 1 mM 1-chloro-2,4-dinitrobenzene (CDNB) in 3% (v/v) ethanol. Final protein concentrations were ~ 1.5 nM. All experiments were performed at $20^{O}C$ on a Hewlett Packard model 8452A-diode array spectrophotometer interfaced with a Vectra CS computer. All reactions were monitored over 60 seconds and the standard error between assays did not exceed 10%. The specific activities of the wild-type and mutant proteins were estimated using identical protein concentrations. A molar extinction coefficient of ε = 9600 M^{-1} cm^{-1} was used to calculate the amount of product, 1-(*S*-glutathionyl)-2,4-dinitrobenzene, formed at 340 nm. All enzymatic reaction rates were corrected for the corresponding non-enzymatic reaction rates.

3.6.2 Kinetic parameters (V_m, K_m) for the wild-type and F51S protein

In order to obtain a kinetic profile of the F51S protein it was necessary to modify the standard assay procedure. Reduced GSH was freshly prepared on a daily basis at a concentration of 0.5 M and pH adjusted to 6.5 prior to use in all assays. The stock concentration of CDNB was 60 mM prepared in absolute ethanol. The wild-type and F51S enzymes were assayed using identical protein concentrations in the presence of 1-150 mM GSH and 2 mM CDNB. The K_m towards GSH was determined from Michaelis-Menten plots. In the same way, the K_m towards CDNB was determined using 0.1-2 mM CDNB and 150 mM GSH. All non-enzymatic reaction rates were subtracted from the assays containing enzyme.

3.6.3 The peroxidase assay using cumene hydroperoxide

The peroxidase activities of the wild-type, F221del and Y8F enzymes were determined using cumene hydroperoxide as the substrate (Lawrence and Burk, 1976). Peroxidase activity was measured at 340 nm in an assay system containing 1 mM GSH, 0.2 mM NADPH, 1.2 enzyme units (E.U)/ml of glutathione reductase and 1.5 mM cumene hydroperoxide. The peroxidase assay buffer contained 50 mM potassium phosphate buffer, pH 7.0, containing 1 mM EDTA and 1 mM sodium azide. Stock solutions of 2 mM NADPH and 10 mM GSH were freshly prepared on a daily basis in peroxidase assay buffer. A stock solution of 15 mM cumene hydroperoxide was prepared in peroxidase assay buffer and stored at $4^{O}C$ until required. The molar extinction coefficient of NADPH at 340 nm is 6220 M^{-1} cm^{-1}. The reaction mixture contained 1 mM GSH, 0.2 mM NADPH, 1.2 E.U glutathione reductase and ~ 30 nM glutathione peroxidase (i.e., wild-type, F221del or Y8F hGSTA1-1) in peroxidase assay buffer. The above reaction mixture was incubated at $20^{O}C$ for 5 minutes. The reaction was initiated by the addition of 1.5 mM cumene hydroperoxide. The total reaction volume was 1 ml. The peroxidase activity was monitored at 340 nm for 5 minutes yielding linear progress curves. All non-enzymatic rates (i.e., glutathione peroxidase was replaced with distilled water) were subtracted from the reactions containing glutathione peroxidase.

3.7 Spectral analysis of wild-type and mutant proteins.

The spectroscopic signatures of wild-type and mutant proteins were measured at identical protein concentrations. Tryptophan residues were selectively excited at 295 nm. The intrinsic fluorescence emission spectra were measured using a Hitachi model 850-fluorescence spectrofluorimeter. The excitation and emission bandwidths were set at 5 nm and emission spectra were collected at a scan rate of 60 nm/minute.

The binding of the amphipathic ligand (i.e., ANS) to the wild-type, F51S and F221del proteins was monitored using fluorescence techniques. ANS (200 μM) was added to 1 μM protein. ANS was selectively excited at 390 nm and the emission spectrum recorded from 390 nm to 600 nm. The contribution of free ANS to the emission spectrum was subtracted from the protein/ANS complex emission spectrum. Free ANS in solution has a

wavelength emission maximum at 540 nm that is blue-shifted to 480 nm upon complex formation with exposed, structured hydrophobic surface area on the protein.

3.8 Determination of secondary structural content using far-UV circular dichroism

Circular dichroism (CD) is an excellent method for analysing the conformation of proteins and peptides in solution. CD is a spectroscopic method that depends on the fact that chromophores in an asymmetrical environment interact differently with right and left handed circularly polarised light. In proteins, the major optically active groups are the amide bonds, peptide backbone and the aromatic side chains (Woody, 1995; Greenfield, 1996; Kelly and Price, 1997). Secondary structural elements (α-helices) in protein molecules have distinctive CD spectra in the far-UV CD region (250-170 nm). α-helices display two negative bands at 222 nm and 208 nm and a stronger positive band at 190 nm.

The loss in secondary structural content for unfolding studies was monitored using a stopped-flow instrument from Applied Photophysics (SX-18MV) in CD mode. Far-UV CD ellipticity values at 222 nm were obtained from an average of 20 runs measured from 224 nm to 220 nm at 0.1 nm increments. Protein samples of 2 μM were used. The path length of the quartz cuvette was 2 mm. The buffer was 20 mM sodium phosphate buffer, pH 6.5 containing 0.1 M NaCl, 1 mM EDTA and 0.02% sodium azide.

Far-UV CD spectral analyses were also performed on 2 μM protein using a Jasco J-810 spectrapolarimeter with a 2 mm pathlength. The data are an average of 20 runs from 250 nm to 200 nm. The CD signal is represented as milli degrees (mdeg).

3.9 Determination of dissociation constants

The affinities of various ligands for the wild-type and mutant hGSTA1-1 proteins were determined by measuring the quenching of the intrinsic protein tryptophan fluorescence. Alternately, the binding affinity of ANS for the various proteins was studied using ANS fluorescence enhancement methods. 1 μM protein concentration in 20 mM sodium phosphate buffer, pH 6.5 containing 0.1 M NaCl, 1 mM EDTA and 0.02% sodium azide

was titrated with increasing concentration of ligand. The final dilution factor did not exceed 10% of the initial volume.

For fluorescence quenching techniques, the tryptophan residues were selectively excited at 295 nm and the wavelength emission was monitored at 325 nm. Because of increasing ligand concentrations during the experiment, it is possible that the higher ligand concentrations can result in a phenomenon known as the primary inner filter effect. The correction for the primary inner filter effect was performed according to Birdsall *et al*. (1983). The absorbance values were obtained at the excitation (295 nm) and emission (325 nm) wavelengths, respectively. First, corrections were made for the protein controls using the equation: $F_1 = F_{obs} - F_{control}$.

The observed fluorescence was also corrected for the contribution due to dilution effects: $F_2 = F_1 \text{ X } V_f/V_i$ where V_f and V_i represent the final and initial volumes, respectively. Correction for the primary absorption effects: $F_{corr} = F_2 \text{ X } 10^{(Aex+Aem)/2}$. The correction for inner filter effects can only be made when $A_{ex} + A_{em}$ is less than 0.2. The dissociation constant is estimated from a double reciprocal pot of $1/\Delta F = K_d/ [\Delta F_{max} (L)] + 1/\Delta F_{max}$, where ΔF is the corrected fluorescence intensity, ΔF_{max} represents the maximum fluorescence signal, [L] is the concentration of the ligand and K_d is the dissociation constant. A plot of $1/\Delta F$ versus 1/[L] yields a straight line with the intercept on the x-axis equal to $-1/K_d$.

3.10 Determination of Stern-Volmer (K_{sv}) constants using acrylamide quenching

Quenching of the proteins intrinsic tryptophan fluorescence by acrylamide was used to determine the exposure of W20. Tryptophan was selectively excited at 295 nm and the wavelength emission maximum was monitored at 325 nm in the presence and absence of acrylamide. Acrylamide (0-0.3 M) was added to 1 μM protein concentrations. The data was analysed according to the equation: $F_o/F = 1 + K_{sv} [Q]$, where F_o is the tryptophan fluorescence in the absence of acrylamide and F is the tryptophan fluorescence in the presence of increasing concentrations of added quenching agent [Q]. K_{sv} is the Stern-Volmer constant.

3.11 Anisotropy studies

Anisotropy decays were measured using a Hitachi model 850-fluorescence spectrofluorimeter with the supplied polarisation attachments. 1 μM protein concentrations were prepared for the native and denatured (i.e., 1 μM in 8 M urea) conformational states of the wild-type and F51S proteins. The excitation wavelength was set at 295 nm and the fluorescence emission wavelength was measured at 325 nm (folded protein) and 355 nm (denatured protein), respectively. The excitation and emission bandwidths were set at 10 nm each.

The anisotropy was calculated using the equations: $A = (I_{VV} – GI_{VH}) / (I_{VV} + 2GI_{VH})$ and $G = I_{HV}/I_{HH}$. G represents the correction factor for the differing efficiencies that the excitation and emission monochromators have for the horizontally and vertically polarised light. The terms I_{VV}, I_{VH}, I_{HV} and I_{HH} represent the fluorescence intensity measured when orienting the polarizers in a horizontal (H) or vertical (V) position Lacowicz, 1983).

3.12 Urea-induced equilibrium unfolding studies

3.12.1 Reversibility studies

The degree of reversibility is important when assessing the conformational stability of proteins using a chemically induced denaturation process. The reversibility of the unfolding event was monitored with all the proteins studied. Reversibility of the unfolding event implies that after chemically denaturing the native protein, the refolding reaction results in a 100% recovery of the native structure of the protein. A 10 μM protein concentration was denatured in 8 M urea and the renaturing of the unfolding reaction was allowed to occur by a 10-fold dilution of the denatured protein. The degree of reversibility was assessed by fluorescence spectroscopy and the results were compared to the native protein structure.

3.12.2 Protein-concentration dependence studies

The protein-concentration dependence of the stability of the proteins in this study was performed in the presence of 4.5 M urea which corresponds to the C_m-value within the

unfolding transition. The concentrations of protein used ranged from 0-5 μM. All experiments were performed in 20 mM sodium phosphate buffer, pH 6.5 containing 0.1 M NaCl, 1 mM EDTA and 0.02% sodium azide. The intrinsic tryptophan fluorescence properties of the protein were exploited by selectively exciting W20 at 295 nm and monitoring the emission wavelength maximum at 325 nm (folded conformation) and 355 nm (denatured conformation). Measuring the rayleigh scatter also monitored the presence or absence of aggregation. There was no evidence of aggregation in the range of protein concentrations used.

3.12.3 Data analysis

All equilibrium unfolding experiments were performed at room temperature in 20 mM sodium phosphate buffer, pH 6.5 containing 0.1 M NaCl, 1 mM EDTA and 0.02% sodium azide. The protein concentrations ranged from 1-2 μM. All the unfolding transition curves are characterised by a single sigmoidal transition that indicated the absence of any thermodynamically stable intermediates. This observation, therefore, allows the unfolding curves to be analysed according to a two-state model. In this model, only the folded and unfolded conformational states are assumed to exist in significant concentrations within the equilibrium unfolding transition region.

The measured fluorescence signal (y_{obs}) was converted to the fraction of the protein populated in the unfolded form (f_U). The fraction of the protein present in the folded (f_F) and unfolded (f_U) conformational states can, therefore, be represented as: $f_F + f_U = 1$. The observed property at any point is therefore: $y_{obs} = y_F f_F + y_U f_U$, where y_F and y_U are the values of the folded and unfolded conformational states of the protein, respectively. The values of y_F and y_U are calculated from the pre- and post-transition baselines observed in the equilibrium unfolding transition curve that are described by the straight line equation: $y_F = ax + c$ and $y_U = ax + c$. By combining the above information, we now arrive at: $f_U = (y_F - y_{obs})/(y_F - y_U)$, where y_{obs} is the observed property (i.e., the ratio of the tryptophan fluorescence intensity of the unfolded (355 nm) to folded (325 nm) protein.

The calculation of the equilibrium constant, K_u, at each point in the transition region for a dimeric protein was performed according to the method of Bowie and Sauer (1989).

K_u

Therefore, $N_2 \Leftrightarrow 2U$ and $K_u = [U]^2 / [N_2] = 2\ P_t\ [f_U^2/(1-f_U)]$, where P_t is the monomeric protein concentration and f_U is the fraction of unfolded protein.

The free energy change could be calculated by using the linear free energy model as described by Schellman (1978) and Pace *et al* (1986). The linear dependence of the Gibbs free energy on unfolding is described as: $\Delta G = -RTlnK_u$, where R is the universal gas constant (1.987 cal/mol/K or 8.314 J/mol/K) and T is the absolute temperature. If one assumes a linear dependence of Gibbs free energy of unfolding on the concentration of denaturant (urea) in the transition region then, $\Delta G = \Delta G(H_2O) - m$ [denaturant], where $\Delta G(H_2O)$ is the difference in Gibbs free energy between the unfolded and folded protein in the absence of denaturant and m represents the slope of the straight line that indicates the change in solvent-accessible surface of the protein as it unfolds.

3.13 The effect of reduced glutathione on the binding of ANS

Identical concentrations (1 μM) of wild-type and F51S proteins were pre-incubated for one hour with 100 μM ANS prior to addition of reduced glutathione (0-20 mM GSH, pH 6.5). The excitation and emission wavelengths were set at 390 nm and 475 nm, respectively. The bandwidths were set at 5.0 nm each. All fluorescence measurements were corrected for the contribution by free ANS in solution (i.e., 100 μM ANS in 20 mM sodium phosphate buffer, pH 6.5 containing 0.1 M NaCl, 1 mM EDTA and 0.02% sodium azide). The corrected ANS fluorescence at 475 nm was plotted versus the glutathione concentration.

3.14 The effect of urea on the binding of ANS to the wild-type and F221del proteins in the presence and absence of *p*-bromobenzylglutathione

Identical protein concentrations (1 μM) of wild-type and F221del in 20 mM sodium phosphate buffer, pH 6.5 containing 0.1 M NaCl, 1 mM EDTA and 0.02% sodium azide

were used. The excitation and emission wavelengths were set at 390 nm and 475 nm, respectively. The excitation and emission bandwidths were 5.0 nm each.

Protein (1 μM) was pre-incubated with 100 μM ANS at varying urea concentrations (0-5.5 M urea) in a final volume of 1 ml in the absence of the active site ligand (*p*-bromobenzylglutathione). The ratio of F/F_o was plotted versus the concentration of urea. F_o and F represent the ANS fluorescence at 475 nm in the absence and presence of urea, respectively.

In order to measure the effect of urea on ANS binding in the presence of the active site ligand, the protein (1 μM) was pre-incubated with 100 μM ANS and *p*-bromobenzylglutathione (100 μM) in the presence of urea (0-5.5 M). The ratio, F/F_o, was plotted versus urea concentration. F/F_o is the ANS fluorescence at 475 nm in the presence and absence of the active site ligand, respectively.

3.15 Thermodynamic studies using isothermal titration calorimetry

3.15.1 Isothermal titration calorimetry (ITC)

Calorimetric studies were conducted using a VP-ITC MicroCalorimeter from MicroCal Incorporated. Titration calorimetry is used to obtain a detailed thermodynamic profile of molecular associations. To date, it is the most sensitive and rigorous method available for the quantitative measurement of protein-ligand interactions. ITC is capable of directly measuring the heat evolved or absorbed during any molecular reaction. This technique, therefore, allows for the direct determination of the standard Gibbs free energy change, (ΔG^O), the binding constant (K_a), the enthalpy change (ΔH^O), the entropy change (ΔS^O) as well as the stoichiometry (N) of the binding interaction in one experiment. By performing identical experiments at different temperatures, it is possible to measure the heat capacity change (ΔC_p) of the protein-ligand binding reaction.

The standard Gibbs free energy change (ΔG^O) of a binding reaction is related to the equilibrium binding constant (K_a) using the equation: $\Delta G^O = -RT\ln K_a$, where R is the universal gas constant (1.987 cal/mol/K or 8.314 J/mol/K) and T is the absolute

temperature. The free energy change (ΔG^O) is associated with the enthalpy (ΔH^O) and entropy (ΔS^O) changes as follows: $\Delta G^O = \Delta H^O - T\Delta S^O$. In this way, ITC provides valuable information about the binding events of protein-ligand, antigen-antibody, enzyme-substrate or enzyme-inhibitor complexes as well as the binding of metal ions to proteins. In order to obtain meaningful ITC data it is extremely important to take special precautions with regard to experimental procedure.

3.15.1.1 Protein and ligand sample preparation

The preparation of ligand-free proteins for ITC studies was accomplished by removing any residual *S*-hexylglutathione that may have bound the proteins during the purification procedure. This was accomplished in three ways. Firstly, the protein (wild-type and Y8F hGSTA1-1) was eluted from the *S*-hexylglutathione affinity column using a high pH as described previously (Cameron *et al*., 1995). Secondly, the proteins were passed through a Sephadex-G25 column. Finally, extensive dialysis was carried out to ensure that the proteins were in the apo-form.

The protein samples were dialysed extensively at 4^OC against 20 mM sodium phosphate buffer, pH 6.5 containing 0.1 M NaCl, 1 mM EDTA, 1 mM TCEP and 0.02% sodium azide. SDS-PAGE and SEC-HPLC was used to assess the purity and homogeneity of the protein samples. Certificates of analyses from the suppliers indicated that the ligands used in this study were chemically pure. Therefore, no further purification of the ligands was attempted. All ligands were prepared in the final dialysate buffer.

3.15.1.2 Dialysis procedure

Proper dialysis is of fundamental importance in obtaining reliable ITC results. Dialysis tubing with a molecular weight cut-off of 3500 Da was used for protein dialysis. Typically, about 5 ml of protein was placed into the dialysis tubing and dialysed for a minimum of 6 hours with each change of dialysis buffers (three consecutive changes of dialysis buffer). The ligand samples were prepared with dialysate buffer from the final dialysis change.

3.15.1.3 Correction of protein concentration due to light scattering effects

The protein concentration was estimated spectrophotometrically at 280 nm using the extinction coefficients reported earlier (section 3.5). Corrections due to light scattering effects was taken into account according to the method suggested previously (Winder and Gent, 1971). A spectrum of the protein sample was obtained from 370 nm to 240 nm. The absorbance from 370 nm to 320 nm was measured at 2 nm or 5 nm intervals. Using this information, a plot of absorbance versus wavelength yielded straight line with the equation: $y = ax + c$, where a and c are obtained from the linear regression curve fit. By substituting $x = 280$ into the above equation, the value of y is obtained. This value represents the contribution due to the light scattering effects of the protein sample. Subtraction of the calculated y-value from the absorbance value at 280 nm of the protein sample yields a corrected A_{280} value. This value is, therefore, used to calculate the corrected protein concentration of the sample.

3.15.2 Thermodynamics of ligand binding to the active site of wild-type and Y8F hGSTA1-1

The wild-type and Y8F proteins were dialysed at $4^{O}C$ against 4 litres of buffer as described earlier. The active site ligands, GSH and GSO_3^-, were prepared at concentrations of 20 mM and 1.2 mM, respectively. Monomeric protein concentrations of ~ 0.10 mM wild-type and 0.08 mM Y8F hGSTA1-1 were used for the GSH binding study. The monomeric protein concentrations used in the GSO_3^- binding study were ~ 0.06 mM and 0.05 mM for the wild-type and Y8F hGSTA1-1 proteins, respectively.

In all the experiments performed, the ligand (GSH or GSO_3^-) was injected in 3 μl increments into the ITC sample cell containing the protein until complete saturation had occurred (~ 50-60 injections). The reference power was set to 25 μcal/sec and the initial delay was 60 seconds. The stirring speed was kept constant at 300 rpm and the spacing between injections was set to 260 seconds. In order to determine the heat capacity of the binding reaction, identical experiments were performed at different temperatures in the range of $5\text{-}25^{O}C$. To correct for heat of dilution effects, control experiments were performed by making identical injections of the ligand into buffer solution. The heat of

dilution was subtracted from the raw data thus obtaining the corrected heat of the interaction between the protein and the ligand. Alternately, the averaged heat of the post-saturation injections was subtracted from each injection. Due to uncertainty in the stoichiometry values during data analysis of the binding interaction between wild-type (and Y8F hGSTA1-1) protein and GSH, the stoichiometry was fixed at one and all the other parameters were allowed to float. The decision to fix the stoichiometry value at one was based on crystal structure evidence which shows that one molecule of GSH is bound per subunit. All data analysis was performed using the computer software package (ORIGIN) supplied with the VP-ITC calorimeter.

3.15.3 Thermodynamics of non-substrate ligand binding to wild-type hGSTA1-1

The wild-type protein concentration used in ANS binding studies was 0.06 mM monomer. The ligand was prepared in the dialysate buffer. The ANS concentration (3.6 mM) was measured spectrophotometrically prior to an ITC experiment using a molar extinction coefficient (at 350 nm) of ε = 18 490 M^{-1} cm^{-1}. An ANS absorbance spectrum was measured between 300 nm and 550 nm. Contribution due to light-scattering effects was measured from 550 nm to 455 nm and the ANS concentration was corrected as described earlier. Identical experiments were performed at different temperatures (5-25°C) in order to calculate the heat capacity change upon binding of ANS to the wild-type protein. During all ITC experiments, 3 µl injection volumes of ANS were added to the protein in the ITC sample cell. All other conditions were the same as described above. The raw data was corrected for heat of dilution effects as described above. All ITC data were fitted according to a model describing one set of binding sites.

The experimental conditions for BSP binding to the wild-type protein are identical to those described for the ANS binding experiments except that the BSP concentration was 3 mM. The corrected data for the BSP binding experiments were fitted to a model describing two sets of binding sites.

3.15.4 ITC data analysis

The raw data obtained from the calorimetric experiments were collected and integrated using the ORIGIN software. All data were corrected for the contribution due to heat of dilution effects. Where necessary, the baseline was adjusted manually before correcting the raw data. The integrated data all fit well to a single site binding model except the BSP binding interaction that was fitted to a binding model describing two sets of binding sites. The stoichiometry of binding of GSH to the wild-type (and Y8F hGSTA1-1) proteins did not accurately reflect the known stoichiometry (from crystal structure evidence) of GSH binding to the wild-type protein. Therefore, the stoichiometry for the wild-type and Y8F protein was fixed (independent parameter) at one (i.e., one molecule of GSH per monomer of dimeric protein). All the other parameters were allowed to float.

The most basic parameters that define a calorimetric titration are the concentrations of the interacting species (i.e., protein and ligand). The ideal protein concentration depends to a large extent on the binding constant of the reaction. The shape of the binding isotherm is described by the c-value. This is a unitless value that is obtained as follows: $c = [M] K_a$, where [M] is the protein concentration (units of M) and K_a is the binding constant with units of M^{-1}. The c-value for the binding interaction between GSH and wild-type as well as the Y8F protein was ~ 0.3. The recommended c-values range from 1-1000 (Wiseman *et al.*, 1989). Although the c-value is less than ideal, thermodynamic parameters can still be obtained. A direct result of a lowered c-value is the difficulty in determining the enthalpy of the binding interaction accurately. In order to increase the c-value, it is possible to use higher protein concentrations providing the protein can be obtained at sufficiently higher concentration without problems due to aggregation.

The c-value for the binding of GSO_3^- to the wild-type and Y8F proteins is ~ 6. This reflects the expected sigmoidal shape of the binding isotherm that reports more accurately on the enthalpy of the binding reaction. The slope of the linear dependence of the binding enthalpy of the reaction on temperature reflects the heat capacity change of the interaction.

3.16 Data analysis and molecular graphics

Unless otherwise stated, all data were fitted and analysed using the programme SigmaPlot for Windows Version 5.00 (Jandel Corporation). The three-dimensional structures of hGSTA1-1 were viewed using the molecular graphics packages, Rasmol (v 26) (Sayle, 1994), Molscript v 2.0 (Kraulis, 1991) and Swiss-PdbViewer (Guex and Peitsch, 1997).

CHAPTER 4

THE ROLE OF PHENYLALANINE 51 IN THE HYDROPHOBIC LOCK-AND-KEY INTERSUBUNIT MOTIF OF HUMAN GLUTATHIONE TRANSFERASE A1-1

4.1 The hydrophobic lock-and-key intersubunit motif of hGSTA1-1

The glutathione transferases exist as stable dimeric structures. Examination of the three-dimensional crystal structures indicates that the GSTs share a similar overall folding topology (Dirr *et al*., 1994b). Two major types of subunit interfaces are observed for the various gene classes. The first is the alpha/mu/pi/Sj26GST type and the second is the sigma/theta type. The subunit interfaces of the first type are represented by a curved topography and are hydrophobic with few polar interactions. The subunit interface is stabilised by the wedging of the hydrophobic side chain of phenylalanine (F51, alpha; F56, mu; F46, pi;) (Ji *et al*., 1995) from one monomer into a hydrophobic pocket in the other monomer. The hydrophobic pocket is formed by side chains of five residues belonging to α-helices 4 and 5 (M93, G97, A134, F135 and V138, alpha; I98, Q102, L136, Y137 and F140, mu; M89, G93, P126, F127 and L130, pi; M9, A97, M131, F32 and R135, *S.japonicum*) (Ji *et al*., 1995). This lock-and key motif physically anchors the two subunits together at either ends of the interface (Figure 1A). A noticeable difference between the squid class sigma and the class alpha GST is the absence of the "key" (phenylalanine) residue at the subunit interface of the class sigma GST (Figure 2). Two of the five "lock" residues in class sigma GST form electrostatic interactions rather than hydrophobic interactions across the dimer interface. The decrease in hydrophobic interactions is compensated for by the increase in electrostatic interactions and it is considered that the class sigma enzyme is more hydrophilic than that of the other classes.

Phenylalanine was replaced with serine at position 51 because the latter residue is found in the class sigma GSTs (Figure 1B and Figure2). Alanine was excluded as the residue of choice because we wanted to exclude any interaction between the hydrophobic side chain of alanine and the hydrophobic "lock". Therefore, by adding a slightly hydrophilic side

chain residue into the hydrophobic “lock” we would prevent any interaction between the serine residue side chain and the hydrophobic “lock”.

4.2 Physicochemical properties of the wild-type and F51S proteins

4.2.1 Identification of the F51S mutant plasmid DNA

Digestion of plasmid DNA with *Eco*R V yielded a linearised fragment of the pKHA1 plasmid DNA thus identifying the possible mutant plasmid DNA incorporating the F51S mutation. The wild-type DNA does not possess the *Eco*R V restriction site and would band as uncut DNA when digested with the diagnostic restriction enzyme. Figure 5 shows the identification of the possible mutant plasmid DNA incorporating the F51S mutation. Lane 9 indicates the banding pattern of the uncut, parental wild-type plasmid DNA. Lane 10 shows the linearised fragment that is generated when the wild-type plasmid DNA is restricted with *Pvu* II. In lane 12 the wild-type DNA was digested with *Sac* I to yield a linearised fragment as well. Lane 5 shows the uncut mutant DNA and lane 6 indicates the linearised fragment that is generated when the plasmid DNA is digested with *Eco*R V.

After the mutant plasmid DNA was identified, the presence of the F51S mutation was confirmed by DNA sequencing. The entire cDNA region of the hGSTA1-1 was sequenced for confirmation of the desired mutation and to ensure the absence of spurious mutations that could have resulted from the PCR amplification step. A segment of the cDNA sequence containing the diagnostic site (*Eco*R V) and the F51S codon change is indicated in Figure 6.

4.2.2 Over-expression and purification

Protein over-expression was achieved by inducing the *E.coli* cells with 0.5 mM IPTG. Although the variant protein was soluble it could not be purified using *S*-hexylglutathione affinity chromatography. The F51S protein was, therefore, purified by means of a CM-Sephadex cation exchange column. The purified mutant protein exhibited a subunit molecular mass of about 27 kDa (Figure 7). SEC-HPLC data (Figure 8) indicated that the

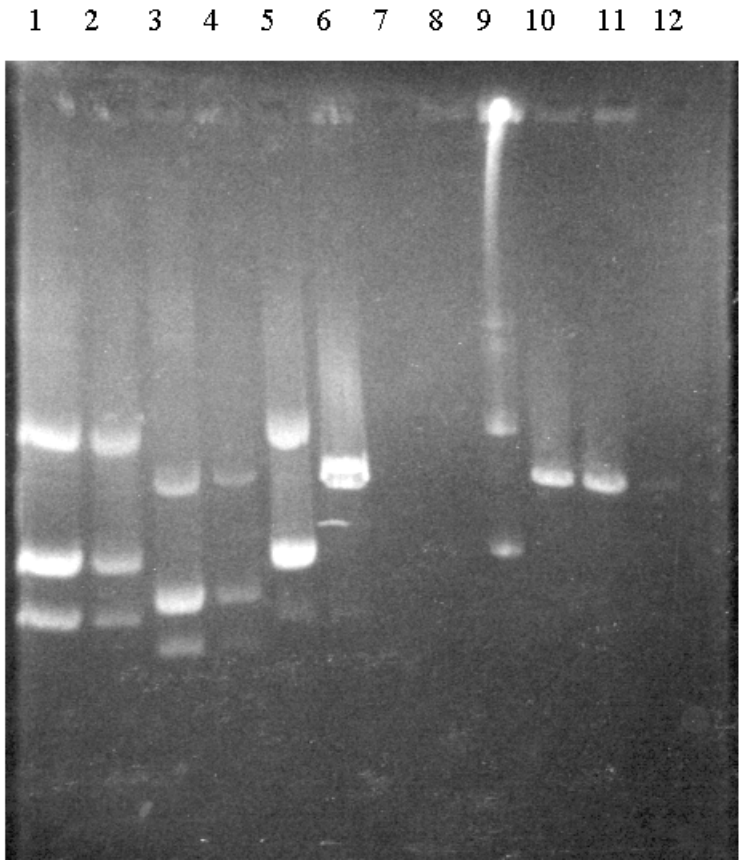

Figure 5. Identification of the F51S mutant plasmid DNA. Products were run on a 1% agarose gel containing ethidium bromide. Lanes 1, 3, and 5 represent uncut mutant plasmid DNA. Lane 9 is the uncut parental wild-type plasmid DNA. Lanes 2, 4, and 6 represent possible mutant plasmid DNA digested with *Eco*R V. Lanes 7 and 8 are empty. Lanes 10, 11 and 12 represent the linearised wild-type plasmid DNA digested with *Pvu* I, *Pvu* II and *Sac* I restriction enzymes, respectively.

A.

5′ GGA TAT TTG ATG TTC CAG CAA GTG CCA ATG 3′

↓ ↓

5′ GGA TAT CTG ATG TCC CAG CAA GTG CCA ATG 3′

B.

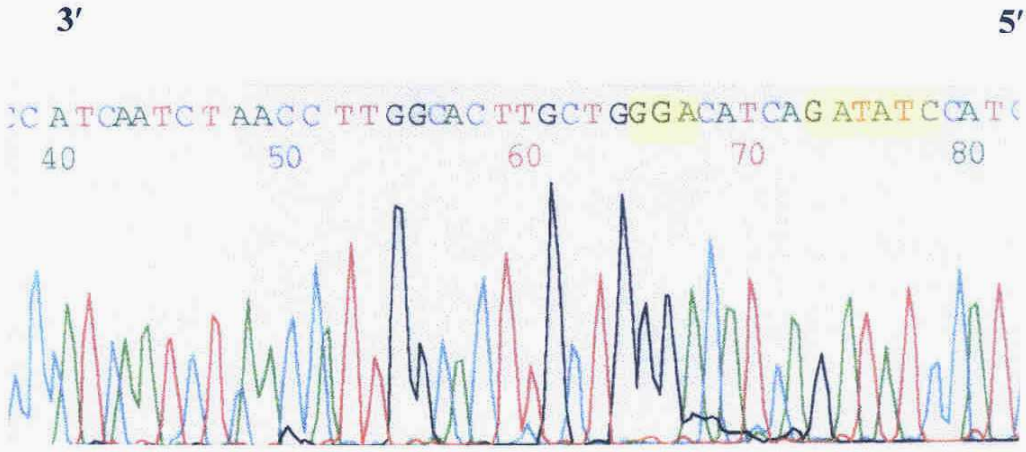

Figure 6. (A) A region of wild-type nucleotide sequence indicating the position of F51 (phenylalanine codon = **TTC**) that was selected for mutagenesis. The codon change for the F51S mutation is **TTC→TCC.** (B) A portion of the nucleotide sequence obtained from DNA sequencing of the F51S mutant plasmid DNA. The primer used for the sequencing reaction generated the 3′ to 5′ sequence of the strand shown in (A). Therefore, the mutation (F51S) is represented by the codon GGA. The presence of the *EcoR* V site (GATATC) and F51S mutation are shaded in yellow.

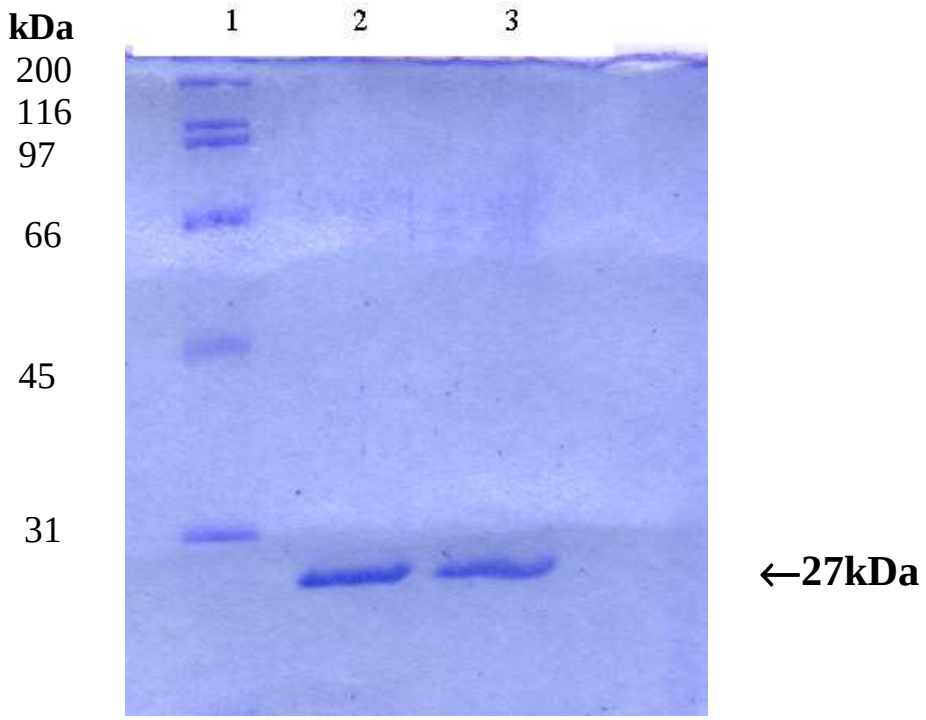

Figure 7. SDS-PAGE gel showing the subunit molecular mass of F51S mutant protein purified using CM-Sephadex cation exchange chromatography. Lane 1: molecular mass markers, lane 2: F51S mutant protein and lane 3: wild-type hGSTA1-1.

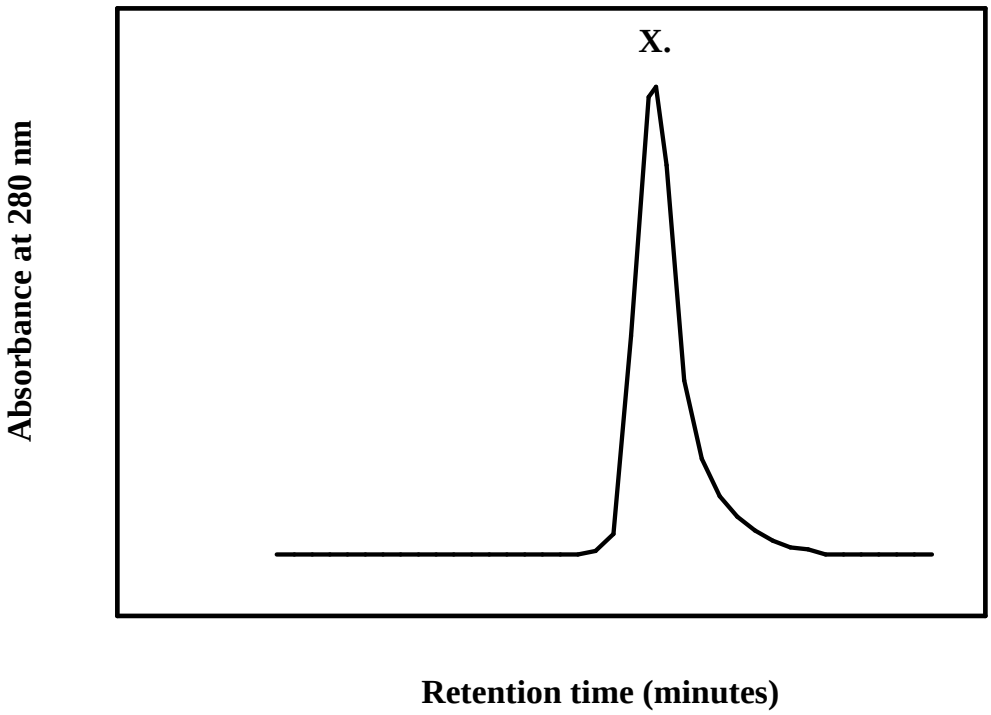

Figure 8. SEC-HPLC elution profile for the purified F51S hGSTA1-1. X in the figure denotes the position of the F51S protein.

hydrodynamic of the mutant remained unchanged and that the homodimeric molecular mass was about 55 kDa.

4.2.3 Fluorescence spectral properties of wild-type and F51S hGSTA1-1

Spectroscopic characterisation of the wild-type and F51S mutant protein was carried out by selectively exciting the lone tryptophan residue at 295 nm. The wavelength emission maximum (325 nm) of the native conformation (absence of urea) of the wild-type and F51S protein was identical (Figure 9A). Since there is no change in the wavelength emission maximum of the F51S variant when compared to the wild-type protein, it can be deduced that the environment of the lone tryptophan residue is not affected by the mutation. The F51S variant, however, does display a decrease in fluorescence intensity when compared to the wild-type protein. This decrease in quantum yield may be because of the tryptophan residue in close proximity to a quenching residue or that it may be located in a slightly more quenching environment. When both proteins are exposed to 8 M urea the emission maximum is red-shifted to 355 nm indicating that both proteins exist in the unfolded conformation (Figure 9B).

4.2.4 Far-UV circular dichroism of wild-type and F51S hGSTA1-1

The F51S variant was characterised with regards to the wild-type hGSTA1-1 protein using circular dichroism as a probe. The secondary structural content of the F51S protein was assessed using far-UV CD (250-218 nm). Normalised protein concentrations (2 μM) for both proteins exhibited two troughs at 222 nm and 208 nm, which are typical of a protein containing alpha-helical content. The results (Figure 10) of the far-UV CD spectra indicated that the alpha-helical content of the F51S variant did not differ significantly from the wild-type protein. The far-UV CD spectra, therefore, indicated that the mutation did not adversely affect the secondary structural content of the F51S variant protein; i.e., the mutation did not induce gross conformational changes in the F51S protein.

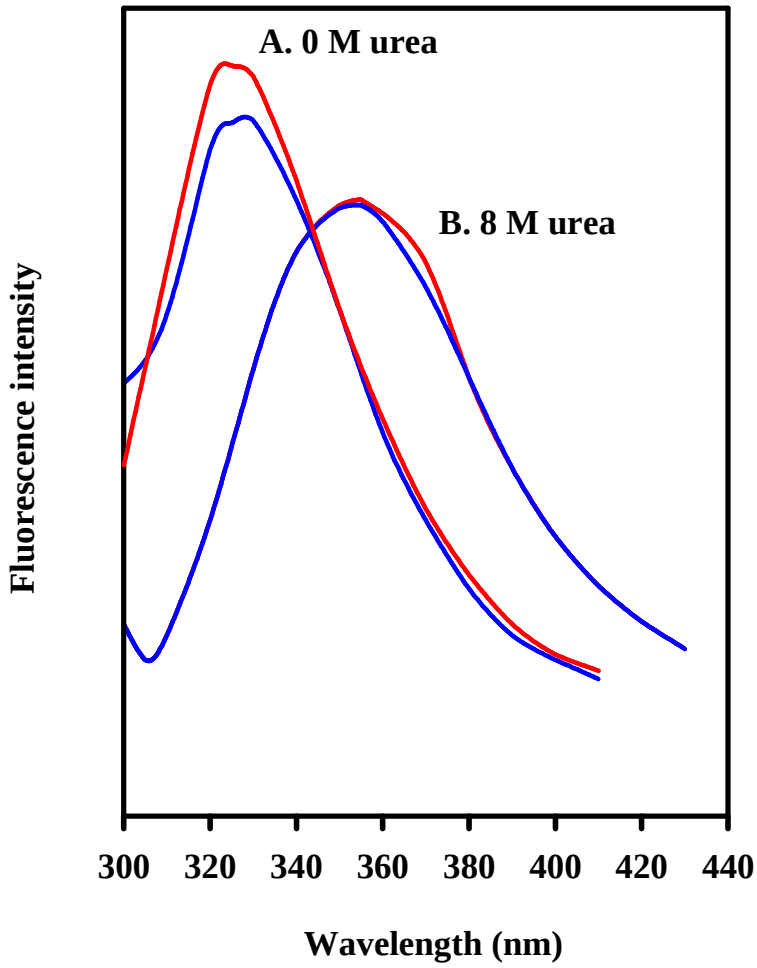

Figure 9. Spectral characterisation of the wild-type and F51S hGSTA1-1 proteins. Solid red and blue lines indicate the wild-type and F51S proteins, respectively. The lone tryptophan was selectively excited at 295 nm and the wavelength emission was monitored. (A) Represents the wavelength emission maximum at 325 nm for the native wild-type and F51S proteins, respectively. (B) represents the wavelength emission maximum at 355 nm for the unfolded wild-type and F51S proteins, respectively.

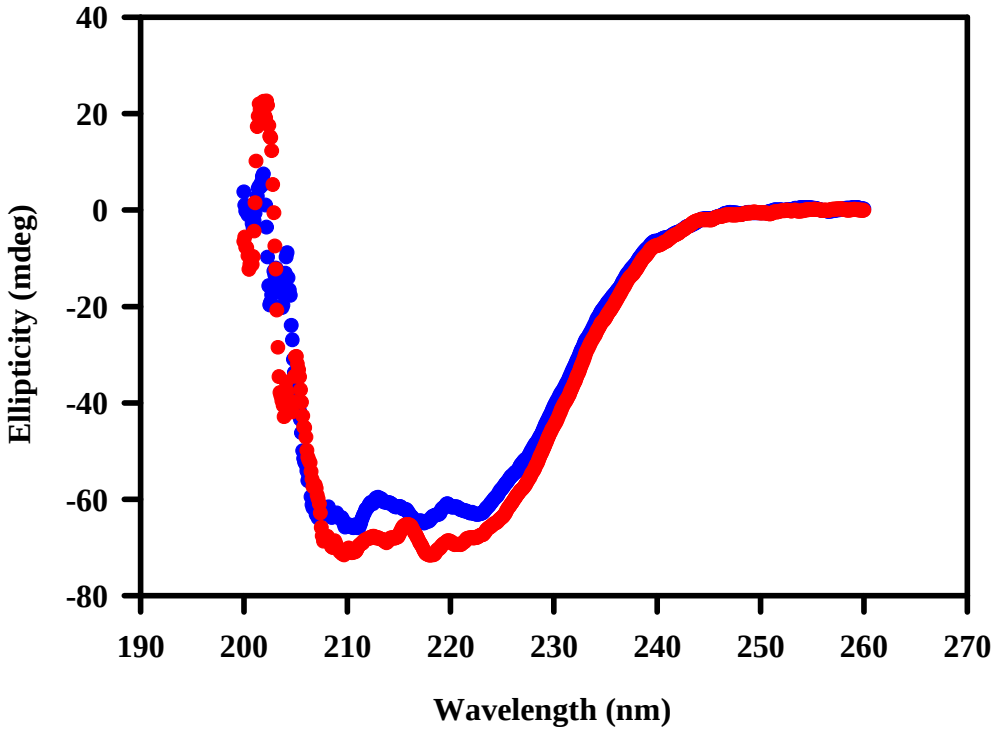

Figure 10. The far-UV circular dichroism spectra of wild-type and F51S hGSTA1-1. The spectra shown in blue and red are for the native wild-type and F51S proteins, respectively. The conditions were 2 μM of each protein in 20 mM sodium phosphate buffer, pH 6.5 containing 0.1 M NaCl. The above spectra represent an average of 16 runs for each protein.

4.2.5 Steady-state kinetic properties of the wild-type and F51S proteins

Steady-state kinetic parameters (V_m, K_m) towards glutathione (GSH) and CDNB were determined for the wild-type and mutant enzymes. The results are listed in Table 2. Using the standard enzyme assay, the mutant enzyme displays only 3% of the wild-type specific activity. The F51S mutant has K_m values for GSH and CDNB that are ~ 54-fold and 4-fold greater than the wild-type protein, respectively. This implies a reduced binding affinity for GSH and CDNB in the F51S mutant. These results are evidence of a structurally compromised active site in the F51S protein. Evidence of a structurally compromised active site was also supported by the fact that the mutant protein could not be purified using *S*-hexylglutathione affinity chromatography.

4.2.6 Dissociation constants for the non-substrate ligands ANS, BSP and *p*-bromobenzylglutathione

The binding affinities of the non-substrate ligands ANS, BSP and *p*-bromobenzylglutathione were assessed using fluorescence quenching techniques. The results are summarised in Table 3. ANS is an anionic dye that binds at/near the dimer interface of hGSTA1-1 (Sluis-Cremer *et al.*, 1996; Sluis-Cremer *et al.*, 1998). The F51S protein binds ANS approximately three times tighter than the wild-type protein. The binding of BSP to the wild-type protein is approximately two-fold stronger than when it binds to the F51S protein. The binding of the glutathione analogue *p*-bromobenzylglutathione is almost identical in both proteins.

4.2.7 ANS binding to the wild-type and F51S proteins

Fluorescence emission spectra of ANS binding to the wild-type and F51S proteins are shown in Figure 11. The spectra indicate enhanced ANS fluorescence intensity of the F51S protein when compared to the wild-type protein. The wavelength emission maxima are 473 nm and 480 nm for the F51S and wild-type proteins, respectively. The blue-shift in the emission maximum from 480 nm (wild-type) to 473 nm (F51S) indicates that the anionic dye is bound to a more hydrophobic surface in the mutant protein.

Table 2. Kinetic parameters for the wild-type and F51S proteins. See section 3.6.2 in Experimental Procedures for conditions used.

	Enzyme:	
	Wild-type	**F51S**
Specific activity (μmol/min/mg):		
CDNB	48.5	1.3
Varied CDNB concentration:		
K_m (mM)	0.44	1.60
V_{max} (μmol/min)	0.15	0.10
Varied GSH concentration:		
K_m (mM)	1.6	70
V_{max} (μmol/min)	0.13	0.14

Table 3. Binding affinities of non-substrate ligands for wild-type and F51S hGSTA1-1 proteins as determined by fluorescence methods. See section 3.9 in Experimental Procedures for method and conditions used.

	Dissociation constant (Kd)(μM)	
Ligand	**Wild-type**	**F51S**
ANS	55.1	18.7
BSP	25.1	47.3
***p*-bromobenzylglutathione**	19.1	22.7

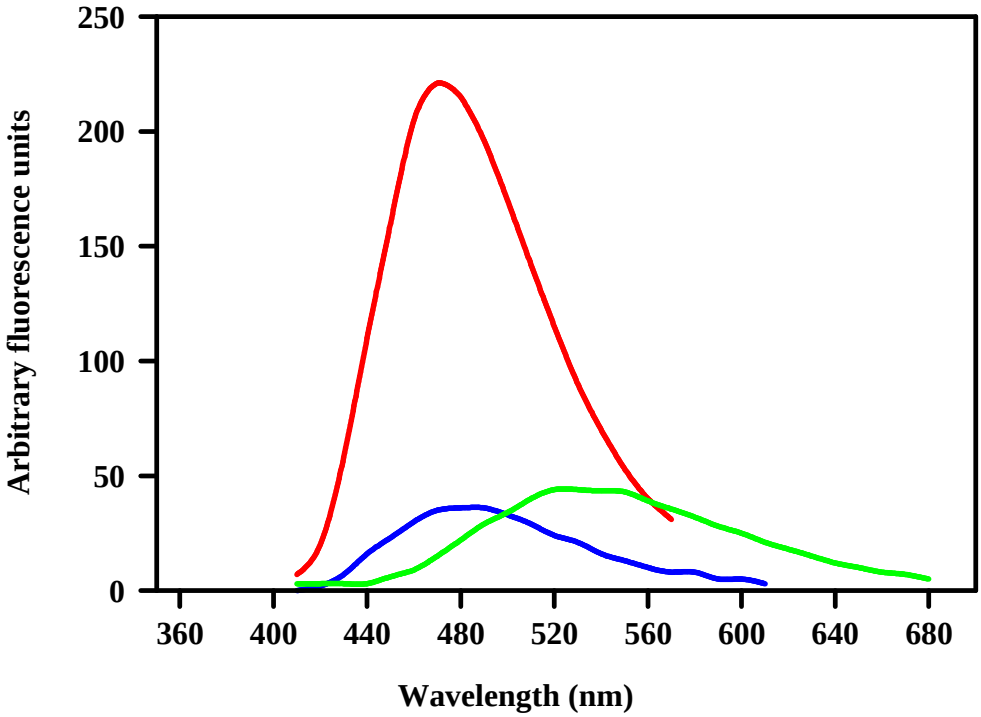

Figure 11. Emission spectra of ANS binding to the wild-type and F51S proteins. 200 μM ANS was added to 1 μM wild-type and F51S protein concentrations. ANS was selectively excited at 390 nm and the emission spectrum read from 400 nm. The spectra of ANS binding to the wild-type and F51S proteins are indicated by the solid blue and red lines, respectively. The above spectra were corrected for the contribution due to free unbound ANS in buffer (solid green line).

4.2.8 The effect of glutathione on the binding of ANS

The addition of glutathione (100 mM) results in a decreased ANS fluorescence intensity for the mutant protein (Figure 12). Although the fluorescence intensity was reduced, there was no change in the emission maximum at 473 nm. The wild-protein, however, exhibited an increase in the ANS fluorescence emission maximum (Figure 12) as well as a blue-shift in the emission wavelength from 480 nm to 475 nm.

4.2.9 Acrylamide quenching of W20 at the domain-domain interface

The ability of acrylamide to quench W20 fluorescence is a useful way of determining the exposure of W20 to the solvent. Stern-Volmer plots at low acrylamide concentrations (0-0.3 M) yielded linear plots with K_{sv} values of 2.1 M^{-1} ($r^2 = 0.998$) and 3.1 M^{-1} ($r^2 = 0.997$) for the wild-type and F51S proteins, respectively (Figure 13). The K_{sv} values obtained indicated a similar exposure of W20 to solvent for the wild-type and F51S proteins.

4.2.10 Steady-state anisotropy studies

Steady-state anisotropy studies are useful in determining the mobility of the W20 residues at the domain-domain interface. Anisotropy values of 0.10 and 0.11 were obtained for the F51S and wild-type protein, respectively. This study, therefore, indicated similar mobilities for W20 in the F51S and wild-type proteins.

4.3 Urea-induced equilibrium unfolding of the wild-type and F51S proteins

4.3.1 Reversibility studies

Fluorescence spectroscopy was employed as a structural probe to determine the reversibility of the urea-induced equilibrium unfolding reaction. A ten-fold dilution of the unfolded protein was allowed to refold. The refolded protein exhibited an emission maximum at 325 nm. The fluorescence intensity of the refolded sample was similar to that of the native sample. The F51S protein yielded > 95% reversibility as monitored by W20 fluorescence. Due to the low specific activity of the F51S protein, it was not possible to use enzyme activity as a functional probe. No evidence of aggregation was observed. A high refolding recovery is essential for the characterisation of the

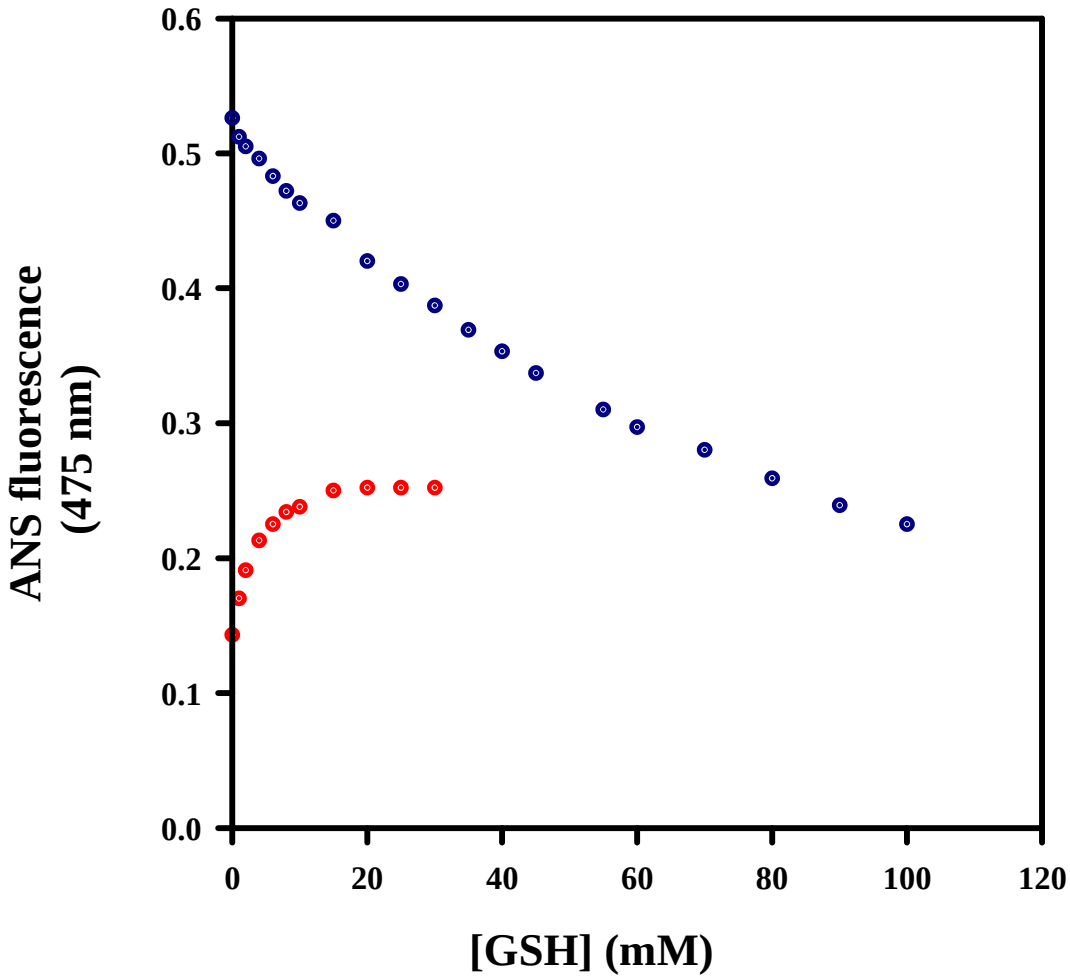

Figure 12. The effect of glutathione on the binding of the anionic ligand, ANS, to the wild-type (filled red circles) and F51S (filled blue circles) hGSTA1-1 proteins. ANS was selectively excited at 390 nm and the wavelength emission maximum was monitored at 475 nm.

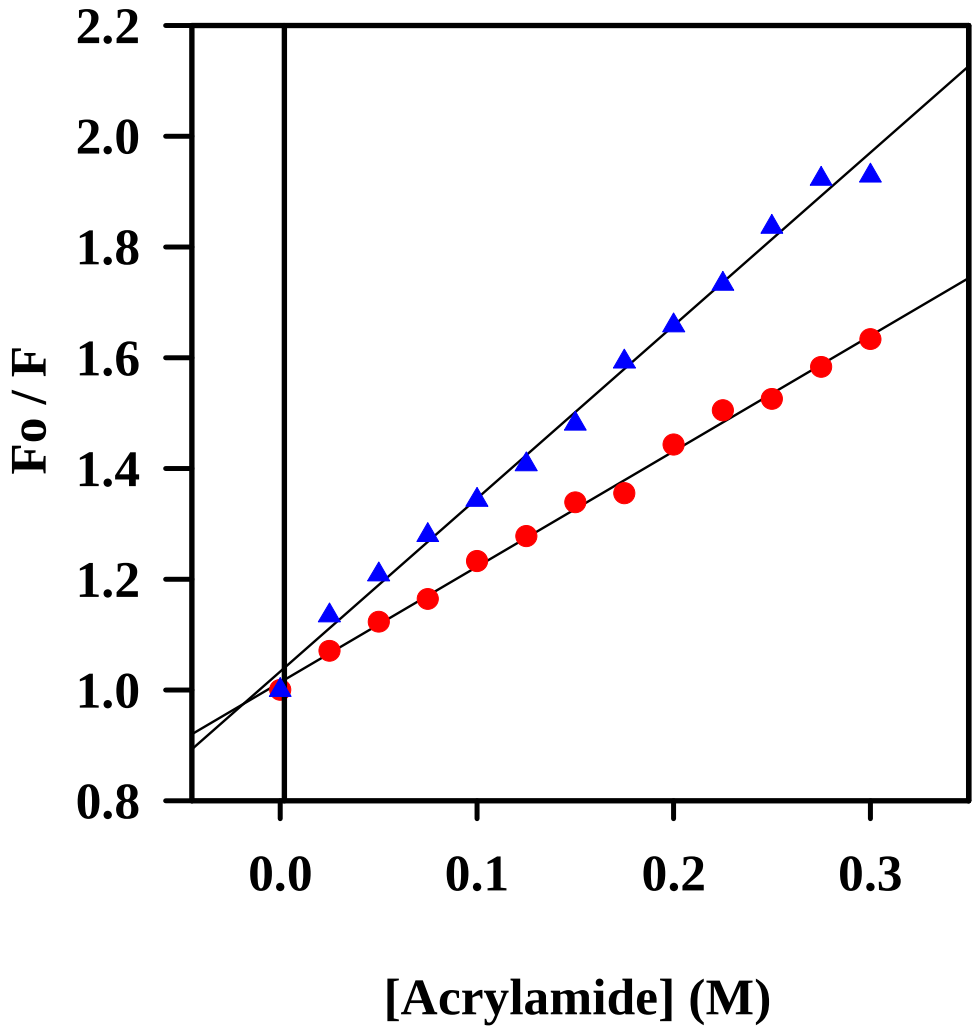

Figure 13. Stern-Volmer plots for the quenching of intrinsic tryptophan 20 fluorescence. The wild-type and F51S proteins are represented as filled blue triangles and filled red circles, respectively. F_o and F are the fluorescence intensities in the absence and the presence of acrylamide, respectively.

equilibrium unfolding transition. High recoveries have also been reported for other classes of cytosolic GSTs (Dirr and Reinemer, 1991; Erhardt and Dirr, 1995; Kaplan *et al*., 1997; Wallace *et al*., 1998a, 1998b).

Far-UV CD unfolding of the F51S mutant in the presence of urea was monitored by measuring the ellipticity at 222 nm at varying urea concentrations (Figure 14). Fluorescence (monitored at 325 nm) and far-UV CD (at 222 nm) data indicated that there was a simultaneous loss in tertiary and secondary structural content as the protein unfolds in the presence of urea (Figure 14).

4.3.2 Protein-concentration dependence of the unfolding transition

In order to establish whether an unfolding process is two-state, one has to determine if the unfolding transition is protein-concentration dependent (Bowie and Sauer, 1989; Neet and Timm, 1994). The urea-induced equilibrium unfolding transitions of the wild-type and F51S proteins show a single sigmoidal transition curve using W20 fluorescence as a structural probe. The C_m-value is understood to represent the midpoint of the equilibrium unfolding transition region. Therefore, at this denaturant concentration 50% of the protein molecules are in the native state and 50% are in the unfolded/denatured state. In this way, the C_m-value was determined to be 4.5 M and 4.1 M urea for the wild-type and F51S proteins, respectively. By varying the mutant protein concentration at a fixed C_m-value (4.1 M urea), it is observed that there is an increase in protein stability with increasing protein concentration (Figure 15). This result is in agreement with a two-state model and can be described as a bimolecular refolding and assembly reaction. It is now possible to estimate the conformational stability parameters. One may describe the equilibrium unfolding reaction of a dimeric protein using one of two models. The models are based on the relative stability of the native folded dimer (N_2), the native-like dimer (M) (or intermediate) and unfolded monomer (U).

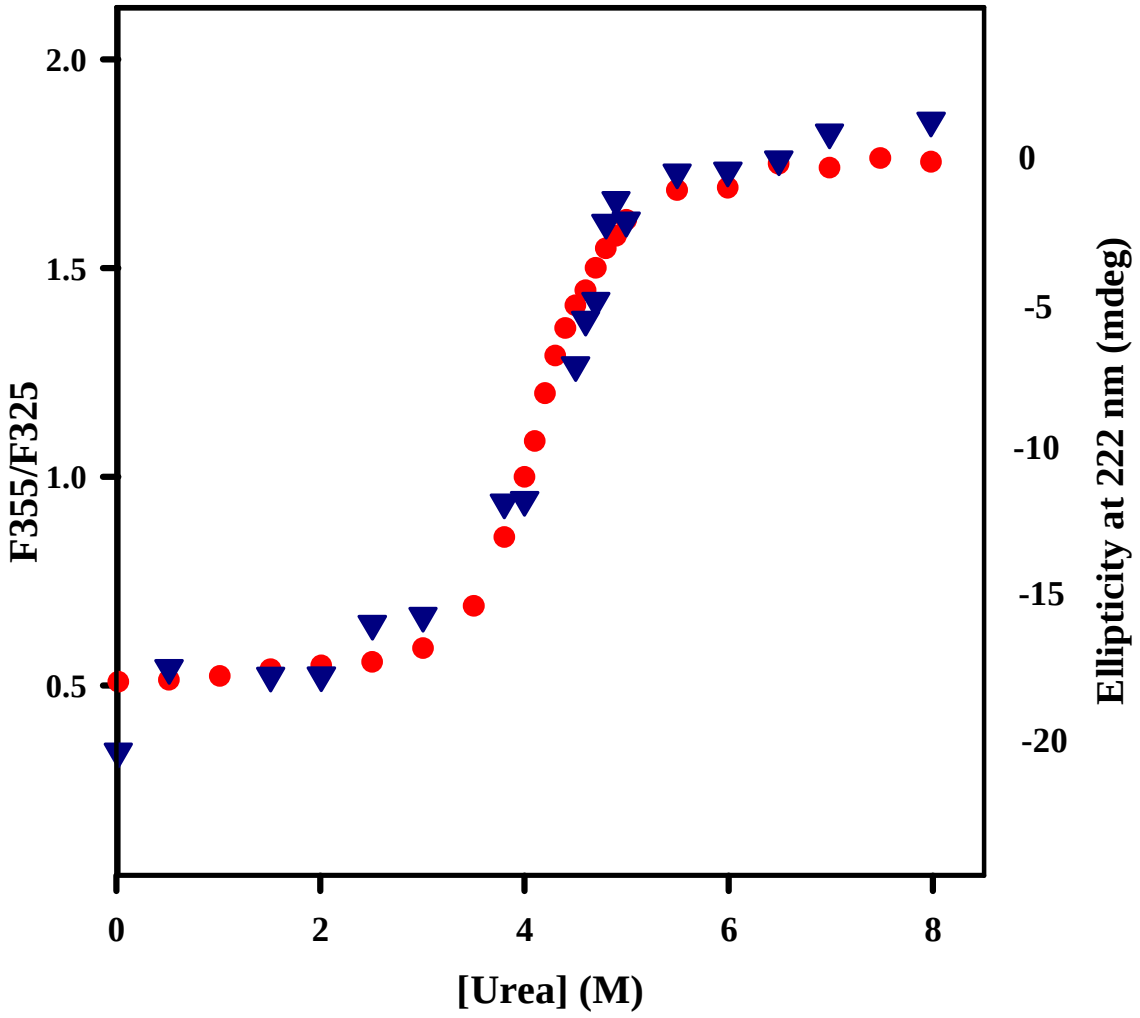

Figure 14. Fluorescence and far-UV circular dichroism unfolding of F51S hGSTA1-1 in the presence of urea. 2 µM protein concentration was incubated at various urea concentrations and fluorescence measurements were made at 325 nm (folded, native conformation) and 355 nm (denatured conformation) (wavelength excitation at 295 nm). The ellipticity at 222 nm was measured as a function of urea concentration.

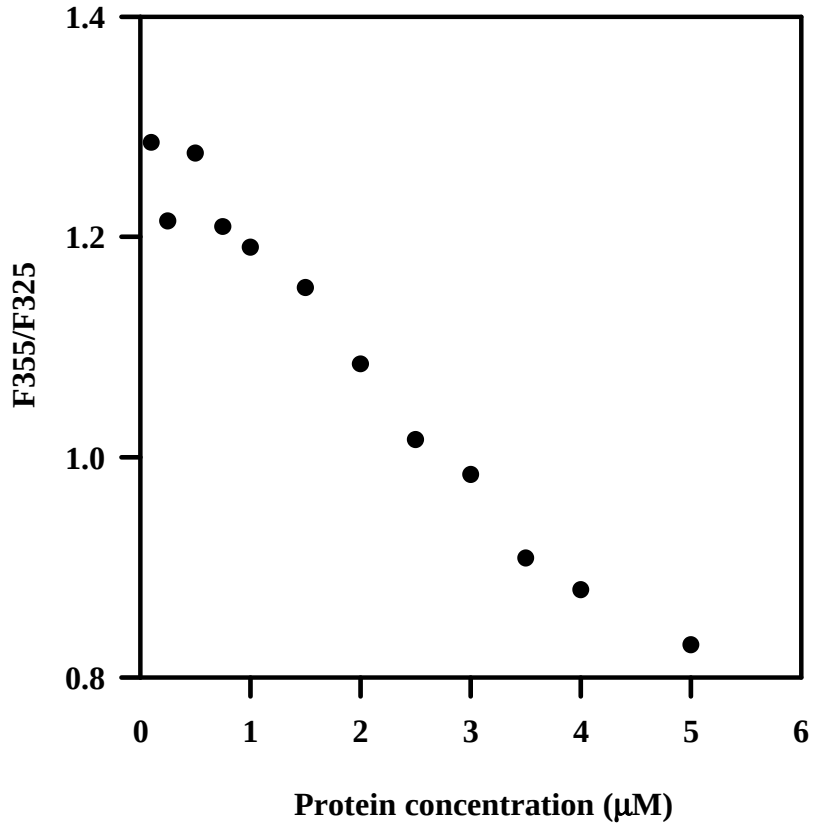

Figure 15. Protein-concentration dependence of the stability of the F51S protein. Various concentrations of F51S protein were incubated in 4.1 M urea (the C_m-value for 2 μM F51S mutant protein). The fluorescence intensity was measured at 325 nm (folded protein) and 355 nm (unfolded protein) (excitation wavelength = 295 nm). The ratio of F355/F325 represents the ratio of unfolded to folded protein.

The first model describes a three-state pathway for the unfolding and dissociation of the native dimer into two structured native-like monomers before unfolding completely to yield two unfolded monomers:

$$N_2 \overset{K_1}{\Leftrightarrow} 2M \overset{K_2}{\Leftrightarrow} 2U$$

where $K_1 = [M]^2 / [N_2]$ and $K_2 = [U] / [M]$. The equilibrium constants K_1 and K_2 refer to the bimolecular and unimolecular reactions, respectively.

The second model describes the native folded dimer and the unfolded monomer. Only these two species are significantly populated at equilibrium:

$$N_2 \overset{K_1}{\Leftrightarrow} 2U$$

where $K_1 = [U]^2/[N_2]$. Here, K_1 represents the equilibrium constant for the bimolecular reaction of the dimeric protein. Therefore, inspection of the above models reveals that only K_1 for the dimeric protein is able to describe a reaction that is protein-concentration dependent (i.e., a bimolecular reaction).

4.3.3 Analysis of the equilibrium unfolding transition and interpretation of $\Delta G(H_2O)$ and *m*-value

The urea-induced equilibrium unfolding of the wild-type and F51S proteins were monitored using the proteins intrinsic tryptophan fluorescence as a structural probe (Figure 16). Data fitting was performed according to a two-state model and the free

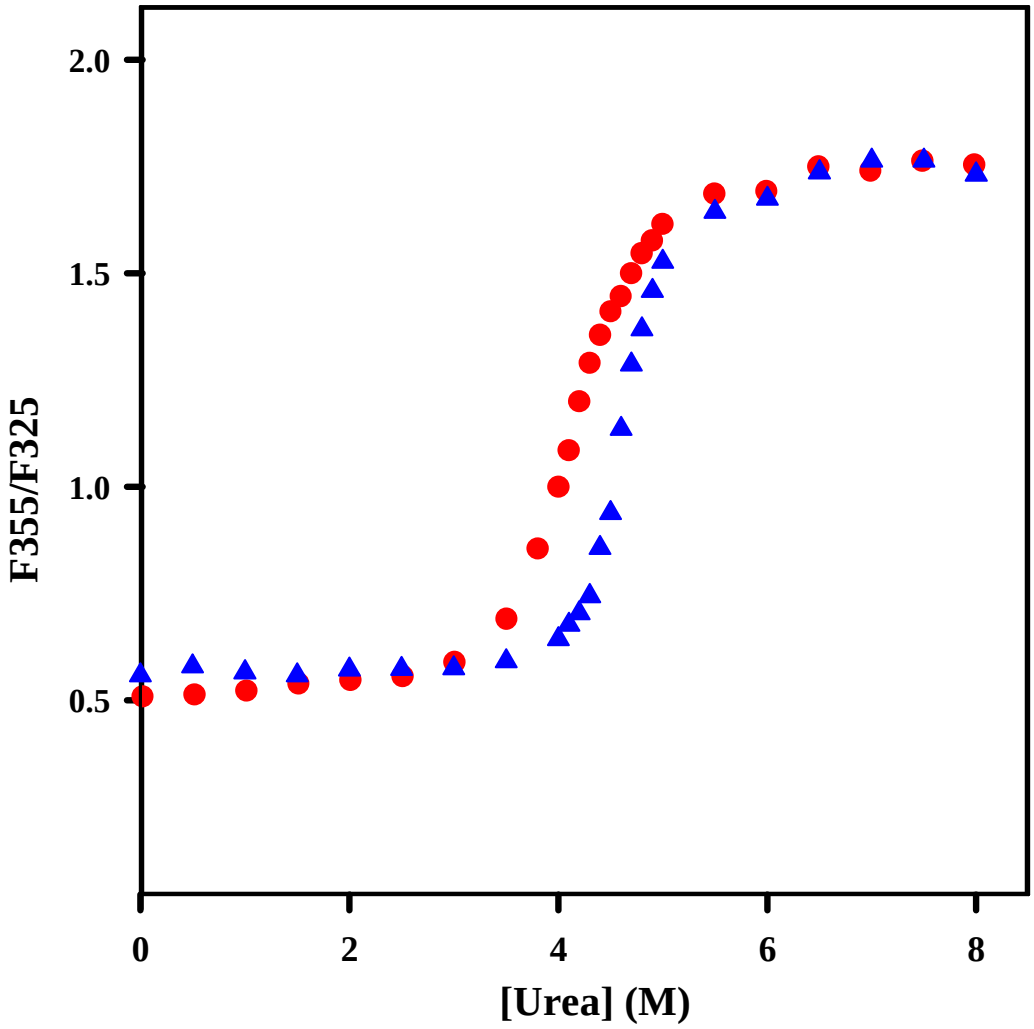

Figure 16. Urea-induced equilibrium unfolding of wild-type and F51S hGSTA1-1. The conformational stability of each protein was determined by monitoring the change in W20 fluorescence in the presence of urea. 2 μM protein concentration was used. The unfolding curves of the wild-type and F51S proteins are shown as filled blue triangles and filled red circles, respectively. The ratio of F355/F325 represents the ratio of unfolded to folded protein, respectively.

energy change in the absence of denaturant ($\Delta G(H_2O)$) was estimated according to the linear extrapolation method of Pace *et al*., (1989). In this way, the relative conformational stability of the wild-type and F51S proteins could be compared. Fitting of the experimental data yielded a $\Delta G(H_2O)$ of 16.8 kcal/mol for the F51S protein. This is significantly different from the wild-type value of 27.5 kcal/mol.

The *m*-value is related to the difference in solvent-accessible surface between the unfolded and native states (Soulages, 1998). This value is also indicative of the co-operativity of the non-covalent interactions required to maintain the native state. It is proportional to the amount of additional surface area exposed upon denaturation, $\Delta A = A_U - A_N$ where ΔA is the amount of additional surface area, A_U is the surface area exposed in the denatured state and A_N is the surface area exposed in the native state (Schellman, 1978). Apart from the difference in conformational stability between the wild-type and F51S proteins, the mutant protein also exhibited a much broader unfolding transition (indicated by *m*-values) when compared to the wild-type protein. The *m*-value was 4.2 kcal/mol/M and 2.1 kcal/mol/M for wild-type and F51S proteins, respectively. A reduced *m*-value value can be interpreted in different ways. Firstly, it may represent differences in the exposed surface area of the native or denatured state. It may also describe a significant decrease in the responsiveness to the denaturant of the reaction to proceed to equilibrium between folded dimer and unfolded monomer (Shortle, 1995; 1996). Secondly, a reduced *m*-value may explain a deviation from two-state behaviour. A reduced *m*-value would be observed if an intermediate state with significantly high conformational stability was present in the unfolding transition. In this case, the unfolding transition would be broader and a lowered *m*-value would be observed. Thirdly, the *m*-value reflects the changes in the interactions of the denaturant with the protein molecules in the denatured state (Arakawa and Timasheff, 1984).

ANS binding to the native wild-type and F51S proteins indicate enhanced exposure of hydrophobic surface area in the F51S protein. Therefore, it is possible that the initial state of the mutant protein prior to unfolding has a larger solvent-accessible surface area than

the wild-type protein. The protein-concentration dependence of the unfolding data suggests the presence of (a) highly populated dimeric state(s) in equilibrium with unfolded monomer within the urea unfolding transition. In the class alpha GST, there have been no reports of stable structured monomeric intermediates although there is evidence of the existence of a transient dimeric unfolding intermediate (Wallace *et al*., 1998b) as well as transient native-like monomeric folding intermediates (Wallace and Dirr, 1999). Stable structured monomeric intermediates have been detected in the GSTs from *Proteus mirabilis* (Sacchetta *et al*., 1993). It has also recently been shown that stable monomeric intermediates exist in the unfolding pathway of the rat class mu isoenzymes (rGSTM1-1 and rGSTM2-2) (Hornby *et al*., 2000). A study of the squid GSTS1-1 indicated the presence of both monomeric and dimeric intermediates (Stevens *et al*., 1998). However, GSTs from the class alpha, pi and Sj26GST are all consistent with the existence of a highly co-operative, concerted two-state equilibrium unfolding model (Wallace *et al*., 1998b; Erhardt and Dirr, 1995; Kaplan *et al*., 1997).

4.4 Discussion

Studies using mammalian GSTs (Dirr and Reinemer, 1991; Erhardt and Dirr, 1995; Wallace *et al*, 1998a, 1998b) and GST from the parasite *Schistosoma japonicum* (Kaplan *et al*., 1997) showed that intersubunit interactions constitute a major source of stabilisation not only for subunit association but also for the tertiary structures of the individual subunits.

In this study, the lock-and-key motif residue in human GSTA1-1, phenylalanine 51 was replaced with serine. The results demonstrated that the F51S protein is dimeric indicating that phenylalanine at the subunit interface is not essential for dimerisation to occur. The evolutionary precursors of the class alpha GST, class sigma and theta, which lack this structural motif also form functional dimers (Armstrong, 1997). The replacement of phenylalanine with serine did not appear to induce any gross structural changes in the secondary structure of the protein. No changes are observed at the domain I-domain II

interface (i.e., environment of W20). This residue serves as a sensitive reporter for any changes that occur at the domain interface within the subunit.

The F51S mutation did, however, affect the functioning of the protein. Although the core structure of the protein remained unaffected, tertiary structural changes have occurred at/near the active site of the protein. The mutation also affected the non-substrate ligand-binding site of the protein. The fact that the F51S protein bound the *S*-hexylglutathione affinity column very weakly was further evidence of a structurally compromised active site. Kinetics data indicated that both the G- and H-sites were affected by the mutation; the G-site being disrupted to a greater extent than the H-site. F51 is located on a loop connecting α-helix 2 and β-strand 3 of domain I. Both secondary structural moieties as well as the elements of the loop form part of the G-site. Arg44 in α-helix 2 forms a salt bridge with the glycine moiety of reduced glutathione and a pair of antiparallel β-strand hydrogen bonds from between the backbone of glutathione and its cysteinyl moiety and the protein backbone at Val54 (Sinning *et al*, 1993). Val54 precedes an invariant *cis*-Pro55 motif at the N-terminus of β-strand 3. Helix 2 makes tertiary contacts with helix 9 located at the C-terminus of the A1 polypeptide (Sinning *et al*., 1993; Cameron *et al*., 1995). Helix 9 is a unique dynamic structural motif observed in the class alpha GST and forms part of the H-site for electrophilic substrates (Board *et al*., 1991). A similar mutation in the class mu enzyme (M1-1) indicated that the function of the enzyme has been compromised despite the absence helix 9 at the C-terminus of the enzyme (J. Hornby, unpublished data). Therefore, it appears that the F51S mutation in hGSTA1-1 affects the functioning of the enzyme by disordering the β3 strand leading to *cis*Pro55 thereby disrupting the active site of the enzyme.

F51 at the subunit interface also impacts on the binding of the non-substrate ligand ANS. This anionic dye binds an amphipathic region at the dimer interface (Sluis-Cremer *et al*., 1996) that is similar to that of aflatoxin B1 (Sluis-Cremer *et al*., 1998), β-estradiol disulfate (Barycki and Colman, 1997) and AEDANS (Wallace *et al*., 1998b; Sluis-Cremer *et al*., 1998). In the wild-type protein, the binding of the physiological substrate

(glutathione) to the G-site, enhances the binding of ANS (Figure 12). The binding sites for these ligands, therefore, do not overlap. This result is similar to that seen elsewhere (Dirr and Wallace, 1999). This enhanced binding effect is attributed to a glutathione-induced immobilisation of helix 9 onto domain I allowing the C-terminus of the GSTA1 polypeptide to contribute toward the ligandin site for ANS (Dirr and Wallace, 1999). In the absence of glutathione, F51S binds more ANS than the wild-type protein.

The F51S mutant also displays diminished conformational stability. The protein-concentration dependence of the unfolding data suggests the presence of (a) highly populated dimeric state(s) in equilibrium with unfolded monomer within the urea unfolding transition. The lock-and-key does stabilise the quaternary structure at the dimer interface although it is not essential for dimerisation to occur. Possible reasons for a reduced *m*-value have been given in section 4.3.3. ANS binding to the native wild-type (wavelength emission maximum at 480 nm) and F51S (wavelength emission maximum at 473 nm) proteins confirmed the existence of enhanced exposure of hydrophobic surface area in the mutant. Therefore, it is reasonable to suggest that the initial state of the mutant protein (native-like dimeric species) prior to the unfolding event has a larger solvent-accessible surface area than the wild-type protein. The lowered *m*-value of the mutant could be indicative of the smaller change in solvent-accessible surface upon total unfolding. In F51S, the protein-concentration dependence of the unfolding data suggests the presence of (a) highly populated dimeric state(s) in equilibrium with the unfolded monomer within the unfolding transition.

4.5 Conclusion

F51 located at the subunit interface was replaced with serine. The mutation resulted in a decreased catalytic activity, which indicated that the mutant protein contained a structurally compromised active site. Kinetics data confirmed that the G-site was disrupted to a greater extent than the H-site. The mutation also affected the ligandin function of the protein because F51S binds more ANS than the wild-type protein. The F51S protein displays a reduced conformational stability. The lock-and-key motif at the

subunit interface is, therefore, not essential for dimerisation to occur but it does stabilise the quaternary structure at the dimer interface.

CHAPTER 5

THE ROLE OF PHENYLALANINE 221 IN THE LIGANDIN FUNCTION OF HUMAN GLUTATHIONE TRANSFERASE A1-1

5.1 The C-terminal of helix 9

The cytosolic GSTs exist as stable dimers. They all share a highly conserved archetypical fold. The dimeric structure of GSTs consists of two subunits and each subunit is composed of two structurally distinct domains. The N-terminal domain contributes towards the formation of the glutathione-binding site (G-site). The C-terminal domain as well as elements from the N-terminal domain forms the hydrophobic substrate-binding site (H-site). The G-sites of all the GST classes are remarkably similar whereas the greatest differences exist in the H-site of these proteins. The GSTs exhibit ~ 75% sequence homology within a class and about 20-30% between classes (Cameron *et al*, 1995).

Comparison of the crystal structures from representatives of the various GST gene classes reveals a unique structural feature at the C-terminus of the class alpha GST. The C-terminus end consists of an amphipathic α-helix (helix 9) which is able to fold onto domain I (Sinning *et al*., 1993; Cameron *et al*., 1995). Although helix 9 is not essential for catalysis (Board and Mannervik, 1991), it does play a role in the specificity towards the binding of hydrophobic (H-site) ligands. Due to the amphipathic character of this helix, the hydrophobic residues that are located on the interior of helix 9 stack onto domain I thereby contributing towards the H-site. In this way, a highly hydrophobic wall is formed for the electrophile-binding pocket. This structural arrangement serves to restrict accessibility of the H-site from surrounding solvent. The highly hydrophobic character of the H-site is also due, in part, to the presence of two highly conserved phenylalanine residues (F219 and F221) from the helix (Sinning *et al*., 1993).

In the crystal structure of hGSTA1-1 in complex with *S*-benzylglutathione (see Figure 1 A), the benzyl group of the ligand is located in a binding site formed by three regions of the enzyme: (1) The N-terminus of α1 (Phe9, Ala11, Arg12, Gly13 and Arg14); (2) The

C-terminus of α4 (Leu106, Leu107, Pro109, Val110 and the side chain of Glu103 salt linking to Arg14), and (3) the contribution of four residues from helix 9 (Leu212, Ala215, Phe219 and Phe221). This structural arrangement results in a highly hydrophobic indentation in the protein surface that in the absence of substrate is completely open to solvent on one side (Sinning *et al*., 1993).

The side chain of F221 is also in van der Waals contact with the ethacrynic acid moiety in the hGSTA1-1 crystal structure in complex with ethacrynic acid and its glutathione conjugate (Cameron *et al*., 1995). When helix 9 becomes immobilised onto domain I due to the binding of active-site ligands, the C-terminal residue of the A1 polypeptide chain (F221) becomes located close to the cleft at the dimer interface. It is also evident from crystal structure data that the side chain of F221 contacts the side chain of Val110 from domain II (Cameron *et al*., 1995). Together they could form a hydrophobic wall that contributes towards the hydrophobic nature of the H-site in the presence of active site ligands (Figure 17). It is possible that F221 contributes toward the formation of a higher affinity non-substrate site at the dimer interface. Inspection of crystal structure data suggests that there are five residues within 4 Å of F221. They are Val110, Leu212, Ala215, Arg216 and Phe219. Four of these residues (Leu212, Ala215, Arg216 and Phe219) are located in helix 9 with the exception of Val110, which is located in domain I. Figure 18A is a representation of the binding environment (≤ 4 Å) of F221 at the C-terminus. In Figure 18B, F221 has been removed from the C-terminus.

In this study, F221 (the C-terminal residue) was targeted for deletion in hGSTA1-1. The impact that this deletion will have on the flexibility of the C-terminal helix 9 as well as the non-substrate ligand binding function of the hGSTA1-1 will be assessed.

5.2 Physicochemical properties of the wild-type and F221del proteins

5.2.1 Identification of F221del mutant plasmid DNA

The strategy for mutant selection was the identification of the incorporation of a *Bgl* II

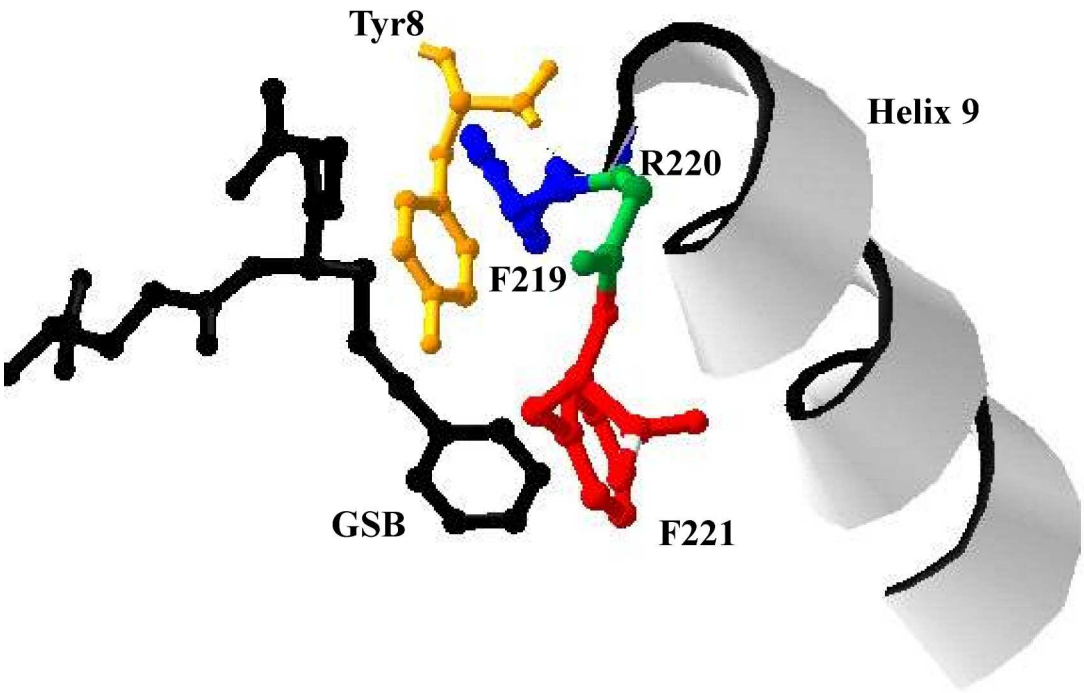

Figure 17. A ball-and-stick representation of the C-terminal environment in human GSTA1-1. The grey ribbon structure represents helix 9 at the C-terminus (residues K210 to F219). The ball-and-stick structures in the figure represent: the active site ligand, *S*-benzylglutathione (black), F219 (violet), R220 (green), F221 (red) and Y8 (yellow).

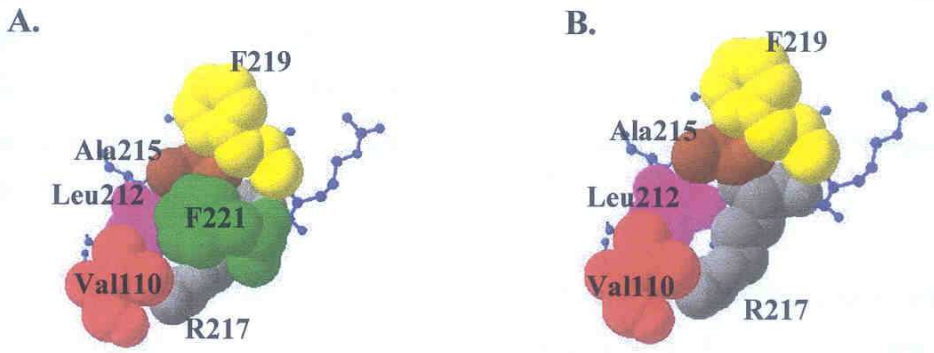

Figure 18. Space-filled representation of the environment of F221 at the C-terminus of helix 9 in human GSTA1-1. (A) The residues located within 4 Å of F221 (green). (B) The same as in (A) except that F221 (green) has been removed to indicate the hydrophobic environment at the C-terminus. The C-terminal helix 9 is shown in ball-and-stick (blue). The figure was generated using Swiss-Pdb viewer.

site. Digestion of possible mutant plasmid DNA with *Bgl* II would yield a linearised fragment on a 1% agarose gel. The wild-type plasmid DNA would not have incorporated the unique restriction site and, therefore, digestion of wild-type DNA with *Bgl* II would be viewed as uncut DNA. In this way, the possible mutant plasmid DNA could be identified (Figure 19).

After selection of the possible mutant plasmid DNA, the entire region coding for the expression of the hGSTA1-1 protein was sequenced to confirm the presence of the F221 deletion and to ensure that no other spurious mutations had occurred. The relevant region of the plasmid DNA incorporating the F221 deletion and the unique *Bgl* II restriction site is indicated in Figure 20.

5.2.2 Over-expression and purification

The F221del protein was over-expressed in *E. coli* cells and purified in the same manner as the wild-type protein (section 3.4). The homogeneity and purity of the F221del protein was assessed by SDS-PAGE (Laemmli, 1970) (Figure 21) and SEC-HPLC (Figure 22), respectively. In this way, the F221del protein was found to have a subunit molecular mass of ~ 27 kDa and a dimeric molecular mass of ~ 54 kDa. The mutation, therefore, did not affect the quaternary structure of the protein.

5.2.2.1 Specific activity of the wild-type and F22del proteins using the CDNB-conjugation assay

Assessment of the specific activity of an enzyme serves as a tertiary structural probe. The specific activity of the wild-type and F221del protein was obtained using the standard CDNB-conjugating assay described under section 3.6.1. Comparable specific activity values of 52 μmol/min/mg and 54 μmol/min/mg were obtained for the wild-type and F221del proteins, respectively. This indicates that the deletion of F221 from the C-

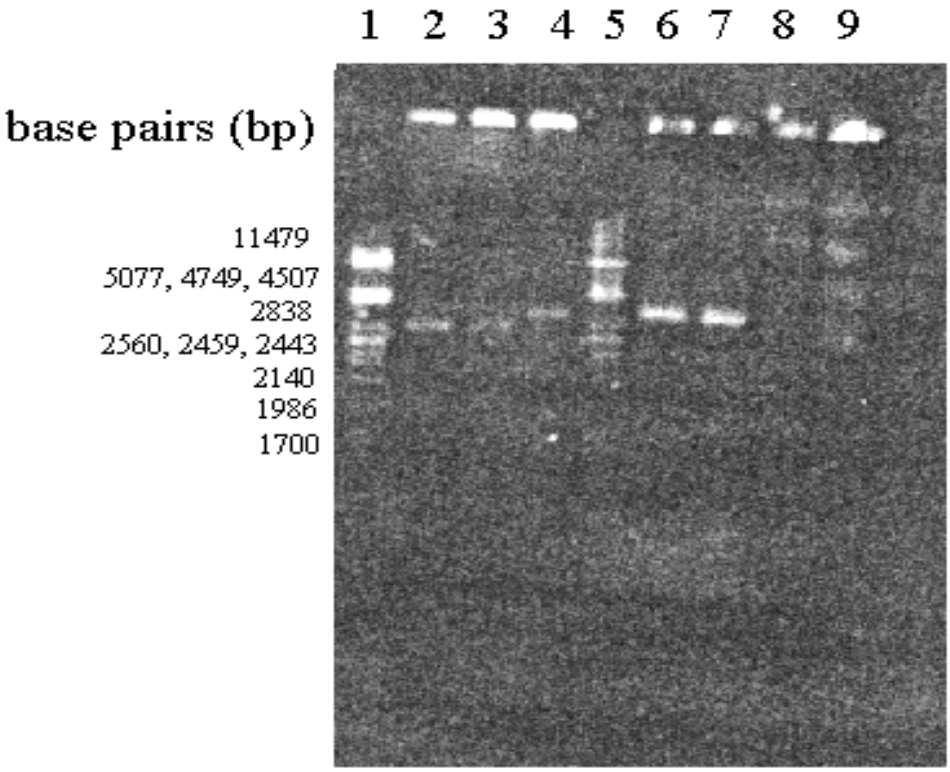

Figure 19. Identification of the F221del mutant plasmid DNA on a 1% agarose gel. Lanes 1 and 5 represent λDNA marker digested with *Pst* I. Lanes 2, 3 and 4 represent three possible mutant plasmid DNA products linearised with the diagnostic restriction enzyme *Bgl* II. Lanes 6 and 7 show the linearised wild-type DNA product generated upon digestion with *Pvu* II and *Sac* I, respectively. Lanes 8 and 9 represent the uncut forms of the wild-type and one of the possible mutants (lane 4), respectively.

A.

5′ GG AAG **ATT** TTC AGG **TTT** TAA TAA CGC AGT CAT GG 3′

↓ ↓

5′ GG A**AG ATC T**TC AGG **TAA** TAA TAA CGC AGT CAT GG 3′

B.

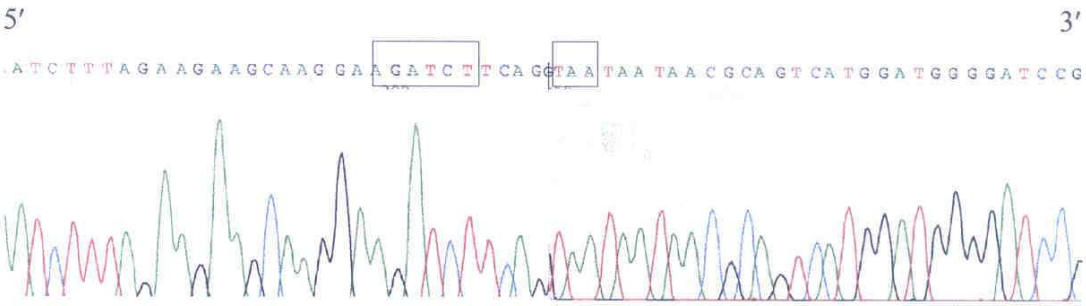

Figure 20. (A) A region of the wild-type nucleotide sequence showing the location of F221 (codon = **TTT**) that was targeted for deletion. The F221 codon was replaced with **TAA** that incorporated a stop signal at F221 thereby effectively truncating the nucleotide sequence at this position. A translationally silent mutation was also engineered into the mutagenic oligonucleotide primer. In this way, Ile218 (codon = **ATT**) was replaced by **ATC**. This alteration caused the introduction of a unique restriction site for the restriction enzyme *Bgl* II (**AG ATC T**) that would be utilised for identification of the mutant plasmid DNA during screening. (B) A segment of the nucleotide sequences obtained from DNA sequencing. The presence of the stop codon at F221 (TAA) as well as the novel *Bgl* II diagnostic restriction site (AG ATC T) are indicated in boxes.

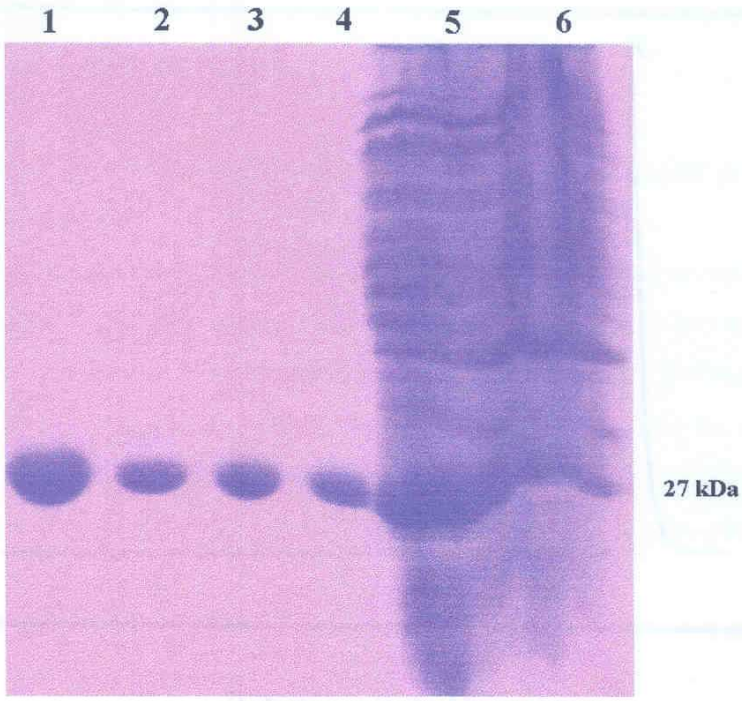

Figure 21. SDS-PAGE of the purified F221del hGSTA1-1. Lane 1 shows the wild-type hGSTA1-1 purified using CM-Sephadex cation exchange chromatography. Lane 2, wild-type hGSTA1-1 purified using *S*-hexylglutathione affinity chromatography. Lanes 3 and 4 represent the F221del protein purified using *S*-hexylglutathione affinity chromatography. Lanes 5 and 6 represent the soluble and insoluble fractions of F221del hGSTA1-1, respectively. The wild-type hGSTA1-1 protein was used as a marker and the subunit molecular mass is shown (27 kDa).

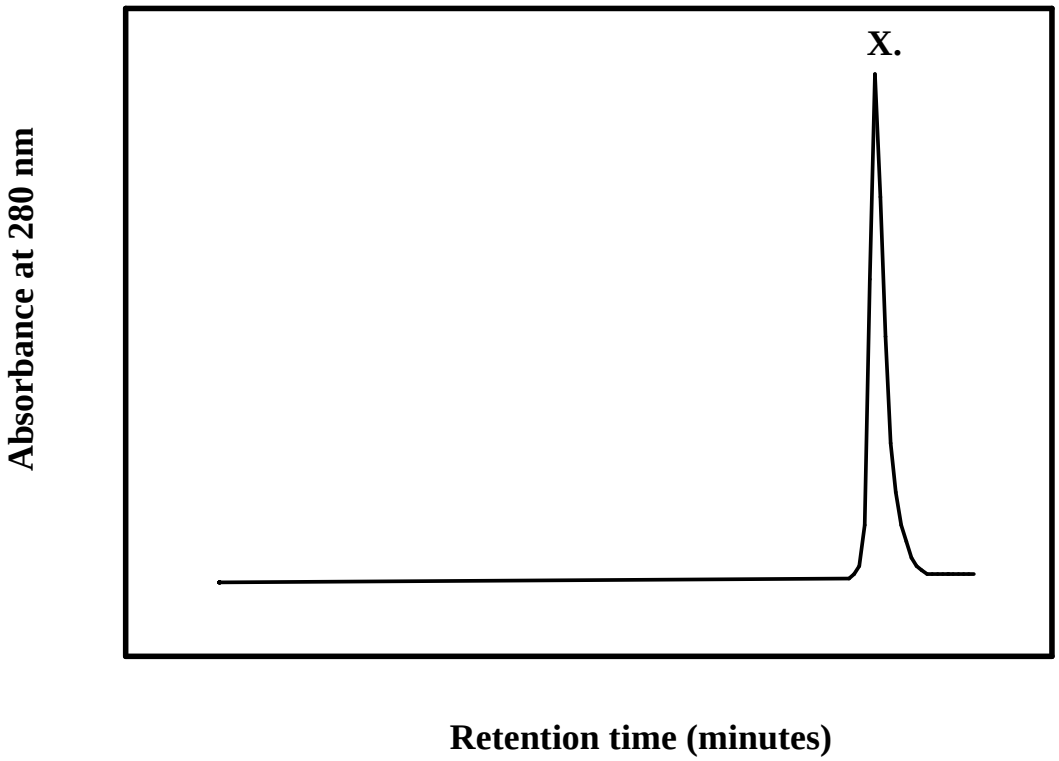

Figure 22. SEC-HPLC elution profile of the purified F221del hGSTA1-1 protein. X in the figure denotes the position of the F221del protein.

terminus of helix 9 does not adversely affect the functioning of the enzyme and that no tertiary structural changes have occurred at/near the region of the active site.

5.2.2.2 Glutathione peroxidase activity of the wild-type and F221del proteins using cumene hydroperoxide

The specific activities of the wild-type and F221del proteins were determined using the cumene hydroperoxide assay system. The wild-type and F221del proteins displayed peroxidase activity towards cumene hydroperoxide as the substrate. The specific activity was calculated as 9.4 ± 0.2 μmol/min/mg and 10.6 ± 0.2 μmol/min/mg for the wild-type and F221del proteins, respectively. These values compare very well with the previously published value of 10 μmol/min/mg for the wild-type hGSTA1-1 protein (Stenberg *et al*., 1991).

The specific activities obtained for F221del hGSTA1-1 with either the CDNB-conjugating assay or the cumene hydroperoxide assay system are comparable to that of the wild-type hGSTA1-1 protein. These results confirm that the mutation does not affect the enzymatic properties of the enzyme.

5.2.3 Fluorescence spectral properties of the wild-type and F221del proteins

The lone tryptophan residue (W20) was selectively excited at 295 nm. The emission spectra obtained indicated that both the wild-type and F221del mutant proteins have an emission maximum at 325 nm (native protein). Although the emission intensity of F221del protein is slightly reduced (Figure 23), they are very similar. Spectral analysis, therefore, suggests that the overall tertiary structure as well as the polarity of the environment of W20 in the F221del protein is unchanged by the deletion. In this way, W20 could serve as a local reporter of any structural changes occurring at the domain I-domain II interface of the F221del protein.

5.2.4 Far-UV circular dichroism

The overall secondary structural content of the wild-type and F221del proteins are highly comparable as can be seen from the characteristic negative peaks at 222 nm and 208 nm,

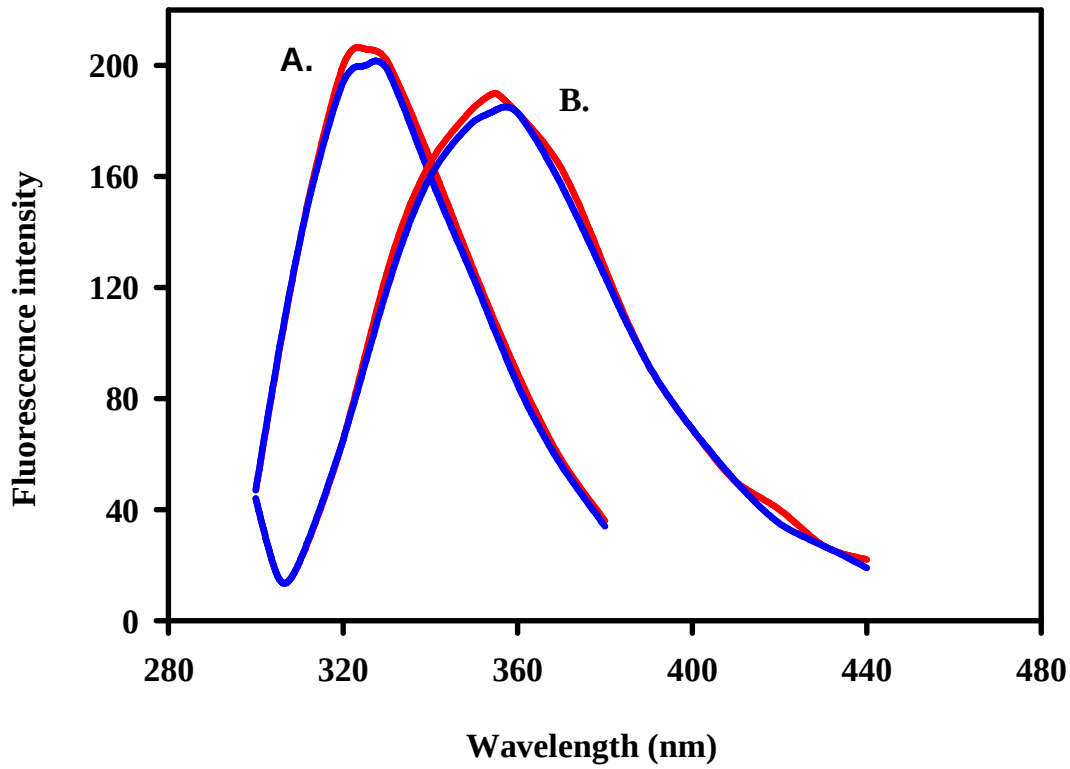

Figure 23. Spectral characterisation of wild-type and F221del hGSTA1-1. The wild-type and F221del proteins are represented as solid red and blue lines, respectively. The lone tryptophan residue of either protein was selectively excited at 295 nm and the wavelength emission spectra were monitored. The wavelength emission maxima are at 325 nm (A) for the native folded proteins in the absence of urea. The wavelength emission maxima are at 355 nm (B) for the unfolded proteins in the presence of 8 M urea.

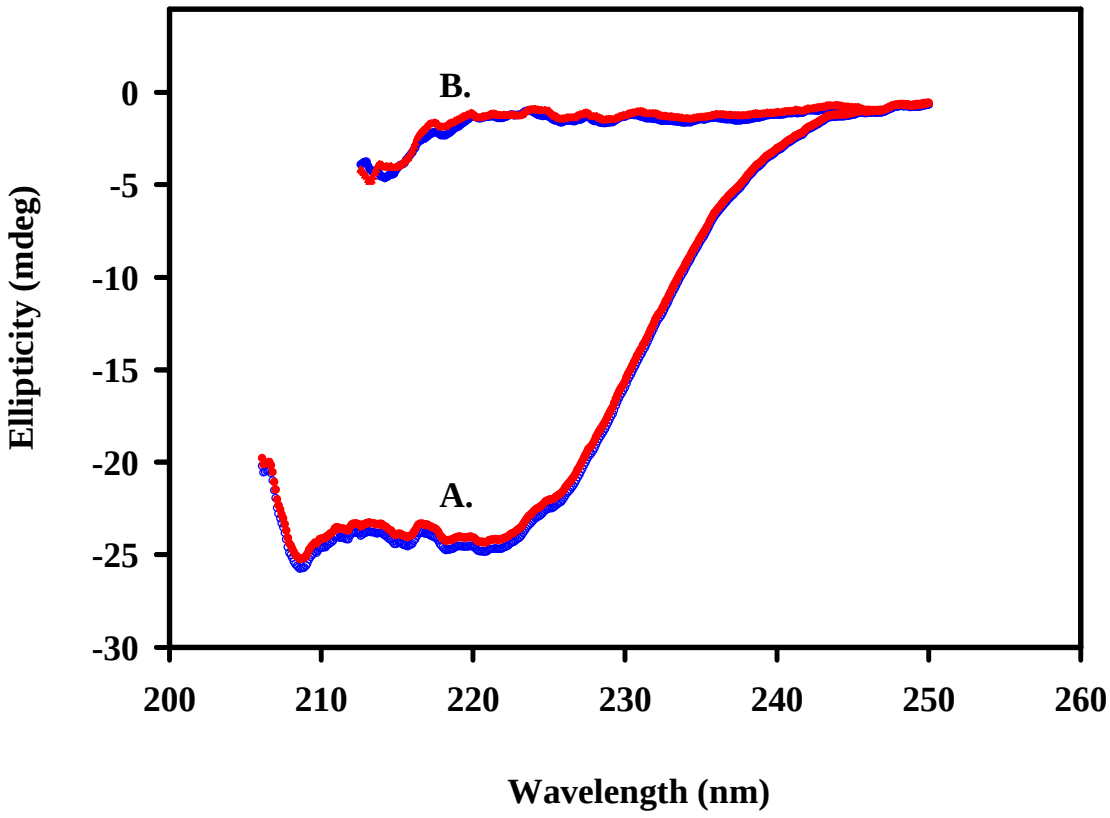

Figure 24. Far-UV circular dichroism spectra for the wild-type (red) and F221del (blue) hGSTA1-1 proteins. (A) The far-UV circular dichroism spectra of wild-type and F221del hGSTA1-1 in the absence of urea (i.e., native folded protein). (B) The far-UV circular dichroism spectra of wild-type and F221del hGSTA1-1 in the presence of 8 M urea (i.e., unfolded protein). The experimental conditions were: 2 μM protein (wild-type or F221del) in 20 mM sodium phosphate buffer, pH 6.5, containing 0.1 M NaCl in the absence (A) and presence of 8 M urea (B).

respectively (Figure 24). Therefore, the deletion of F221 from the C-terminus of hGSTA1-1 does not disrupt the secondary structural content of the protein.

5.2.5 ANS binding to the wild-type and F221del proteins

ANS is an anionic dye that binds a site at the dimer interface of hGSTA1-1 (Sluis-Cremer *et al*., 1996; Sluis-Cremer *et al*., 1998). ANS is extremely effective in monitoring the appearance/disappearance of hydrophobic surfaces on proteins that are undergoing structural changes. In the absence of protein (i.e., 100 μM ANS in protein storage buffer alone), ANS exhibits an emission maximum at 540 nm (direct ANS excitation at 390 nm). When ANS is bound to protein, the emission spectrum is blue-shifted to 480 nm for the wild-type and F221del proteins (Figure 25). The spectra indicate the differences in emission intensity at 475 and 480 nm for the wild-type and F221del proteins, respectively. The wild-type protein exhibits an enhanced ANS fluorescence which is ~ 1.6 times greater than the F221del protein. A comparison between the two proteins reveals that the emission maximum wavelength remains unchanged. This result, therefore, indicates that there is no significant difference in exposed hydrophobic surface area between the wild-type and F221del proteins although the ANS-binding capacity is diminished in the F221del protein. The decreased capacity of ANS binding to the F221del mutant may indicate decreased hydrophobicity of the ANS binding environment. This will be dealt with later in the Discussion section (Section 5.4).

5.2.6 The dissociation constant for ANS

The affinity of each of the proteins for the anionic dye ANS was measured using fluorescence quenching and enhancement techniques. By means of fluorescence enhancement, dissociation constant (K_d) values of 10.9 ± 0.9 μM and 11.6 ± 0.8 μM ANS were obtained for the wild-type and F221del proteins, respectively (Figure 26). These values are comparable and indicate that the F221del protein binds ANS with a similar affinity to that of the wild-type protein. Therefore, deletion of F221del from the C-terminus of hGSTA1-1 causes the protein to bind ANS with a similar affinity but reduced capacity (see Section 5.2.5).

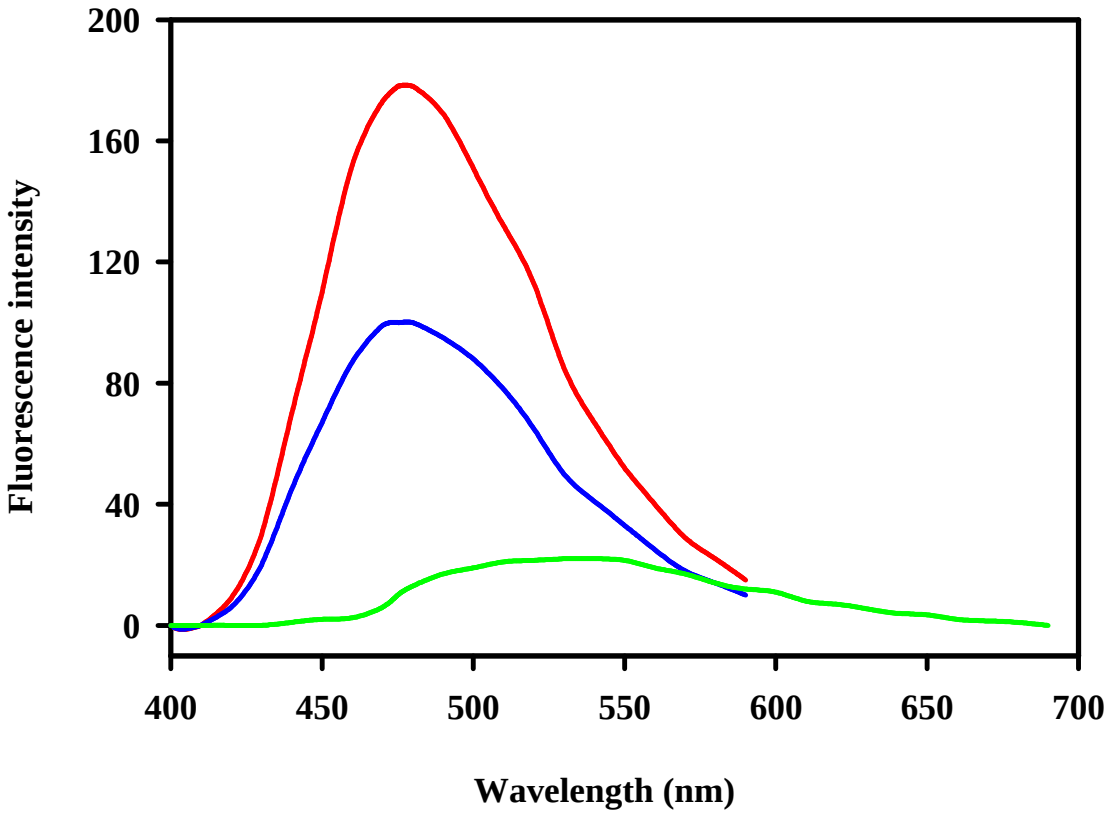

Figure 25. Emission spectra of ANS binding to wild-type and F221del hGSTA1-1. 100 μM ANS was added to 1 μM wild-type and F221del protein. ANS was selectively excited at 390 nm and the wavelength emission spectra were monitored. The spectra of ANS binding to wild-type and F221del proteins are represented as solid red and blue lines, respectively. The above spectra were corrected for the contribution due to free unbound ANS in buffer (solid green line).

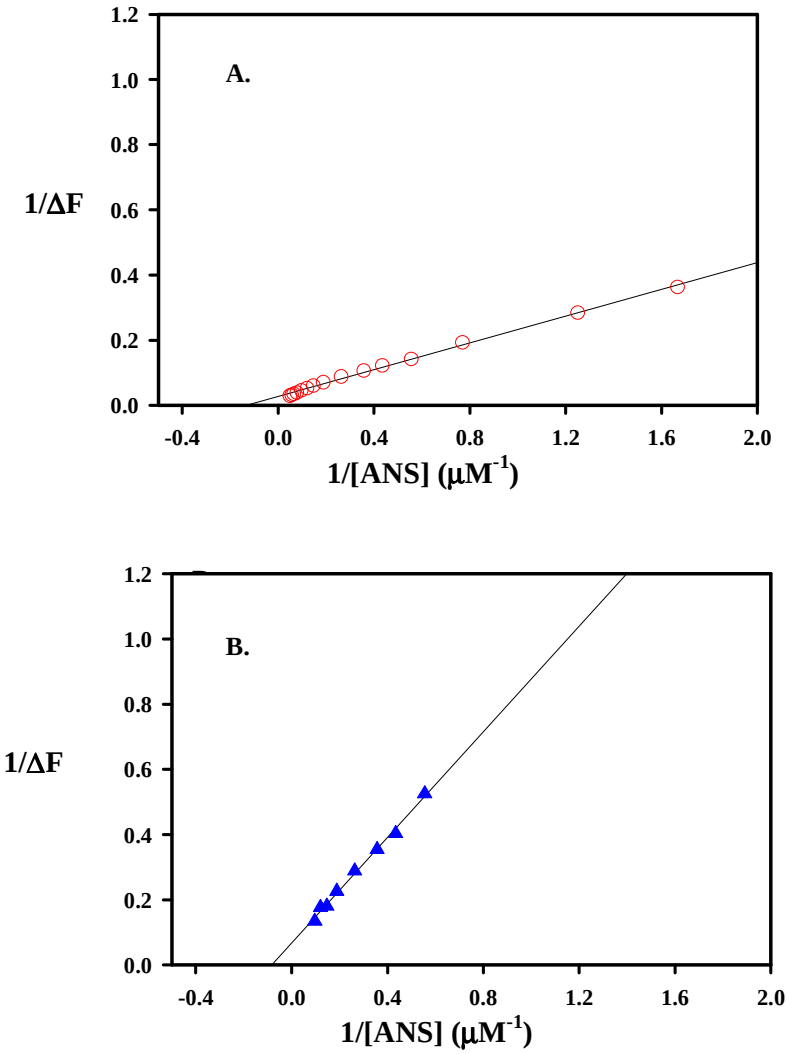

Figure 26. Determination of the dissociation constant (K_d) for ANS. The fluorescence enhancement technique was used to determine the K_d for the wild-type and F221del proteins, respectively.

5.2.7 The effect of urea on the binding of ANS in the presence and absence of *p*-bromobenzylglutathione

ANS is a widely used hydrophobic probe that monitors the conformational changes in protein molecules during folding/unfolding studies (Erhardt *et al*., 1995; Wallace *et al*., 1998a; Stevens *et al*., 1998). ANS has been shown not to affect the stability of the wild-type hGSTA1-1 protein implying that this fluorescent dye does not affect the conformation of the protein (Wallace *et al*., 1998a).

The effect of urea on the binding of ANS to the wild-type hGSTA1-1, helix 9 deletion mutant as well as the F219W mutant has already been demonstrated (Dirr and Wallace, 1999). This type of assay is extremely useful in assessing the conformational dynamics of helix 9 (Figure 27). Essentially, ANS binding to the above proteins was monitored between 1 and 4 M urea concentrations in the absence and presence of active site ligands. This is also the urea concentration region corresponding to the fluorescence pre-transition region baseline for wild-type and F221del proteins (Figure 28) as well as the initial urea-induced deactivation of hGSTA1-1 (Dirr and Wallace, 1999). Therefore, the extent of helix 9 flexibility is easily monitored in this concentration range.

The effect of urea on the binding of ANS to the wild-type and F221del proteins was studied in the presence and absence of the active site ligand, *p*-bromobenzylglutathione. The range of urea concentrations used in this study corresponds to the region of the fluorescence pre-transition baseline as observed in Figure 28.

5.2.7.1 ANS binding in the absence of *p*-bromobenzylglutathione

Figure 27A demonstrates that ANS binding to the wild-type hGSTA1-1 protein is enhanced in the absence of the active site ligand (from 0-4 M urea). There also appears to be a very dramatic decrease in ANS fluorescence intensity in the uncomplexed wild-type protein from 4.5-5.5 M urea. The F221del protein exhibits enhanced ANS binding behaviour at lower urea concentrations than the wild-type protein (Figure 27B). ANS binding to the uncomplexed mutant protein is greatly diminished from 3.5 M urea. This effect has been observed previously (section 5.2.5).

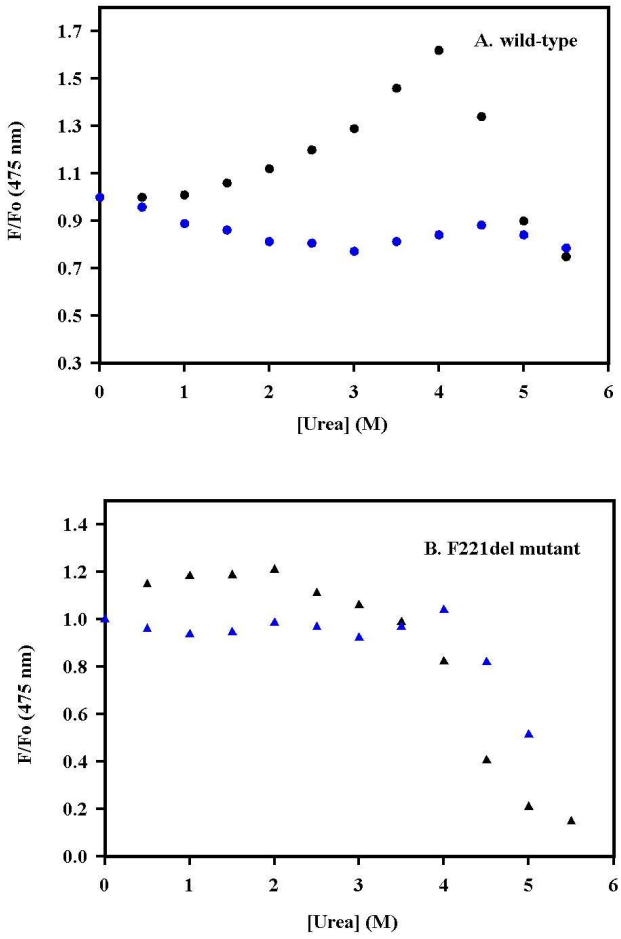

Figure 27. ANS binding to wild-type (A) and F221del (B) hGSTA1-1 in the presence of urea. The wild-type and F221del proteins are represented as filled circles (A) and filled triangles (B), respectively. ANS was selectively excited at 390 nm and the emission wavelength maximum was monitored at 475 nm in the absence of any ligand (black filled symbols), as well as the presence of 200 μM *p*-bromobenzylglutathione (A, filled blue circles and B, filled blue triangles). Experimental conditions were: 1 μM protein dimer and 100 μM ANS in 20 mM sodium phosphate buffer, pH 6.5. The ratio, F/Fo, represents ANS fluorescence monitored in the presence (F) and absence of ligand (Fo).

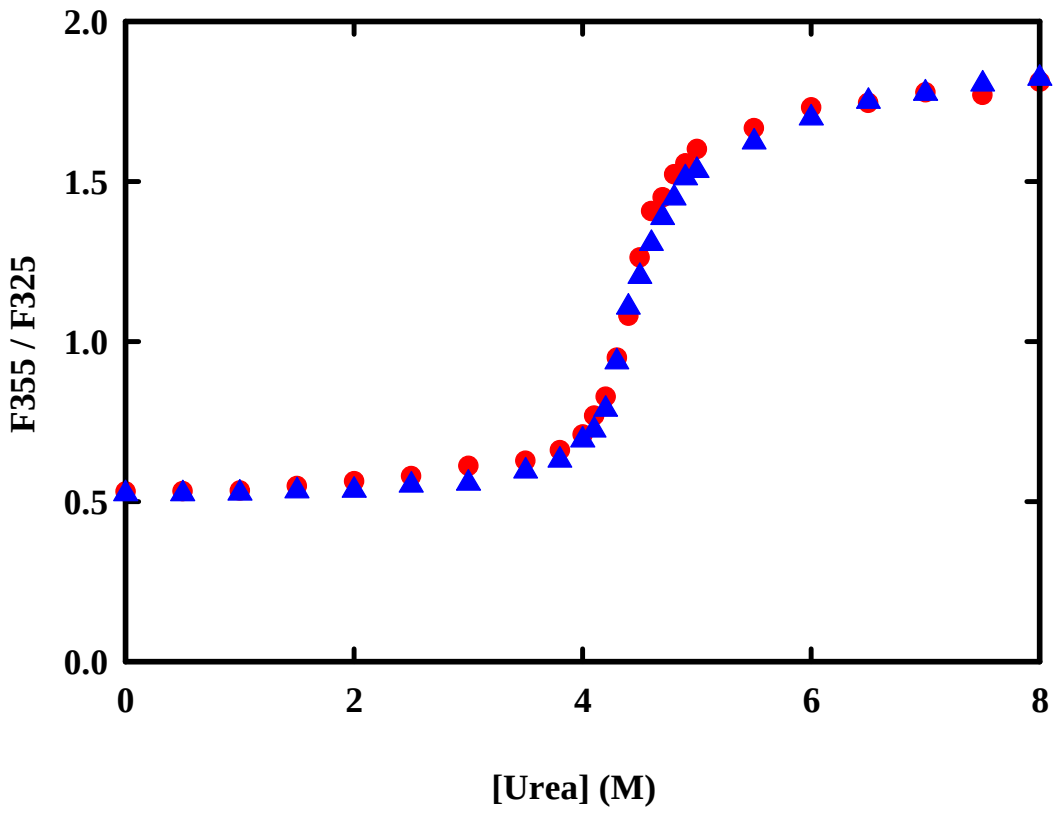

Figure 28. Urea-induced equilibrium unfolding of wild-type and F221del hGSTA1-1. The conformational stability of each protein was determined by monitoring the change in fluorescence of tryptophan 20 in the presence of urea. Protein concentration = 1 μM. The unfolding curves of the wild-type and F221del proteins are represented as filled blue triangles and filled red circles, respectively. The ratio of F355/F325 represents the ratio of unfolded to folded protein.

5.2.7.2 ANS binding in the presence of *p*-bromobenzylglutathione

The enhanced ANS binding ability that is observed in the uncomplexed wild-type protein is almost completely lost when *p*-bromobenzylglutathione is present. ANS does not have the ability to bind the wild-type protein at low urea concentrations. An increase in ANS fluorescence intensity for the wild-type protein is observed from 0-4 M urea but diminishes at higher urea concentrations as the protein unfolds (Figure 27A). The F221del mutant and the wild-type protein exhibit the same ANS binding behaviour when *p*-bromobenzylglutathione is complexed at the active site (Figures 27A and B). The enhanced ANS binding effect diminishes from 4.5 M urea for both the wild-type and F221del proteins.

The result obtained for the F221del mutant in this study is very similar to that obtained in another study by Dirr and Wallace (1999). In that study, the F219W mutant also binds ANS at lower urea concentrations when compared to the wild-type protein. When the F219W mutant protein is complexed with *p*-bromobenzylglutathione, ANS binding is reduced at lower urea concentrations but not at the higher urea concentrations. ANS binding to the F219W mutant diminishes beyond 4 M urea as the mutant protein unfolds. In the F219W mutant, the enhanced ANS binding behaviour at lower urea concentrations suggests a weaker association of helix 9 with domain I of the protein (i.e., helix 9 is more mobile or less “ordered”) (Dirr and Wallace, 1999).

5.3 Urea-induced equilibrium unfolding of the F221del mutant protein

5.3.1 Reversibility studies

Fluorescence spectroscopy was utilised as a structural probe in order to study the reversibility process. The lone tryptophan emission spectrum (excitation at 295 nm) of the native folded F221del mutant protein has an emission maximum at 325 nm. The tryptophan emission maximum is red-shifted to 355 nm for the denatured protein. The emission maximum wavelength observed for the F221del protein in the native and denatured states is identical to that of the wild-type protein. The percentage reversibility of the mutant protein as assessed by the regain in emission fluorescence intensity at 325 nm was greater than 95%.

5.3.2 Dependence of unfolding transition on protein-concentration

The urea-induced equilibrium unfolding reaction of F221del was monitored using steady-state tryptophan florescence. Figure 28 shows that the unfolding reaction proceeds through a single sigmoidal transition. The single transition suggests a two-state unfolding process proceeding from a folded dimer to unfolded monomer. Analysis of the sigmoidal transition curve indicated that the unfolding transition for 1 μM F221del has a midpoint at 4.4 M urea (the C_m-value). The C_m-value compares very well with the wild-type hGSTA1-1 value of 4.5 M urea determined previously (Wallace *et al*., 1998a; Sayed *et al*., 2000). As mentioned previously (section 4.3.2), protein-concentration dependence at the midpoint of the protein unfolding transition (i.e., the C_m-value) using tryptophan fluorescence is indicative of a two-state unfolding reaction (Neet and Timm, 1994).

Varying concentrations of F221del protein (0-5 μM) were incubated with 4.4 M urea (C_m-value) and the intrinsic tryptophan emission maximum of the protein was monitored at 325 nm and 355 nm for the folded and unfolded conformations, respectively (tryptophan excitation wavelength = 295 nm). Figure 29 shows that there is an increase in protein stability with increasing protein concentration. This result is consistent with a two-state model that defines the unfolding/refolding reaction as:

$$N_2 \overset{K_1}{\Leftrightarrow} 2U$$

where the equilibrium constant $K_1 = [U]^2 / [N_2]$. This result is evidence that the deletion of F221 from the C-terminus of helix 9 does not impact on the two-state equilibrium unfolding/refolding process.

5.3.3 Analysis of the equilibrium unfolding transition and interpretation of the $\Delta G(H_2O)$ and *m*-value

Figure 28 shows the urea-induced equilibrium unfolding transition of the wild-type and F221del protein in the presence of urea. Analysis of the equilibrium unfolding data indicated that both proteins fit a two-state model. This pre-requisite enables one to

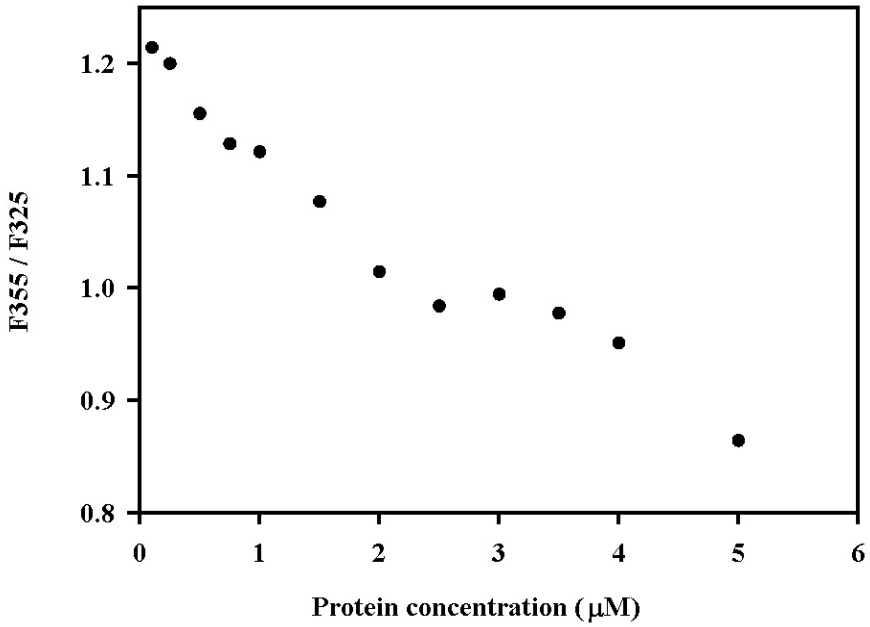

Figure 29. Protein-concentration dependence of the stability of F221del hGSTA1-1. Varying concentrations of F221del protein were incubated in 4.4 M urea (the C_m-value for F221del hGSTA1-1). The lone W20 residue was excited at 295 nm and the fluorescence intensity was measured at 325 nm (folded protein) and 355 nm (unfolded protein). The ratio of F355/F325 represents the fraction of unfolded to folded protein.

estimate the $\Delta G(H_2O)$ (i.e., the free energy change in the absence of denaturant) as well as the difference in solvent-accessible surface area between the native and unfolded states (*m*-value) (Schellman, 1978; Shortle, 1995). A comparison of the values obtained for these two parameters for a wild-type and mutant protein allows one to assess the role of certain residues and interactions in the structure and stability of a protein (Matthews, 1995; Shortle, 1995). Neet and Timm (1994) have stated that a linear correlation exists between the number of amino acid residues in the monomer (N) and the value of the $\Delta G(H_2O)$ using the equation: $\Delta G(H_2O) = 8.8 + 0.08$ N. The calculated $\Delta G(H_2O)$ values are 26.5 kcal/mol and 26.4 kcal/mol for the wild-type and F221del proteins, respectively. This value correlates the tertiary/quaternary stabilisation with the size of the dimer. The experimentally determined $\Delta G(H_2O)$ values are 26.6 kcal/mol and 28.2 kcal/mol for the wild-type and F221del proteins, respectively. This large stabilisation energy is common to the GSTs studied thus far (Dirr and Reinemer, 1991; Erhardt and Dirr, 1995; Kaplan *et al*., 1997; Wallace *et al*., 1998a). The large stabilisation energy of dimers is related to the intersubunit interactions and thus lends support to the formation of oligomers. The magnitude of the conformational stability is related to the size of the polypeptide in the subunit and depends upon the type of structure in the subunit interface (Neet and Timm, 1994). A good correlation of the $\Delta G(H_2O)$ values for both proteins exists between the experimentally determined values as well as those calculated from the above equation. The conformational stability of the F221del mutant when compared to that of the wild-type protein indicates the non-disruptive nature of the deletion mutation.

According to Myers *et al.* (1995), the theoretical *m*-value can be estimated by relating the amount of surface area buried with the number of amino acid residues. This can be expressed by the equation: $m = 374 + 0.11(\Delta ASA)$, where ΔASA is the change in the solvent-accessible surface area upon unfolding. The change in solvent-accessible surface area is calculated as follows: $\Delta ASA = -907 + 93(N)$ where N represents the number of amino acid residues in the dimeric protein. ΔASA for the dimeric wild-type and F221del proteins are, therefore, calculated as 40199 $Å^2$ and 40013 $Å^2$, respectively. The theoretical *m*-values are 4.79 kcal/mol/M urea and 4.78 kcal/mol/M urea for the wild-type and F221del proteins, respectively. The experimentally determined *m*-values were 4.16

kcal/mol/M and 4.43 kcal/mol/M for the wild-type and F221del proteins, respectively. It appears, therefore, that there is strong agreement between the *m*-values obtained for the wild-type and mutant proteins both theoretically and experimentally. As pointed out by Myers *et al*., (1995), there is also a strong correlation between the *m*-value and the amount of accessible surface area upon unfolding. This has also been found with heat capacity changes. Therefore, for proteins undergoing simple two-state unfolding behaviour, the ΔASA is the main structural determinant for both the *m*-value and ΔC_p. The similarity in the *m*-values for the wild-type and mutant protein suggests that there is no/very little difference in the solvent-accessible surface area between the two proteins. Both proteins indicate a highly co-operative two-state unfolding process with a high degree of co-operativity between the non-covalent interactions stabilising the folded state. Therefore, deletion of F221 from the C-terminus of helix 9 does not impact on the conformational stability and accessible surface area of the protein.

5.4 Discussion

It is clear from crystal structure data that the alpha class GSTs alone possesses a unique secondary structural element, helix 9, at the C-terminus of the protein. This helix has been the subject of very intensive research with respect to catalytic (Board and Mannervik, 1991; Gustafsson *et al*., 1999; Allardyce *et al*., 1999; Nieslanik and Atkins, 2000) and ligandin function and conformational stability studies (Dirr and Wallace, 1999). This helix is not essential for catalytic activity but it is a structural determinant for the specificity toward hydrophobic electrophiles. In the presence of active site ligands, helix 9 packs onto domain I and becomes an integral part of the H-site thus providing a highly hydrophobic environment for the electrophile-binding pocket. In this way, the H-site is protected from the bulk solvent. It has been suggested that helix 9 contributes towards the ionisation of Y8 in the rat GSTA1-1 (Atkins *et al*., 1997). Y8 is a conserved catalytic residue that is required for the activation of the thiol group of reduced glutathione.

In the present study, SEC-HPLC data suggests that the deletion of F221 from the C-terminus of hGSTA1-1 does not affect the quaternary structure of the protein. The far-UV

circular dichroism spectra are highly comparable between the wild-type and F221del proteins. The mutant protein displays two ellipticity minima at 208 nm and 222 nm, respectively. The removal of F221, therefore, does not disrupt the secondary structural content of the protein. Helix 9 alone contributes 4.5% toward the total helical content of the protein and has not been found to impact on the secondary structural content of the helix 9 deletion mutant (Dirr and Wallace, 1999). The sensitivity of CD does not allow for the observation of a 4.5% reduction in CD signal.

Fluorescence spectral data indicated that the deletion of F221 does not impact on the tertiary structure of the protein. W20 is a sensitive probe for any changes that occur at the domain interface. The polarity of the environment of W20 in F221del is unchanged when compared to the wild-type protein. Therefore, no structural changes have occurred at/near the domain I-domain II interface of the mutant protein.

The non-disruptive nature of the mutation with regards to the tertiary structure of the protein was studied using enzyme activity as a functional probe. Both the wild-type and mutant proteins displayed similar enzyme activities when using either the CDNB or cumene hydroperoxide (peroxidase) assay method. The results demonstrate that the active site (i.e., the G- and H-sites) of the F221del protein is not affected by the mutation because a structurally competent active site is required for the enzyme to be catalytically active.

The binding of the amphipathic dye ANS to proteins serves as a very powerful probe for monitoring the appearance/disappearance of structured hydrophobic surfaces on proteins. ANS exhibits a wavelength emission maximum at 540 nm in the absence of protein (excitation wavelength = 390 nm), and the emission maximum is blue-shifted to 480 nm in the protein/ANS complex. The wild-type protein exhibits an emission maximum at ~ 475 nm whereas the mutant displays an emission maximum at 480 nm in the protein/ANS complex. Therefore, there appears to be an increase in exposure of hydrophobic surface area in the F221del protein when compared to the wild-type protein. Interestingly, the wild-type protein also binds ~ 1.6 times more ANS than the F221del mutant protein

(Figure 25). The K_d values for ANS indicate that both proteins bind the anionic dye with the same affinity (Figures 26A and B). The F221del mutant, however, binds ANS with a reduced capacity (Figure 25). In the crystal structure of wild-type hGSTA1-1 complexed with *S*-benzylglutathione (Sinning *et al*., 1993), the bulky side chain of F221 located at the C-terminus of helix 9 becomes located close to the V-shaped cleft at the subunit interface. In the presence of active site ligands, helix 9 becomes immobilised over the active site thus effectively excluding the active site from bulk solvent. The result is the formation of a highly hydrophobic environment for the binding hydrophobic electrophilic compounds at the H-site. Also, the side chain interactions between F221 and Val110 (from domain I) could result in the formation of a hydrophobic wall for the ANS binding site (Figure 18A). F221 contributes towards the formation a highly hydrophobic region at the C-terminus of the protein (Figure 18A and B). In light of the results from an ITC study of the binding interaction between ANS and the wild-type hGSTA1-1 protein (see Chapter 6), we propose that this is also the region that functions as an ANS binding site. ITC studies indicated that one molecule of ANS is bound per protein monomer. The binding of ANS to hGSTA1-1 results in the reduction of non-polar surface area exposed to solvent. Therefore, the proposed ANS binding site is the region adjacent to domain I that becomes buried when helix 9 is immobilised. This is the same region that contributes to the formation of the highly hydrophobic environment in the presence of F221 at the C-terminus. Therefore, removal of F221 at the C-terminus of helix 9 could result in lowering of the hydrophobic character of this region.

One of the structural features distinguishing the class alpha GST from the other GST classes is the existence of a unique C-terminal alpha helix, helix 9. The mobility of helix 9 in the F221del protein was compared to the wild-type protein. The results indicated that when the wild-type protein is complexed to *p*-bromobenzylglutathione, there is a great reduction in the urea-induced exposure of hydrophobic surface area. This is explained by the reduced ANS binding behaviour when the wild-type protein is complexed to the active site ligand. Helix 9 at the C-terminus, therefore, appears to be tightly bound to the GST protein when the active site is occupied with ligand. An earlier study has highlighted this behaviour for the wild-type hGSTA1-1 enzyme (Dirr and Wallace,

1999). In that study, the authors also found that helix 9 is more tightly bound to the GST protein with *p*-bromobenzylglutathione and glutathione than with ethacrynic acid.

Crystallographic data has shown that helix 9 at the C-terminus is highly flexible in the uncomplexed protein, and upon occupancy of the active site, helix 9 becomes highly ordered (Sinning *et al*., 1993). In contrast to this, a crystal structure of human GSTA4-4 showed the presence of a highly ordered and structured C-terminal helix 9 in the absence of any ligand (Bruns *et al*., 1999).

The effect of urea on the exposure of hydrophobic surface area in the uncomplexed F221del mutant is very different from the wild-type protein. Figure 27B shows that the uncomplexed F221del mutant is capable of binding ANS at much lower urea concentrations when compared to the wild-type protein. This suggests that helix 9 at the C-terminus is more flexible (or less ordered) in the F221del mutant than the wild-type protein. Upon occupation of the active site with *p*-bromobenzylglutathione, helix 9 appears to be more tightly associated with the F221del protein in the complexed form than it is in the uncomplexed form. In both proteins, occupancy of the G- and H-sites, with *p*-bromobenzylglutathione, immobilises helix 9 over the active site of domain I thus effectively shielding it from bulk solvent. Therefore, F221 may be required for controlling the dynamics of helix 9 at the C-terminus of hGSTA1-1.

Recently, a study by Gustafsson *et al*. (1999) showed that the rate of glutathione binding to the hGSTA1-1 was modulated by the C-terminal helix 9. The binding rate of GSH to the wild-type hGSTA1-1 as well as different mutants appear to be linked to the accessibility of the active site to solvent and, therefore, the flexibility of helix 9 at the C-terminus. Interestingly, the rate of GSH binding to the active site of class pi GSTP1-1 is enhanced due to the accessibility of the active site to bulk solvent because of the absence of a C-terminal helix 9 in the class pi GSTP1-1.

Helix 9 is a unique structural feature at the C-terminus of the class alpha enzymes. However, the various GSTA1-1 isoforms display noticeable differences both in residue

content as well as the length of helix 9 at the C-terminus of the protein (Figure 30). Inspection of the structures indicates that the length of helix 9 as well as the helical content will reflect the degree to which helix 9 is ordered at the C-terminus. The role of various residues in helix 9 localisation at the C-terminus were examined in rat GSTA1-1. For example, a comparison of 1ev9 (W20F; single mutant) and 1ev4 (W20F/F219; double mutant) in rat GSTA1-1 (Adman *et al*., 2001) indicates that helix 9 in the double mutant is much shorter and possibly more flexible at the C-terminus of the protein than the W20F mutant. This suggests a possible role for F219 in helix localisation and flexibility at the C-terminus. Possible reasons for the decrease in helix 9 stability in these mutants are also related to the substrate (GSO_3^-) used in the protein crystallisation studies. It is interesting to note that the human GSTA4-4 structure (Figure 30, 1gul and 1gum) possesses an ordered helix 9 at the C-terminus in both the complexed (*S*-(2-iodobenzyl) glutathione) and uncomplexed structures (Bruns *et al*., 1999). The GSTA1-1 isoforms, therefore, indicate that the degree of occupancy (G-site, H-site, both or neither) of the active site as well as the residues located at the C-terminal of the protein will determine the extent of helix 9 flexibility at the C-terminus.

The protein-concentration dependence of the unfolding data for F221del suggests the presence of a highly populated dimeric state in equilibrium with unfolded monomer within the urea unfolding transition. No significant changes in the *m*-values were obtained between the wild-type and F221del proteins. A lowered *m*-value usually indicates a deviation from two-state pathway (Pace, 1986). Based on the similar *m*-values for the wild-type and F221del proteins, it is reasonable to assume that the F221del mutant follows a two-state unfolding/refolding pathway. The magnitude of the *m*-value is also an indication of the co-operative nature of the non-covalent interactions that stabilise the

GSTA1-1

1guh **E^{209} K^{210} S^{211} L^{212} E^{213} E^{214} A^{215} R^{216} K^{217} I^{218} F^{219}** R^{220} F^{221}

1gse **E^{209} K^{210} S^{211} L^{212} E^{213} E^{214} A^{215} R^{216} K^{217} I^{218} F^{219}** R^{220} F^{221}

1gsf E^{209} **K^{210} S^{211} L^{212} E^{213} E^{214} A^{215} R^{216} K^{217} I^{218} F^{219}** R^{220} F^{221}

1gsd ----------

1ev4 K^{210} Q^{211} I^{212} E^{213} **E^{214} A^{215} R^{216} K^{217} I^{218}** Y^{219} K^{220} F^{221}

1ev9 **K^{210} Q^{211} I^{212} E^{213} E^{214} A^{215}** R^{216} K^{217} I^{218} F^{219} K^{220} F^{221}

1f3a **A^{209} K^{210} Q^{211} I^{212} Q^{213} E^{214} A^{215} R^{216}** K^{217} A^{218} F^{219} K^{220} I^{221}

1f3b **A^{209} K^{210} Q^{211} I^{212} Q^{213} E^{214} A^{215} R^{216} K^{217} A^{218} F^{219}** K^{220} I^{221}

GSTA4-4

1gul **E^{209} I^{210} Y^{211} V^{212} R^{213} T^{214} V^{215} Y^{216} N^{217} I^{218}** F^{219} R^{220} P^{221}

1gum **E^{209} I^{210} Y^{211} V^{212} R^{213} T^{214} V^{215} Y^{216} N^{217} I^{218}** F^{219} R^{220} P^{221}

Figure 30. Schematic diagram of helix 9 at the C-terminal end of various class alpha GST isoforms. The bold underlined segments represent the residues that are involved in the formation of the C-terminal helix 9. The dashed line (1gsd) indicates that helix 9 is crystallographically "invisible" because of the absence of clear electron density information in the crystal structure. The positions of the residues at the C-terminus are indicated by superscripts. Depending on the isoform, the N-terminal end is indicated by E^{209}, A^{209} or K^{210} and the C-terminal by F^{221}, I^{221} or P^{221}. The PDB accession codes are indicated. 1guh, human GSTA1-1 complexed with *S*-benzylglutathione (Sinning *et al*., 1993). 1gse, human GSTA1-1 complexed with GSH-EA conjugate (Cameron *et al*., 1995). 1gsf, human GSTA1-1 complexed with ethacrynic acid (EA) (Cameron *et al*., 1995). 1gsd, the apo-form of human GSTA1-1 (Cameron *et al*., 1995). 1ev4, a double mutant (W20F/F219Y) of the rat GSTA1-1 complexed with glutathione sulfonate (Adman *et al*., 2001). 1ev9, W20F mutant of rat GSTA1-1 complexed with glutathione sulfonate (Adman *et al*., 2001). 1f3a; murine GSTA1-1 complexed with GSH (Gu *et al*.,

2000); 1f3b, murine GSTA1-1 complexed with the GS-Bpd glutathione conjugate (Gu *et al*., 2000). 1gul, human GSTA4-4 complexed with *S*-(2-iodobenzyl) glutathione (Bruns *et al*., 1999) and 1gum, the apo-form of human GSTA4-4 (Bruns *et al*., 1999).

native state.

One question that we may ask is whether the results of the $\Delta G(H_2O)$ and *m*-value obtained for F221del from a single physical method could be affected by the presence of an undetected intermediate. If the unfolding of the wild-type protein is consistent with a two-state unfolding process, a comparison of the results obtained between the wild-type and mutant protein can answer this question. To discard the presence of an intermediate one should observe no changes in the *m*-value or a slight increase (see section 5.3.3 for the *m*-values). The presence of an intermediate will always translate into an underestimation of the *m*-values for the N $\Leftrightarrow$ U process. (Soulages, 1998). The urea-induced equilibrium unfolding studies for F221 are consistent with the two-state model previously proposed for the wild-type hGSTA1-1 (Wallace *et al*., 1998b). Therefore, F221 situated at the C-terminus of the protein does not affect the conformational stability of hGSTA1-1.

5.5 Conclusion

F221 is the last residue located at the C-terminus of helix 9 of hGSTA1-1. The removal of this residue does not affect the gross structural properties of the protein because no changes in secondary, tertiary and quaternary structure were observed. In addition, F221 is not required for catalysis nor does it impact on the conformational stability of the protein. The deletion of F221 from the C-terminus of hGSTA1-1 does, however, impact on the ligandin function of the protein. The deletion mutant also exhibits a more mobile C-terminal helix 9 than the wild-type protein. Therefore, a possible role for F221 is the stabilisation of helix 9 at the C-terminus of hGSTA1-1.

Chapter 6

THERMODYNAMICS OF LIGAND BINDING TO HUMAN GLUTATHIONE TRANSFERASE A1-1 USING ISOTHERMAL TITRATION CALORIMETRY

6. Glutathione and glutathione sulfonate binding to wild-type and Y8F hGSTA1-1

6.1 Role of Y8 in the catalytic mechanism of hGSTA1-1

The cytosolic GSTs are composed of two active sites per dimer, which behave independently of one another (Danielson and Mannervik, 1985). Each active site consists of a highly specific site (G-site) for glutathione binding and a less specific hydrophobic binding site for hydrophobic electrophilic substrates (H-site). The lack of specificity allows the GST enzymes to bind a variety of substrates at the H-site. A conserved overall active site core region is observed in the GSTs. A ββα motif in the cytosolic GSTs is responsible for the recognition of the γ-glutamyl moiety of the glutathione tripeptide. This structural element commences with a *cis*-proline residue just before β3 and continues through the α3-helix and supplies hydrogen bonding partners that recognise the amino and carboxylate groups at the chiral α-carbon of the γ-glutamyl residue. These interactions involve two residues located in the turn between strand β4 and the α3-helix, a glutamine/glutamate residue followed by a serine/threonine. The *cis*-prolyl residue that precedes this region helps to conserve the overall fold of the domain (Armstrong, 1997).

An evolutionary conserved tyrosine residue (Tyr8, class alpha; Tyr6, class mu; Tyr7, classes pi and sigma) located in the G-site has been shown to be essential for the activation of glutathione in all the gene classes except the class theta enzymes. The class theta enzymes have recruited a hydroxyl group from a serine residue located near the N-terminus of the polypeptide to activate the sulfhydryl group of bound glutathione (Wilce *et al*., 1995; Board *et al*., 1995). A key feature in the catalytic mechanism is the lowering of the pK_a of the thiol of reduced glutathione from 9 in solution to between 6 and 7 when bound to the protein (Graminski *et al*., 1989a, 1989b; Liu *et al*., 1992; Wang *et al*., 1992; Kong *et al*., 1992; Atkins *et al*., 1993).

To date, the actual role of the tyrosyl hydroxyl group (classes alpha, mu, pi and sigma) at the active site remains a matter of much debate. The two proposed mechanisms differ over the position of the protons in the active site. The question posed is whether the active site tyrosyl residue acts a hydrogen bond donor or a hydrogen bond acceptor (general base). The arguments in favour of the active site tyrosyl residue acting as general base (Atkins *et al*., 1993; Dietze *et al*., 1996a; Karshikoff *et al*., 1993; Meyer *et al*., 1993) is based on the observation that the hydroxyl group of tyrosine in the class alpha enzyme has an unusually low pK_a value (~ 8.5) (Bjornestedt *et al*., 1995). In contrast, the pK_a of the hydroxyl group in M1-1 enzyme is ~ 10 (Xiao *et al*., 1996). If one considers that at neutral pH much less than 50% of the tyrosyl side chain is ionised then the argument that the hydroxyl group acts as a general base is not appropriate. A better explanation would be in favour of the tyrosyl hydroxyl group acting as a hydrogen bond donor. The evidence for this comes from a study in which all fourteen tyrosyl residues in the class mu enzyme were replaced with 3-fluorotyrosine and it appears that the active site tyrosine acts as a surrogate solvent molecule that donates a hydrogen bond that stabilises the thiolate anion (Parsons and Armstrong, 1996). Also, the fact that glutathione sulfonate and γ-Glu-AspGly binds to the enzyme with a higher affinity than does reduced glutathione argues against a significant ionisation of the active site hydroxyl in uncomplexed enzymes (Graminski *et al*., 1989a; Dirr *et al*., 1994a). This evidence, therefore, argues in favour of the tyrosyl hydroxyl group acting as a hydrogen bond donor and not as a general base in the catalytic cycle of cytosolic GSTs.

It is currently held that the tyrosine 8 hydroxyl group at the active site controls the dynamics of helix 9 in the class alpha GSTs and is required for efficient product release. Additionally, the phenolic hydroxyl group may also affect the rates of ligand binding and dissociation (Gustafsson *et al*., 1999; Nieslanik and Atkins, 2000).

In the present study, a comparison of the binding thermodynamics of active site ligands (reduced glutathione and glutathione sulfonate) to the wild-type and Y8F mutant proteins were investigated using isothermal titration calorimetry (ITC). In addition to their catalytic function, GSTs also function as ligand binding proteins. ITC was, therefore, also

used to characterise the thermodynamic parameters of non-substrate ligand binding to the wild-type protein using ANS and BSP.

6.1.1 Construction and identification of the Y8F mutant plasmid DNA

Possible mutant plasmid DNA was identified using restriction enzyme digestion analysis. The products of a *Hind* III digestion of wild-type and mutant plasmid DNA were electrophoresed on a 1.2% agarose gel containing ethidium bromide. The results are shown in Figure 31. Lanes 2 and 4 show the expected fragment sizes (~ 3000 bp) of two individual mutant plasmid DNA preparations. Lane 6 represents the wild-type plasmid DNA also digested with *Hind* III and the DNA fragment bands at the expected position around 3300 bp. Lanes 3, 5 and 7 confirms that the undigested mutant plasmid DNA is the correct size as the wild-type plasmid DNA. The banding positions of the wild-type and mutant plasmid DNA are as predicted thus confirming the successful incorporation of the additional *Hind* III diagnostic restriction site in the mutant plasmid DNA. The entire cDNA region of the mutant plasmid DNA was sequenced. The relevant region containing the *Hind* III diagnostic restriction site and the Y8F mutation is indicated in Figure 32. No spurious mutations were observed in the mutant plasmid DNA.

6.1.2 Over-expression and purification of the Y8F mutant

The Y8F mutant protein has a subunit molecular mass of ~ 27 kDa (tertiary structure) and a dimeric molecular mass of ~ 55 kDa (quaternary structure). The purity of the mutant protein was confirmed using SEC-HPLC.

6.2 Biochemical characterisation of Y8F hGSTA1-1

6.2.1 Fluorescence spectral properties of Y8F hGSTA1-1

The lone tryptophan residue was selectively excited at 295 nm. The emission spectra for the Y8F mutant exhibited wavelength emission maxima of 325 nm and 355 nm for the folded and the unfolded conformations, respectively (Figures 33A and B). The emission spectrum is similar to that observed for the wild-type protein (Figure 23A). This result implies that no structural changes have occurred at the domain I-domain II interface. Thus, the tertiary structure and polarity of the environment of the tryptophan residue is

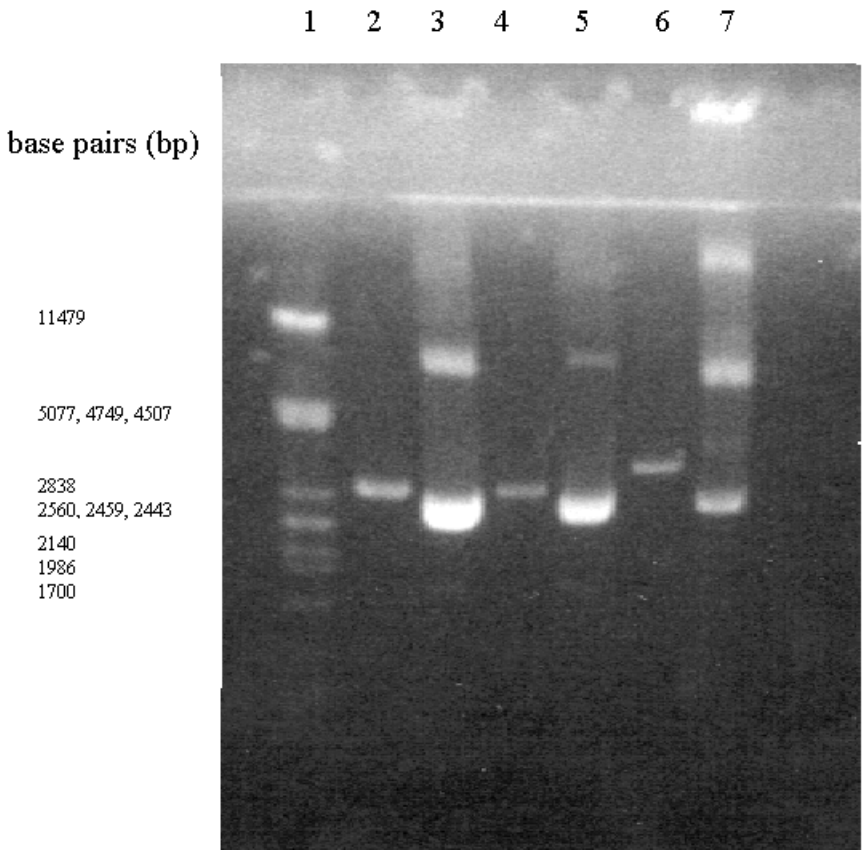

Figure 31. Identification of the Y8F mutant plasmid DNA on a 1.2% agarose gel. Lane 1: λDNA digested with *Pst* I. Lanes 2 and 4: two possible mutant plasmid DNA constructs digested with the diagnostic restriction enzyme, *Hind* III. Lanes 3 and 5 represent the uncut mutant plasmid DNA corresponding to lanes 2 and 4, respectively. Lane 6: wild-type plasmid DNA digested with *Hind* III. Lane 7 shows the uncut wild-type plasmid DNA.

A.

5′ AAG CCC AAG **CTC** CAC **TAC** TTC AAT GCA CGG GGC 3′

5′ AAG CCC **AAG CTT** CAC **TTC** TTC AAT GCA CGG GGC 3′

B.

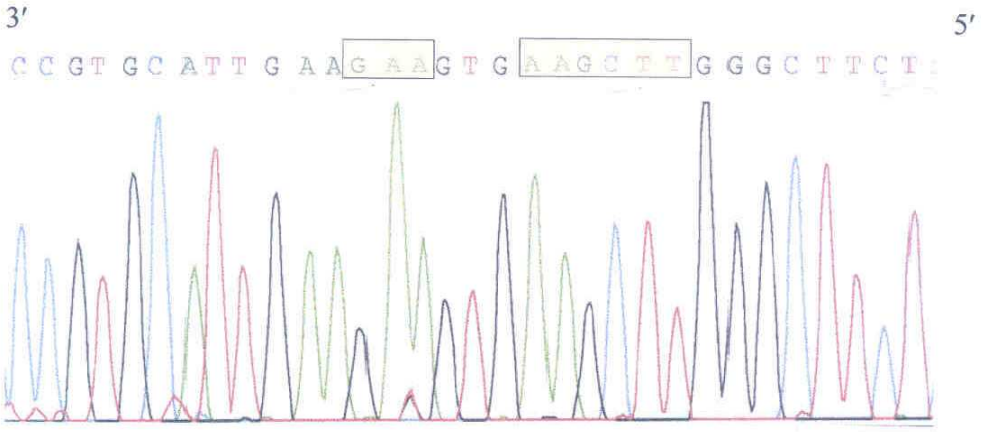

Figure 32. (A) Region of the wild-type nucleotide sequence showing the location of Y8 (codon = **TAC**). Tyrosine at position 8 was replaced with phenylalanine (codon change from **TAC→TTC**). A translationally silent mutation was also incorporated into the mutagenic oligonucleotide primer. The codon for leucine (**CTC**) was changed to **CTT** thus engineering an additional *Hind* III restriction site (**AAG CTT)** in the Y8F mutant plasmid DNA. (B) Results of the Y8F mutant plasmid DNA sequencing reaction. The primer used for the sequencing reaction generated the 3′ to 5′ sequence of the strand shown in (A). Therefore, the mutation (F8) corresponds to GAA. The presence of F8 (codon = GAA) and the diagnostic restriction site (AAG CTT) are boxed in.

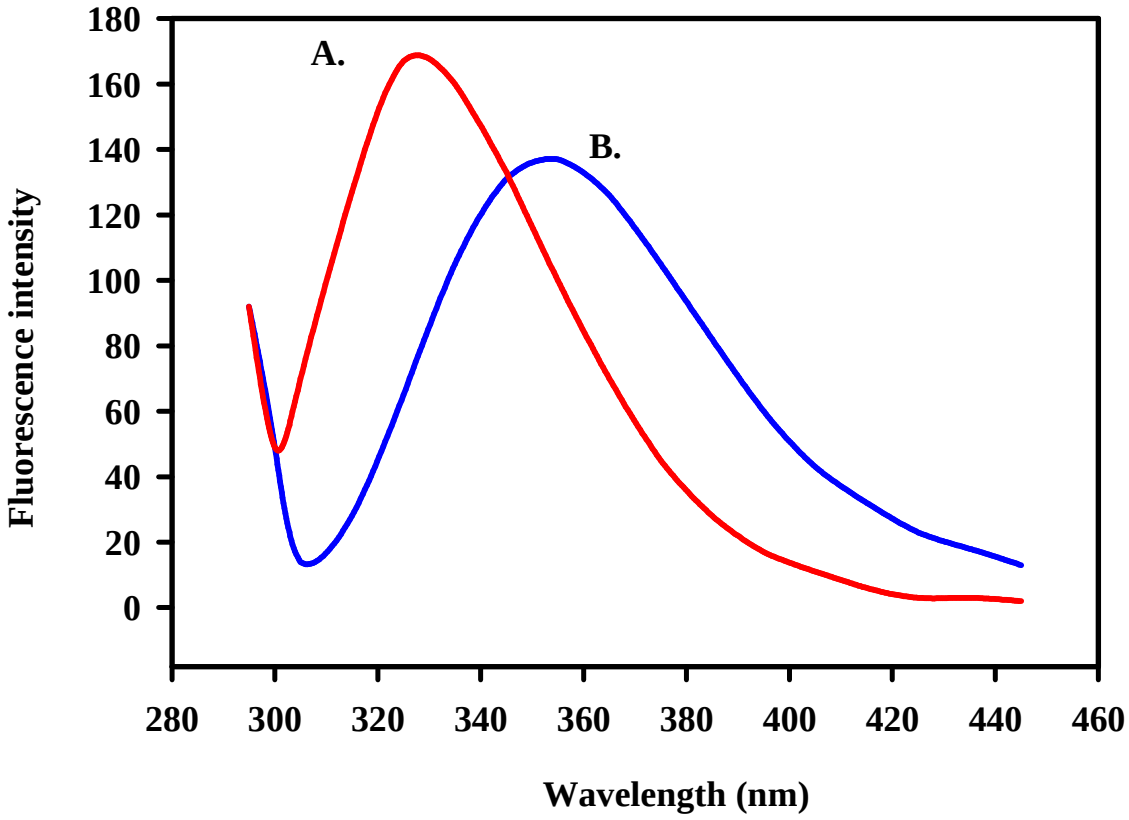

Figure 33. Spectral analysis of the Y8F mutant. The lone tryptophan 20 residue was selectively excited at 295 nm and the emission was monitored from 295 nm. (A) The wavelength emission maximum at 325 nm in the absence of urea and (B) the wavelength emission maximum at 355 nm in the presence of 8 M urea.

unchanged. Tryptophan 20, therefore, retains its ability to serve as a local reporter of events occurring at the interdomain interface.

6.2.2 Far-UV circular dichroism

Far-UV circular dichroism measurements of the Y8F mutant indicated that the mutation does not impact on the secondary structural content of the protein. The spectrum exhibited two ellipticity minima at 222 nm and 208 nm. This is typical for a protein that contains a high α-helical content. The spectrum of the Y8F mutant (Figure 34) is similar to that of the wild-type protein (Figure 24).

6.2.3 Specific activity measurements using the CDNB-conjugation assay

The specific activity of the Y8F mutant was determined under standard enzyme assay conditions of 1 mM reduced GSH and 1 mM CDNB as the substrates. The results are summarised in Table 4. It is evident that the mutant enzyme displays ~ 6% of the wild-type specific activity under the assay conditions. This indicates that the Y8 residue located in the active site of hGSTA1-1 is not essential in the catalytic mechanism of the protein. This result is similar to that of Stenberg *et al.* (1991). This group reported that the Y8F mutant has ~ 3% of the wild-type specific activity under the same conditions.

6.2.4 Specific activity measurements using the cumene hydroperoxide assay

The human class alpha GSTs are known to exhibit peroxidase activity as demonstrated previously (Lawrence and Burk, 1976; Stenberg *et al.*, 1991). The peroxidase activity of the Y8F mutant was determined using cumene hydroperoxide as the substrate. The specific activities for the wild-type and Y8F proteins are given in Table 4. The Y8F mutant represents ~ 6% of the specific activity of the wild-type protein. The mutant peroxidase activity presented here is also in agreement with that found by Stenberg *et al*. (1991).

6.3 Thermodynamics of ligand binding to G-site of wild-type and Y8F hGSTA1-1

In order to understand the structural basis for protein-ligand and protein-protein interactions and molecular recognition in general, one is required to characterise the

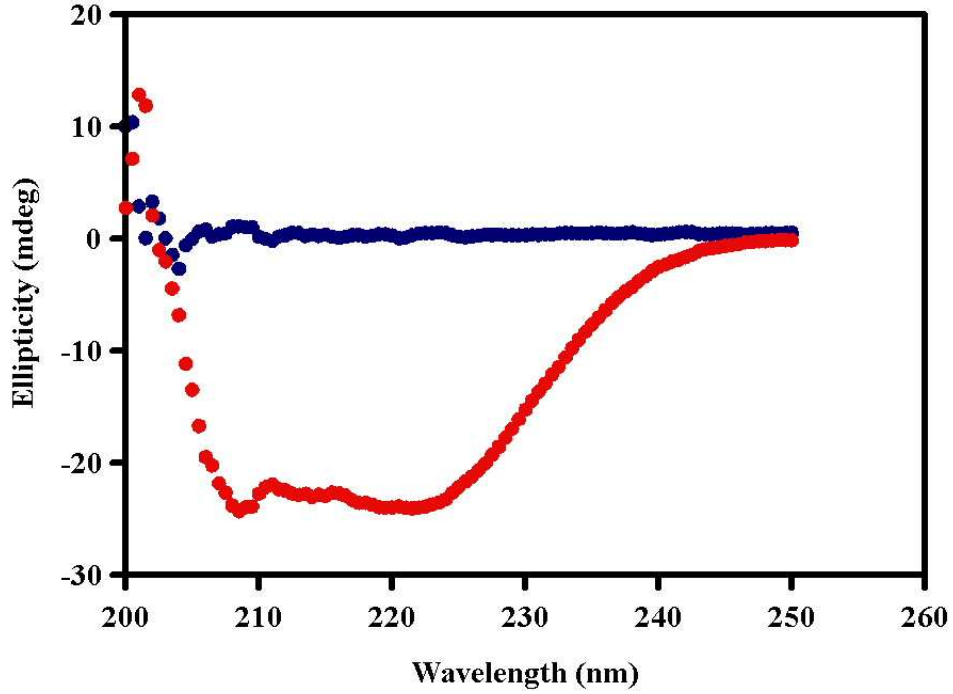

Figure 34. Far-UV circular dichroism spectrum for Y8F hGSTA1-1. The spectra shown in red and blue are for the native Y8F protein and buffer, respectively. The conditions were 2 μM native protein in 20 mM sodium phosphate buffer, pH 6.5, containing 0.1 M NaCl. The above spectra are an average of 20 runs.

Table 4. Specific activities of the wild-type and Y8F proteins using two different enzyme assay systems. The standard assay system involves conjugation between reduced glutathione and CDNB. The peroxidase system involves determination of peroxidase activity towards cumene hydroperoxide (CuOOH) as the substrate (see Chapter 3).

Protein	Specific activity (μmol/min/mg) towards substrate: CDNB	CuOOH
Wild-type hGSTA1-1	52.2	9.4
Y8F hGSTA1-1	3.3	0.5

binding energetics completely and then correlate the energetics with the structures involved. ITC measures directly the energetics of ligand-binding reactions at constant temperature by measuring the heat evolved or absorbed in the stepwise addition of a ligand to a solution containing a macromolecule until saturation of the available binding sites on the macromolecule has been achieved.

Isothermal titration calorimetry (ITC) was used to obtain a complete energy profile of the association of the active site ligands, glutathione and glutathione sulfonate, with wild-type and Y8F hGSTA1-1 proteins. In particular, the role of tyrosine 8 hydroxyl group at the active site in ligand binding will be addressed.

6.3.1 Glutathione (GSH) binding to wild-type and Y8F proteins

The binding energetics of the physiological tripeptide glutathione (γ-Glu-Cys-Gly) to the wild-type and Y8F proteins were measured using ITC. Figures 35 and 36 show representative results of calorimetric titrations of glutathione binding to the wild-type and Y8F proteins, respectively. All the raw data were corrected and fitted using the ORIGIN software. Control reactions in which ligand was injected into buffer represented the heat of dilution. The heat of dilution was very similar to that seen at the end of a titration of the protein with glutathione. To correct for any heat of dilution, the integrated areas of the post-saturation peaks were averaged and then subtracted from the raw data (Figures 35A and 36A). The sum of the areas of the peaks after each injection are normalised per amount of ligand in the ITC sample cell and represents the enthalpy of the binding of glutathione to each of the proteins (Figures 35B and 36B). The most notable feature of all the binding isotherms is that the binding of glutathione to the wild-type and mutant protein is exothermic. All the data from each experiment fit well to a single-site binding

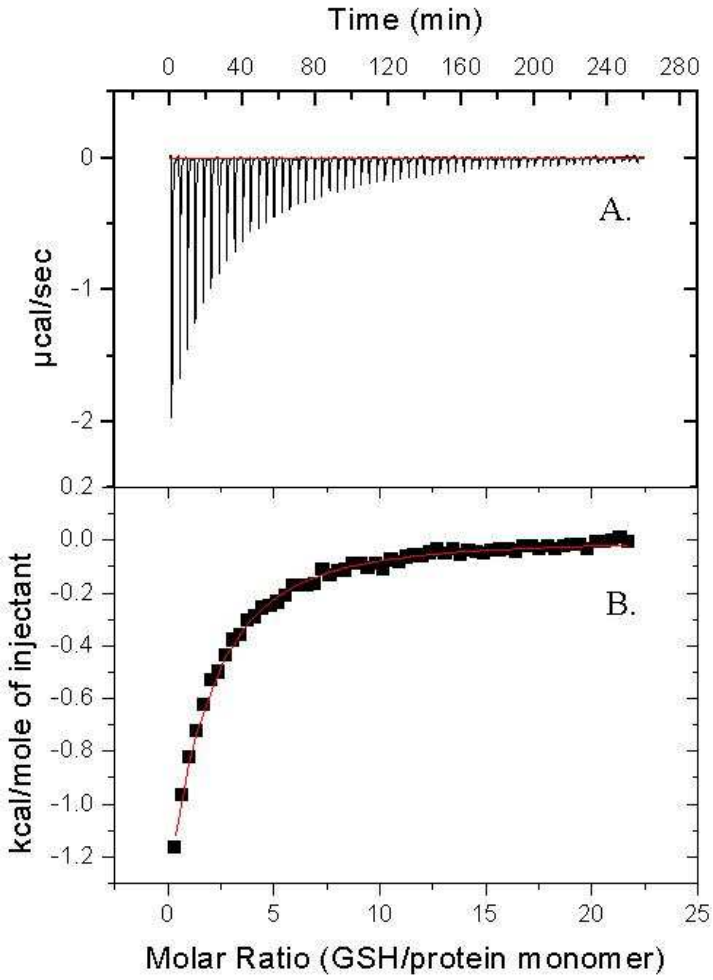

Figure 35. A representative calorimetric titration profile of the binding of reduced glutathione to the wild-type hGSTA1-1 protein. The experiment was performed at 20°C. The conditions were: 0.12 mM protein monomer concentration and 20 mM reduced glutathione in 20 mM sodium phosphate buffer, pH 6.5, containing 0.1 M NaCl, 1 mM EDTA, 0.02% sodium azide and 1 mM *tris*-(carboxyethyl)-phosphine (TCEP). Panel A shows the exothermic heat effects associated with the injection of reduced glutathione into the ITC sample cell containing the wild-type protein. Panel B shows the binding isotherm (corrected for heats of dilution) corresponding to the data in panel A. The solid line through the data represents the best fitted curve obtained using the ORIGIN software.

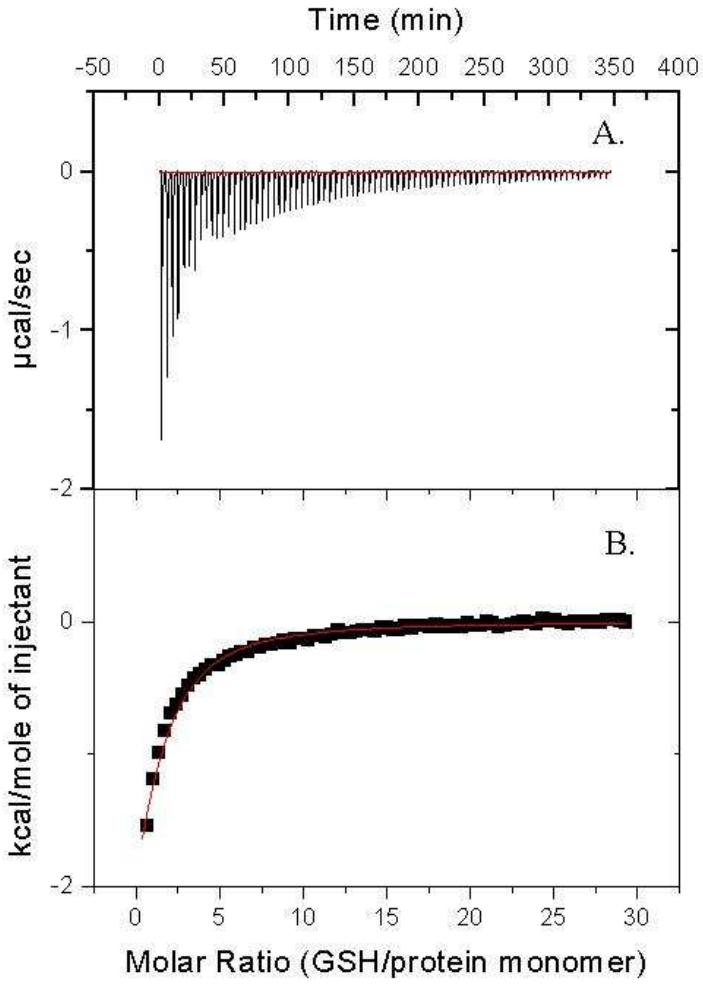

Figure 36. A representative calorimetric titration profile of the binding of reduced glutathione to the Y8F mutant protein. The experiment was performed at 20°C. The conditions were: 0.08 mM protein monomer concentration and 20 mM reduced glutathione in 20 mM sodium phosphate buffer, pH 6.5, containing 0.1 M NaCl, 1 mM EDTA, 0.02% sodium azide and 1 mM *tris*-(carboxyethyl)-phosphine (TCEP). Panel A shows the exothermic heat effects associated with the injection of reduced glutathione into the ITC sample cell containing the mutant protein. Panel B shows the binding isotherm (corrected for heats of dilution) corresponding to the data in panel A. The solid line through the data represents the best fitted curve obtained using the ORIGIN software.

model. The titration curve exhibits a decrease in the exothermic heat of binding after each successive injection. The reaction is, therefore, characterised by a series of negative peaks representative of a favourable enthalpy change.

Table 5 summarises the experimental parameters obtained for the binding of glutathione to the wild-type (Table 5A) and Y8F (Table 5B) mutant proteins, respectively. In order to achieve a satisfactory fit, the stoichiometry of the reaction was fixed (independent parameter) at a value of one based on the stoichiometry data from GST X-ray crystal structures with GSH. Unlike the GSX product analogues, which can bind sites other than the G-site (Ji *et al*., 1996), crystallographic data suggests that there is no evidence for the existence of additional GSH binding sites (Reinemer *et al*., 1991; Sinning *et al*., 1993; Cameron *et al*., 1995). Therefore, one molecule of glutathione binds to one protein subunit. Atkins and co-workers also found that the stoichiometry of ligand binding of GS-EA to the rat class alpha GSTA1-1 was one molecule of GS-EA per protein monomer (Nieslanik *et al*., 2001). The binding of glutathione sulfonate to the wild-type hGSTA1-1 also displays a stoichiometry of one molecule glutathione sulfonate per protein monomer (see section 6.3.2 of this thesis). The ITC results (Table 5) show that the strength of glutathione binding to wild-type and mutant is greater at lower temperature and decreases as the temperature is increased. A comparison of the binding constants for the wild-type hGSTA1-1 protein and GSH obtained using spectroscopic techniques (Allardyce *et al*., 1999; Dirr and Wallace, 1999; Gustafsson *et al*., 1999) are in agreement with the measurements obtained using ITC. The removal of the phenolic hydroxyl group in the Y8F mutant, however, displays different binding affinities when compared to the wild-type protein. Overall, it appears that the Y8F mutant binds GSH tighter than the wild-type protein. Allardyce *et al*. (1999) recently found that the Y8F hGSTA1-1 binds the glutathione conjugate, *S*-dinitrophenylglutathione, 20-fold more tightly than the wild-type protein. The explanation for this effect was that the hydroxyl group of Y8 is situated close to the sulfur atom of *S*-benzylglutathione complexed with enzyme, and the absence of the tyrosyl hydroxyl group allows the ligand to adopt a more favourable binding mode. Therefore, the binding interactions for both the GSH and

Table 5. Energetics of the interaction between wild-type (A) and Y8F (B) hGSTA1-1 with reduced glutathione (GSH) at different temperature conditions. All the values are based on a single experiment and the errors were obtained by fitting the titration data using the ITC software programme (ORIGIN 5.0).

A.

Temperature (^{O}C)	N	K_d (mM)	ΔH^{O} (kJ/mol)	ΔS^{O} (J/mol/K)	ΔG^{O} (kJ/mol)
5.1	1	0.18±0.01	-11.1±0.1	32.1	-20.0
10.1	1	0.21±0.01	-12.9±1.7	24.9	-20.0
15.0	1	0.23±0.02	-14.1±0.1	20.6	-20.1
20.0	1	0.31±0.01	-17.9± 0.2	6.1	-19.7
25.0	1	0.37±0.01	-19.5±0.3	0.3	-19.6

B.

Temperature (^{O}C)	N	K_d (mM)	ΔH^{O} (kJ/mol)	ΔS^{O} (J/mol/K)	ΔG^{O} (kJ/mol)
5.1	1	0.1±0.01	-9.0±0.3	48.4	-22.5
10.1	1	0.1±0.01	-15.3±0.4	22.5	-21.6
20.1	1	0.2±0.01	-23.8±0.4	-9.3	-21.1
25.5	1	0.3±0.01	-33.8±0.6	-46.1	-20.1

dinitrophenyl moieties are optimised.

For all the glutathione-binding experiments performed, an increase in temperature resulted in an increase in the binding enthalpy of the reaction. The heat capacity change was determined by performing the calorimetric experiments at different temperatures under the same pH and buffer conditions. The heat capacity change associated with the binding reaction (protein-ligand complex formation) is estimated from the slope of the linear regressions (Figures 37A and B). The ΔC_p is -0.4 kJ/mol/K and -1.2 kJ/mol/K for the wild-type and Y8F proteins, respectively. The slopes are negative in both cases but the values differ greatly. It has been shown that the heat capacity change associated with protein-protein interactions as well as protein unfolding experiments can be correlated to changes in the solvent-accessible surface area for a given process (Makhatadze and Privalov, 1990; Spolar *et al*., 1992; Spolar and Record, 1994; Makhatadze and Privalov, 1995; Baker and Murphy, 1997; Luque *et al*., 1998c; Todd and Freire, 1999). The negative ΔC_p is a good indicator of the changes in hydrophobic interactions with binding, being negative if hydrophobic bonds are formed and positive if they are broken (Luque *et al*., 1998b). The binding processes observed for the wild-type and Y8F mutant proteins are characteristic of a binding process driven by the gain in solvent entropy associated with the burial of solvent-accessible hydrophobic surface area.

6.3.2 Glutathione sulfonate (GSO_3^-) binding to wild-type and Y8F proteins

Glutathione sulfonate is a competitive inhibitor of GSTs. X-ray crystal structure data of the GST in complex with glutathione sulfonate indicate that one molecule of glutathione sulfonate binds per protein monomer (Reinemer *et al*., 1991; Adman *et al*., 2001). Glutathione sulfonate makes 15 direct polar contacts and four water-mediated contacts with the protein molecule (Dirr *et al*., 1994a). The interactions observed between pGSTP1-1 and GSO_3^- are very similar to those seen in the structure of *S*-benzylglutathione complexed to hGSTA1-1 at the G-site (see Figure 4) (Sinning *et al*., 1993).

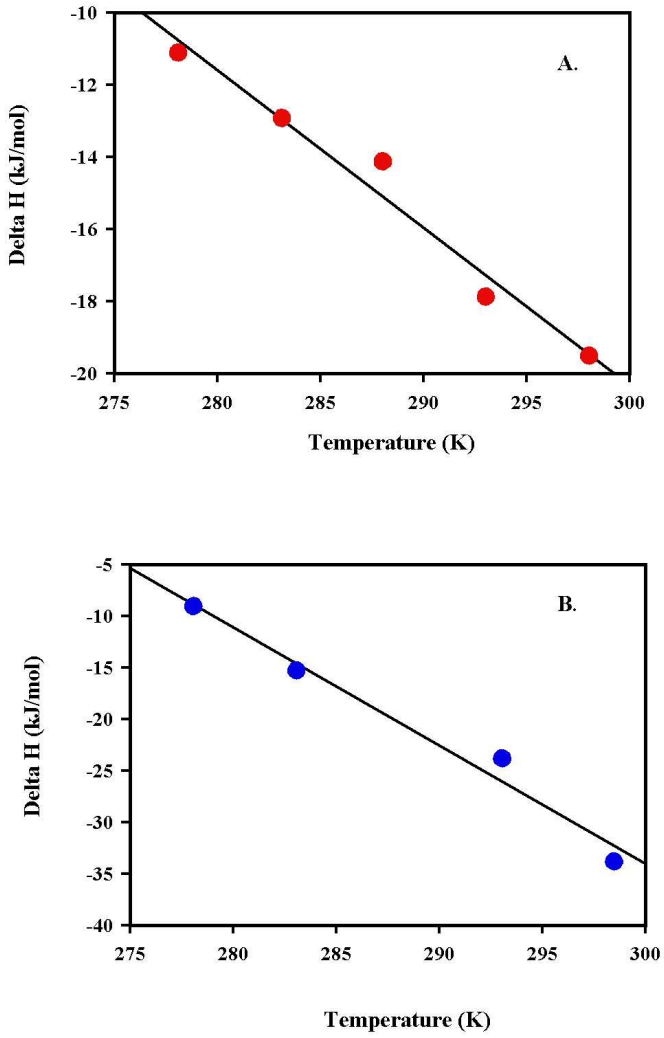

Figure 37. Temperature-dependence of the enthalpy change, ΔH^{O}, upon binding of glutathione to the (A) wild-type (filled red circles) and (B) Y8F (filled blue circles) hGSTA1-1 protein, respectively. The data are summarised in Table 7. The solid line through the points is the linear regression fit to the data. The slope of the linear regression yields the change in heat capacity (ΔC_p) upon ligand binding to each of the proteins. The correlation coefficient for (A) and (B) is 0.99 and 0.98, respectively.

The energetics of the association of glutathione sulfonate and the wild-type and Y8F hGSTA1-1 proteins were measured using ITC. Figures 38 and 39 show typical calorimetric titrations of ligand to the wild-type and Y8F proteins, respectively. The peaks in panel A (Figures 38 and 39) correspond to the heat evolved upon addition of ligand to the protein sample; i.e., an exothermic interaction. The area under each peak diminishes with each successive injection of glutathione sulfonate into the protein solution. The small peaks observed towards the end of each titration experiment are representative of the heat of dilution. At this point, all the available ligand binding sites on the protein molecule have been saturated. The averaged heat of the post-saturation peaks was subtracted from the raw data to obtain the heat evolved from each injection. The ΔH^O is obtained by integrating the area under each peak and dividing this by the moles of ligand added. All calculations were performed using the ORIGIN software provided with the ITC machine. The ΔH^O for the wild-type and Y8F mutant protein is shown in panel B (Figures 38 and 39), respectively.

ITC experiments were performed as a function temperature from 5-25°C with all other experimental conditions kept constant; i.e., buffer and pH conditions. Under these conditions, ITC provided thermodynamic parameters for the association of glutathione sulfonate to the wild-type and Y8F proteins. All the titration data from the wild-type and Y8F proteins are exothermic and each experiment fits well to a single-site binding model.

Analyses of the ITC data reported stoichiometry values of ~ 1 for the wild-type and Y8F proteins. These values are consistent with X-ray crystal structure data that shows a stoichiometry of one molecule of glutathione sulfonate binding per monomer of wild-type protein (Dirr *et al*., 1994a; Adman *et al*., 2001). The stoichiometry values obtained for the wild-type and Y8F proteins are summarised in Table 6A and B, respectively.

The binding affinities (K_d) for glutathione sulfonate are in the micromolar range for the wild-type and Y8F proteins. A comparison of the K_d values obtained for glutathione and glutathione sulfonate suggests that glutathione sulfonate binds the wild-type protein with a higher affinity at the active site. Both proteins exhibit decreasing binding affinity and

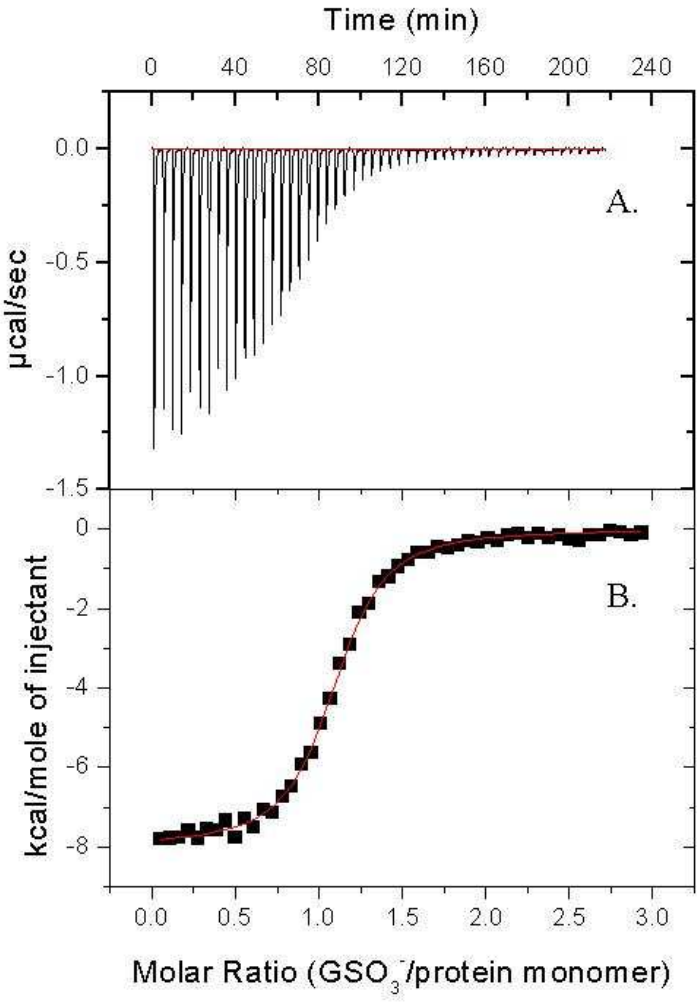

Figure 38. A representative calorimetric titration profile of the binding of glutathione sulfonate to the wild-type protein. The experiment was performed at 5°C. The conditions were: 0.06 mM protein monomer concentration and 1.1 mM glutathione sulfonate in 20 mM sodium phosphate buffer, pH 6.5, containing 0.1 M NaCl, 1 mM EDTA, 0.02% sodium azide and 1 mM *tris*-(carboxyethyl)-phosphine (TCEP). Panel A shows the exothermic heat effects associated with the injection of glutathione sulfonate into the ITC sample cell containing the wild-type protein. Panel B shows the binding isotherm (corrected for heats of dilution) corresponding to the data in panel A. The solid line through the data represents the best fitted curve obtained using the ORIGIN software.

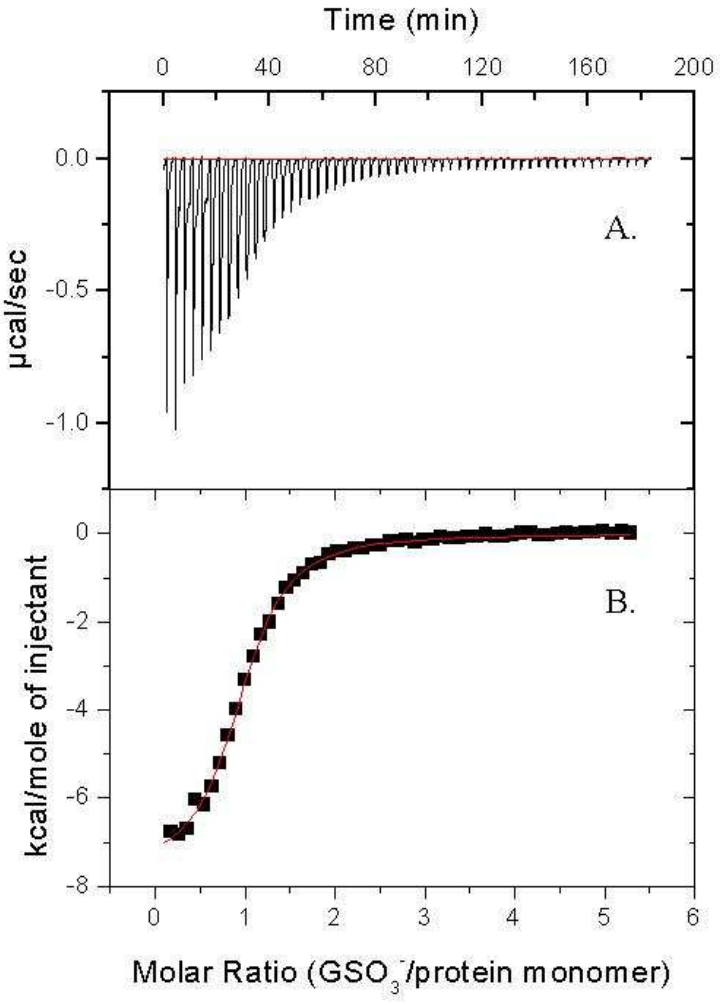

Figure 39. A representative calorimetric titration profile of the binding of glutathione sulfonate to the Y8F mutant protein. The experiment was performed at 10°C. The conditions were: 0.05 mM protein monomer concentration and 1.1 mM glutathione sulfonate in 20 mM sodium phosphate buffer, pH 6.5, containing 0.1 M NaCl, 1 mM EDTA, 0.02% sodium azide and 1 mM *tris*-(carboxyethyl)-phosphine (TCEP). Panel A shows the exothermic heat effects associated with the injection of glutathione sulfonate into the ITC sample cell containing the wild-type protein. Panel B shows the binding isotherm (corrected for heats of dilution) corresponding to the data in panel A. The solid line through the data represents the best fitted curve obtained using the ORIGIN software.

Table 6. Energetics of the interaction between (A) wild-type and (B) Y8F hGSTA1-1 with the anionic inhibitor glutathione sulfonate (GSO_3^-) at different temperature conditions. All the values are based on a single experiment and the errors were obtained by fitting the titration data using the ITC software programme (ORIGIN 5.0).

A.

Temperature (^OC)	N	K_d (μM)	ΔH^O (kJ/mol)	ΔS^O (J/mol/K)	ΔG^O (kJ/mol)
6.3	1.1±0.01	1.3±0.1	-33.4±0.2	-6.8	-31.5
10.0	1.1±0.01	1.6±0.1	-35.4±0.2	-14.4	-31.4
16.0	1.0±0.01	2.1±0.1	-38.6±0.3	-24.7	-31.4
20.0	1.1±0.01	2.7±0.2	-40.9±0.4	-32.9	-31.3
25.0	1.0±0.01	4.0±0.3	-41.8±0.6	-36.7	-30.8

B.

Temperature (^OC)	N	K_d (μM)	ΔH^O (kJ/mol)	ΔS^O (J/mol/K)	ΔG^O (kJ/mol)
5.1	1.0±0.01	2.1±0.2	-23.1±0.4	26.0	-30.3
10.1	1.0±0.01	3.8±0.2	-32.1±0.3	-9.8	-29.4
15.1	1.0±0.01	4.5±0.3	-36.5±0.5	-24.1	-29.5
25.0	1.0±0.02	11.5±0.7	-51.3±1.3	-77.5	-28.2

increasing observed binding enthalpy (ΔH^O) with increasing temperature. The enthalpy of the interaction suggests that the binding of glutathione sulfonate is comparable between the wild-type and mutant proteins.

The association reaction of the anionic ligand with wild-type and Y8F proteins is characterised by a linear decrease in the observed enthalpy of the reaction, ΔH^O, with temperature. The slopes of these plots are indicative of the constant heat capacity change, ΔC_p, for wild-type and Y8F hGSTA1-1 proteins and are shown in Figures 40A and B, respectively. The Y8F mutant protein displays a ΔC_p value that is ~ 3-fold greater than the wild-type protein. The ΔC_p values are -0.47 kJ/mol/K and -1.38 kJ/mol/K for wild-type and Y8F proteins, respectively.

6.4 Discussion

Isothermal titration calorimetry (ITC) is an extremely sensitive and powerful technique that can be used to obtain detailed thermodynamic parameters involving molecular associations. Molecular recognition, as in protein-ligand interactions, is one of the most relevant fields in structural biology today. A wealth of structural and functional information exists for the GST superfamily. Recently, a kinetics study was the first to report on a model for the folding and assembly of dimeric human glutathione transferase (Wallace and Dirr; 1999). Extensive information has also been reported on the role of a unique C-terminal helix 9 in catalysis, ligandin function and conformational stability of the class alpha GSTs (Dirr and Wallace, 1999; Nieslanik and Atkins, 2000; Board and Mannervik, 1991; Gustafsson *et al*., 1999; Allardyce *et al*., 1999). Despite this, very little is known about the thermodynamics of ligand binding to the GST superfamily. Presently, there are only two reports on the thermodynamics of ligand binding to GSTs (Nieslanik and Atkins, 2000; Nieslanik *et al*., 2001). Therefore, an understanding of the forces that drive ligand binding are required for a clearer understanding of the functional properties of this important class of enzymes. Isothermal titration calorimetry (ITC) is an ideal method for the study of the thermodynamics of ligand binding to GSTs. The study presented here is the first to describe the energetics of binding of active site ligands, glutathione and glutathione sulfonate, to the wild-type and Y8F hGSTA1-1 proteins.

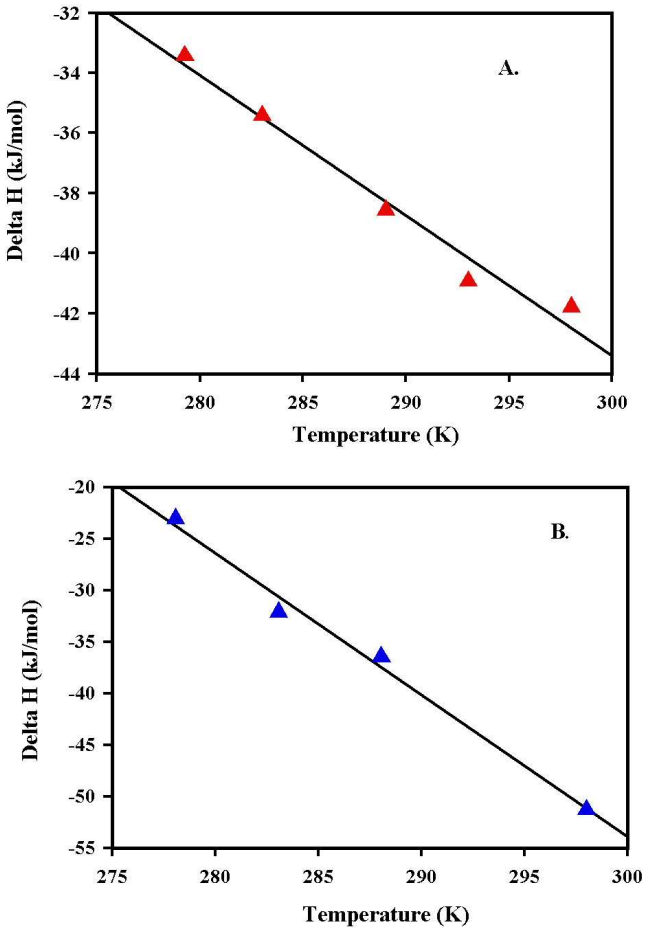

Figure 40. Temperature-dependence of the enthalpy change, ΔH^{O}, upon binding of glutathione sulfonate to the (A) wild-type (filled red triangles) and (B) Y8F (filled blue triangles) hGSTA1-1 protein, respectively. The data is summarised in Table 7. The solid line through the points is the linear regression fit to the data. The slope of the linear regression yields the change in heat capacity (ΔC_p) upon ligand binding to each of the proteins. The correlation coefficient for (A) and (B) is 0.90 and 0.99, respectively.

Binding energetics of reduced glutathione to wild-type and Y8F hGSTA1-1. The binding of glutathione to the wild-type and Y8F proteins was conducted under the same conditions with respect to buffer, pH and temperature. The stoichiometry was fixed at one and the other variables (K_a, ΔH^O and ΔS^O) were allowed to float in order to obtain the best fit. Structural data has shown that GSH binds with a stoichiometry of one molecule GSH per protein monomer to the G-site in the class alpha GST (Cameron *et al*., 1995; Sinning *et al*.,1993). A stoichiometry of one molecule of glutathione sulfonate per protein monomer was also observed in another ITC study (section 6.3.2).

Under the experimental conditions studied, the binding isotherms observed for both proteins were characteristic of a hyperbolic, saturation curve. Ideally, one should obtain a few points in the pre-transition region that would assist in accurately defining the ΔH^O of the protein-ligand interaction.

The c-value is a unitless value that is used to describe the shape of the binding isotherm and depends on the product of K_a $[M_t]$, where K_a is the binding constant and $[M_t]$ is the concentration of macromolecule in the ITC sample cell (Wiseman *et al*., 1989). Under these experimental conditions, the c-value was determined as 0.3. Wiseman *et al*. (1989) have suggested that ideal c-values are between 1 and 1000. Therefore, in order to obtain a binding isotherm that has a c-value value of, e.g., 40, the experiment would require a 10 mM protein concentration. Technically, we were unable to concentrate the protein to such high concentrations. Also, if it were possible to obtain the protein at such high concentrations for ITC studies, it would be difficult to saturate the ligand binding sites due to the low binding affinity of glutathione for hGSTA1-1 (K_d = 0.27 mM GSH) (Dirr and Wallace, 1999). Under the experimental conditions, we were approximately 10-fold away from the required protein concentration. However, even under these conditions, the binding affinity obtained for the wild-type protein was very similar to those previously determined using fluorescence techniques (Dirr and Wallace, 1999; Gustafsson *et al*., 1999). The reliability of the binding affinity constant, therefore, allowed for the calculation of the Gibbs free energy of binding using the equation: $\Delta G^O = -RT\ln K_a = \Delta H^O - T\Delta S^O$. Interestingly, the ΔG^O values obtained for the binding interaction are very similar

whether one uses the experimentally obtained K_a values ($\Delta G^O = -RT\ln K_a$) or the experimentally derived ΔH^O value ($\Delta G^O = \Delta H^O - T\Delta S^O$) in order to calculate the Gibbs free energy of binding (ΔG^O).

Analysis of the interaction of wild-type protein with the physiological tripeptide glutathione (Table 5A) indicates that the interaction is enthalpically favourable (negative ΔH^O values). The observed entropy is also favourable (positive ΔS^O) although there is a decrease with a corresponding increase in temperature. It appears that both enthalpy and entropy serve as the driving forces in the association of glutathione with the wild-type protein. Binding of glutathione to the Y8F protein (Table 5B) indicates that the interaction is also enthalpically favourable (negative ΔH^O). The binding reaction, however, is entropically unfavourable (negative ΔS^O values) at 20 and 25^OC and entropically favourable (positive ΔS^O values) at 5 and 10^OC.

Determination of the Gibbs free energy (ΔG^O) values for the wild-type (Table 5A) indicates that ΔG^O is similar at each temperature. The same is true for the Y8F protein (Table 5B). This is an example of the enthalpy-entropy compensation effect that is common to many binding processes (Baron *et al.*, 1989; Sigurskjold *et al.*, 1991). However, one cannot exclude the existence of some type of "extra-thermodynamic" compensation i.e., "a linear relationship between ΔH and ΔS that cannot be a priori deduced from the laws of statistical thermodynamics" (Sharp, 2001). The large and favourable enthalpy term is attributed to hydrogen bonding and van der Waals interactions in the complex formation (see Figure 4) and these overcome the unfavourable entropy change. This explains the overall favourable Gibbs free energy of binding observed for both proteins. The individual contributions of the enthalpy and entropy terms to the overall Gibbs free energy in the wild-type and Y8F proteins suggest that, in both cases, the binding processes are enthalpically-driven. Recently, an ITC study indicated that the binding of the ligand GS-NBD (NBD, 4-nitrobenzo-2-oxa-1,3-diazole) to the wild-type rat GSTA1-1 at 25^OC is favoured both enthalpically (-23.93 kJ/mol) and entropically (31.29 J/mol/K). The study also looked at the binding energetics of GS-NBD

with a Y8F rGSTA1-1 mutant and the results indicated that the reaction was enthalpically favourable (-40.08 kJ/mol) but entropically unfavourable (-10.96 J/mol/K) (Nieslanik and Atkins, 2000). A more recent study by the same group on the binding energetics of GS-EA (glutathione-ethacrynic acid conjugate) with the wild-type rGSTA1-1 indicated very similar binding behaviour as described above for the wild-type hGSTA1-1 protein and GSH (Nieslanik *et al*., 2001). Therefore, the binding of GS-EA to the wild-type rGSTA1-1 protein is also enthalpically (-31.79 kJ/mol) and entropically (24.43 J/mol/K) favourable. A comparison of the binding energetics for the rat wild-type and Y8F proteins in complex with either GS-NBD or GS-EA with the results in the present study at 25°C (Table 5), indicates that the results compare very well. Therefore, in the present study, the binding of GSH to the wild-type hGSTA1-1 at 25°C is enthalpically (-19.5 kJ/mol) and entropically (0.3 J/mol/K) favourable. The binding of GSH to the hGSTA1-1 Y8F mutant at 25°C, however, is enthalpically favourable (-33.8 kJ/mol) but entropically unfavourable (-46.1 J/mol/K). The majority of the energy, therefore, stems from hydrogen bonding and van der Waals interactions. The role of the hydrogen bond is recognised as an interaction of fundamental importance in determining the structures of proteins as well as their complexes with ligands (Connelly *et al*., 1994). Despite this, there are still conflicting views on the relative contributions of hydrogen bonds and interactions involving non-polar groups to the thermodynamics of protein folding and ligand binding (Murphy and Gill, 1991; Yang *et al*., 1992; Murphy *et al*., 1990; Baldwin, 1986; Spolar *et al*., 1992).

Table 5 shows the overall Gibbs free energy of GSH binding to the wild-type and Y8F hGSTA1-1 proteins. It is evident that the overall ΔG^{O} is slightly more favourable for the Y8F mutant than the wild-type protein. This observation may be explained in terms of the binding energy and the ionisation of GSH. The wild-type enzyme predominantly binds the thiolate form (GS^{-}) whereas the Y8F mutant binds the reduced form of glutathione (GSH). Therefore, the wild-type enzyme would utilise some of its intrinsic binding energy in order to remove the proton from the neutral form of GSH so as to generate the thiolate form (GS^{-}). In this way, the tyrosyl (Y8) hydroxyl group stabilises the thiolate ion at the active site. The Y8F mutant, however, lacks the hydroxyl group and is unable

to stabilise the thiolate ion and, therefore, most of the intrinsic binding energy is utilised in the actual binding interaction. Intuitively, however, one would have expected the opposite to be true since the mutation involves the removal of the hydroxyl group thus eliminating the formation of a hydrogen bond/s between the protein and the ligand. In the apo-structure of the hGSTA1-1, three active site water molecules are located close to the hydroxyl group of tyrosine 8 (Figure 41). The distances between the oxygen atom of the hydroxyl group and the oxygens of the water molecules are 2.93 Å, 4.50 Å and 7.30 Å. Therefore, one water molecule is within hydrogen bonding distance of the tyrosyl hydroxyl group. All three water molecules are displaced when *S*-benzylglutathione is bound to the active site (Figure 41) (Sinning *et al*., 1993; Párraga *et al*., 1998).

Crystal structures of the wild-type hGSTA1-1 protein complexed to GS-EA conjugate indicate that the GSH moiety is well structured at the G-site. All the hydrogen-bonding interactions observed in the *S*-benzylglutathione structure (see Figure 4) are maintained in the wild-type protein complexed to GS-EA. Although the interactions of the dichlorophenoxy group of the EA moiety and the wild-type GST are mainly hydrophobic in nature, it is evident that the carbonyl oxygen of EA is in hydrogen bonding distance with the hydroxyl group of Y8. The carbonyl oxygen of EA, therefore, acts as a hydrogen-bond acceptor from the tyrosyl hydroxyl group. The tyrosyl hydroxyl group is thought to exist in the protonated form and, therefore, acts as a hydrogen bond donor (Cameron *et al*., 1995). It also forms hydrogen bonds to the thiolate form of glutathione as well as the peptide nitrogen of Arg14 (Sinning *et al*., 1993; Dirr *et al*., 1994a, 1994b). Removal of the hydroxyl group by replacement with phenylalanine, therefore, effectively eliminates two hydrogen bonds from the protein-glutathione active site in the Y8F mutant protein and the mutation appears to favour the overall binding enthalpy in the Y8F mutant protein when compared to the wild-type protein. The results show that ΔG^{O} is slightly more favourable in the Y8F protein and, therefore, more stabilising due to the removal of the tyrosyl hydroxyl group. This behaviour has been observed before where tyrosine 82 was replaced with phenylalanine in FKBP-12 (Connelly *et al*., 1994). The role of the hydroxyl group of Y6 in the catalytic mechanism of rat GSTM1-1 has also previously been reported using X-ray crystal structure data, enzyme activity and pK_a

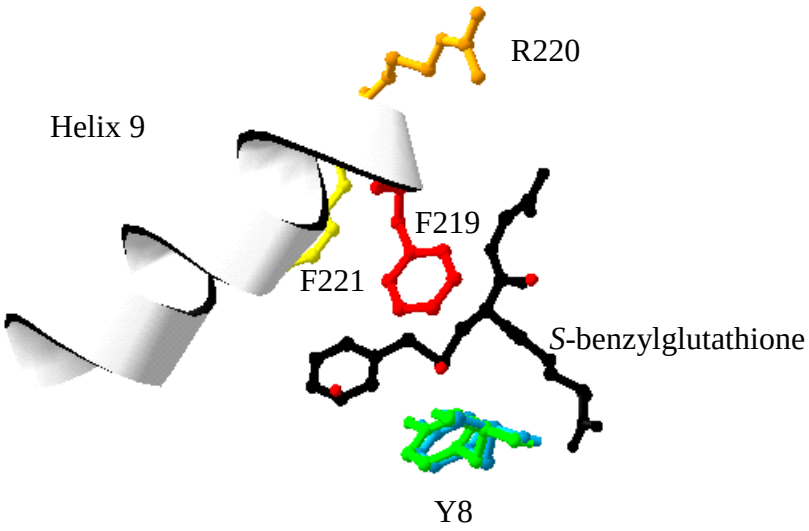

Figure 41. Representation of the active site structure of human GSTA1-1. The figure was generated by superimposing the structures of two hGSTA1-1 structures; (1) the apo-form of the protein (1gsd), and (2) the protein complexed with *S*-benzylglutathione (1guh). The C-terminal helix 9 is shown as a ribbon structure and is only visible when the active site is occupied (1guh; Sinning *et al*., 1993). Helix 9 is crystallographically "invisible" in the apo-form of the protein (Cameron *et al*., 1995). The following structures are represented in ball-and-stick: *S*-benzylglutathione (black), R220 (mustard), F221 (yellow), F219 (red), Y8 from 1gsd (light blue) and Y8 from 1guh (green). The red dots indicate the positions of three water molecules (present in the apo-form only) located nearest to the active site Y8 hydroxyl group. The distances of the water molecules from the Y8 hydroxyl group are 2.93 Å, 4.50 Å and 7.30 Å. All three of these water molecules are displaced when the active site is complexed with *S*-benzylglutathione.

measurements (Liu *et al*., 1992). The results indicated that in the binary complex of enzyme and GSH, the predominant ionisation state of GSH in the active site of the wild-type protein is the thiolate form (GS^-) whereas the neutral thiol (GSH) form was observed for the Y6F mutant. This group also suggested that the tyrosyl hydroxyl might function in stabilising the thiolate anion and also act as a participant in the removal of the proton of GSH from the active site of the wild-type enzyme. This pathway would, therefore, not be available to the Y6F mutant. Structural evidence also indicated that the tyrosine 6 hydroxyl group specifically hydrogen bonds to the GSH and stabilises the thiolate anion by about 1.4 to 2.2 kcal/mol (Liu *et al*., 1991).

The observed enthalpy difference between the wild-type and Y8F proteins is due to the difference in the enthalpy of the interaction of the tyrosyl hydroxyl group with the water molecule and the peptide nitrogen of Arg14 (effectively two hydrogen bonds). The fact that the formation of the wild-type-glutathione complex is enthalpically less favourable but more entropically favourable than the Y8F protein is evident from the results in Table 5. It has been suggested that the overall formation of hydrogen bonds in ligand binding may be unfavourable due to the unfavourable enthalpy of desolvation (Ben-Naim, 1991).

The entropy of a molecule in solution is composed of four contributions relating to four types of motion: translational, rotational, vibrational and conformational entropy (Finkelstein and Janin, 1989). Glutathione is bound at the active site in an extended conformation and most of the polar atoms in the tripeptide are involved in hydrogen bonds or salt links (Sinning *et al*., 1993). Upon binding of glutathione to the wild-type (or Y8F) proteins, all four entropy terms will change unfavourably for both the ligand and the macromolecule because of greater motional restrictions. In order for the overall entropy change to contribute favourably to the binding, the liberation of solvent molecules bound to the surface of the ligand and/or the binding site of the macromolecule must occur to an extent sufficiently high to overcome the entropy changes for the ligand and the macromolecule (Sigurskjold *et al*., 1991). It is, therefore, possible that solvent displacement occurs upon binding of glutathione to the wild-type and Y8F proteins. Figure 41 represents the active site structure of wild-type hGSTA1-1 and the location of

the active site water molecules. A study by Párraga *et al.* (1998) indicated the existence of a well-defined network of water molecules in the active site of mouse GSTP1-1. Crystal structure data from that study indicated the existence of three water molecules in the apo-enzyme. One of the water molecules was displaced when the enzyme was complexed with GSH and a second water molecule was displaced when the electrophilic binding site was occupied, thus resulting in the formation of a GSH-conjugate. The crystal structure data also showed that the thiolate anion (GS^-) is stabilised by the presence of three water molecules as well as the tyrosyl hydroxyl group at the active site. The tyrosine 7 hydroxyl group is not ionised in the free or in the GSH complex at physiological pH. The authors also suggested that one of these water molecules might be responsible in assisting the release of the proton from GSH thiol group.

As a ligand enters the binding site of a macromolecule, the more strongly it is bound (the more negative the ΔH^O of binding), the more its rotational and translational freedom will be restricted (the more negative the ΔS^O) (Eftink *et al.*, 1983). A comparison of the binding constants reveals that the Y8F mutant protein binds glutathione tighter than the wild-type protein. A recent study on the binding of the GS-NBD product conjugate to the Y8F protein in rat GSTA1-1 indicated that the binding was enhanced compared to the wild-type rat GSTA1-1 protein (Nieslanik and Atkins, 2000). A different study on the Y8F hGSTA1-1 mutant bound the ligand, *S*-dinitrophenylglutathione, 20-fold more tightly than the wild-type protein (Allardyce *et al.*, 1999). Recently, an ITC study conducted by Nieslanik and Atkins (2000) reported the binding of a GS-NBD conjugate to the Y8F mutant in rat GSTA1-1. They found that the interaction is enthalpically more favourable but that this comes at an entropic cost. The results of a recent binding study of a glutathione-ethacrynic acid product conjugate (GS-EA) to the wild-type rat GSTA1-1 indicated the C-terminus is required for the entropically-driven ligand binding reaction (Nieslanik *et al.*, 2001).

The high unfavourable entropic cost of glutathione binding to the hGSTA1-1 Y8F mutant (at 20 and 25^OC) also probably reflects the degree of immobilisation of the ligand, thus decreasing its flexibility and increasing its rigidity at the active site. The overall effect of

the removal of the tyrosyl hydroxyl group is that the mutation is entropically destabilising but enthalpically stabilising at increasing temperatures. The presence of the tyrosyl hydroxyl group at the active site, therefore, stabilises the wild-type protein entropically.

It has been proposed that the basis for the heat capacity changes observed in protein-ligand binding is related to the changes in the solvation of the protein and ligand during the binding process (Sturtevant, 1977; Eftink *et al*., 1983). The changes in heat capacity upon binding of glutathione to the wild-type and Y8F hGSTA1-1 proteins indicated that the burial of solvent-exposed non-polar surface area occurs to a larger extent in the Y8F mutant than in the wild-type protein (Table 7). The burial of hydrophobic surface upon occupation of the active site by glutathione involves the immobilisation of helix 9 onto the surface of domain I in the hGSTA1-1 protein (Gustafsson *et al*., 1999; Dirr and Wallace, 1999). A comparison of the ΔC_p values (Table 7) for both proteins indicate that the Y8F mutant exhibits a 2.7-fold greater reduction of exposed hydrophobic surface area when compared to the wild-type. This is quite striking and is probably related to the observation that GSH also binds the Y8F mutant tighter than the wild-type protein thus stabilising helix 9 to a larger degree. Dirr and Wallace (1999) have found that helix 9 flexibility in hGSTA1-1 is modulated by the absence/presence of various ligands at the active site. In the presence of active site ligands (e.g., *p*-bromobenzylglutathione), the conformational flexibility of helix 9 is restricted thereby causing it to become more tightly associated with the H-site of the protein. Because of the amphipathic character of helix 9, the hydrophobic residues located on the inner wall of helix 9 form favourable hydrophobic interactions with residues located at the H-site. The C-terminal helix 9, therefore, forms a "lid" which folds over onto the hydrophobic surface area of domain I thereby effectively shielding the active site bulk solvent (Sinning *et al*., 1993). A direct consequence of this would be a reduction in the solvent-accessible non-polar surface area surface in the complexed protein. The amount of solvent-accessible non-polar surface area that becomes buried (ΔA_{np}/monomer), due to the localisation of helix 9 over the active site, may be estimated using the theoretical relationship shown in Table 7. Theoretical calculations of ΔA_{np} ($Å^2$) indicate that a larger amount of solvent-accessible non-polar surface area becomes buried when GSH binds the Y8F mutant than the wild-

Table 7. The change in heat capacity (ΔC_p) upon binding of reduced glutathione (GSH) and glutathione sulfonate (GSO_3^-) to the wild-type and Y8F hGSTA1-1 proteins. The non-polar surface area that becomes buried (ΔA_{np}) upon protein-ligand interaction may be estimated using the following equation: $\Delta C_p = 1.046\ \Delta A_{np}$, where ΔA_{np} has the units ($Å^2$) and ΔC_p has the units J/mol/K (Spolar and Record, 1994; Livingstone *et al*., 1991).

	(ΔC_p) (J/mol/K)		**(ΔA_{np}) ($Å^2$)**	
	Experimental		**Theoretical**	
	GSH	GSO_3^-	GSH	GSO_3^-
wild-type hGSTA1-1	-437	-467	-418	-447
Y8F hGSTA1-1	-1150	-1380	-1099	-1319

type hGSTA1-1 protein. Therefore, this may refer to the presence of a more stabilised conformation of helix 9 at the C-terminus in the theY8F mutant protein than the wild-type. In another study, Gustafsson *et al*. (1999) have shown the rate of GSH binding to the active site of hGSTA1-1 correlates with the accessibility of the active site to GSH. The extent to which the active site is exposed to solvent is related to the flexibility of the C-terminal helix 9. Therefore, the existence of a more conformationally flexible C-terminal helix 9 in the wild-type, when compared to the Y8F mutant, would facilitate the diffusion of GSH through a more open entrance to the G-site. The ITC results from our work suggests that the tyrosyl hydroxyl group located at the active site of hGSTA1-1 is required for controlling the dynamics of helix 9 at the C-terminus. Nieslanik and Atkins (2000) have also proposed that the catalytic Y8 residue in the rat GSTA1-1 controls the dynamics of the C-terminus. Crystal structure evidence also shows that the C-terminal helix 9 is crystallographically "invisible" in the apo-form of the enzyme (Cameron *et al*., 1995; Adman *et al*., 2001). In the presence of active site ligands, the C-terminus is localised (immobilised) over the active site on domain I (Sinning *et al*., 1993; Cameron *et al*., 1995).

The fact that the wild-type protein has a reduced heat capacity change could have functional significance for the wild-type protein. The wild-type protein binds reduced glutathione at the active site following which it is activated to the GS^- thiolate form. It is in this state (as a potent nucleophile) that glutathione is complexed to a variety of non-polar electrophilic substances at the H-site. Upon completion of the nucleophilic substitution reaction, the more water-soluble glutathione-conjugate is eventually released from the active site and eliminated via the mercapturate pathway. If helix 9 closes too tightly over domain I (high heat capacity), there would be an enthalpic penalty to break the bonds between the hydrophobic face of the amphipathic helix and the H-site in order to release the glutathione-conjugate.

An intriguing question is how does Y8, at the active site, control the dynamics of helix 9 in class alpha GSTs? Recently, Nieslanik and Atkins (2000) showed that the binding of the glutathione-conjugate, GS-NBD, to the rat GSTA1-1 Y8F mutant was enhanced

compared to the wild-type protein. Using stopped-flow kinetic analysis it was observed that the increase in binding affinity was associated with the decrease in rates for the C-terminal order-disorder transition. The same effects were reported for a second glutathione conjugate, GS-EA. It is reasoned that the phenolic oxygen of tyrosine 8 (our numbering) provides a mechanism for communication between the active site and the C-terminus. This could be achieved through an on-face electrostatic interaction between F219 and Y8 (Nieslanik and Atkins, 2000).

It appears that ligand binding to the class alpha GSTs occurs via a two-state mechanism. The first step involves the "docking" of the ligand to the active site. This is followed by an isomerisation step in which the C-terminal helix 9 is transformed from a dynamic (mobile) helix to a localised (immobile) helix. The following reaction is adapted from Nieslanik *et al*. (2001) and is represented as follows:

$$\text{GSTA1-1} + \text{ligand} \underset{k_{1}}{\overset{k_{-1}}{\rightleftharpoons}} [\text{GST}\bullet\text{ligand}]_{\text{dynamic}} \underset{k_{2}}{\overset{k_{-2}}{\rightleftharpoons}} [\text{GST}\bullet\text{ligand}]_{\text{localised}}$$

where, $[\text{GST}\bullet\text{ligand}]_{\text{dynamic}}$ and $[\text{GST}\bullet\text{ligand}]_{\text{localised}}$ represents the pre-complex of GSTA1-1 protein with a dynamic (i.e., mobile) C-terminal helix and the final equilibrium complex of protein and ligand with a localised (i.e., immobile) helix, respectively. The "docking" of the ligand to the active site of the protein is represented as k_1 and k_2 is the slow isomerisation step that leads to the formation of the localised helix 9.

The results presented in Table 5 demonstrate that at 25°C, the favourable binding enthalpy (-33.8 kJ/mol) of glutathione to the Y8F mutant comes at a large entropic cost (-46.1 J/mol/K). Similar results were observed with the binding of GS-NBD to the Y8F mutant from rat GSTA1-1; i.e., the more favourable ΔH^{O} of binding is accompanied by an entropic penalty. The reason that was advanced was the possibility of decreased solvent displacement from the active site when helix 9 is localised. What is clear is that Y8F at the active site decreases the rate at which the ligand "docks" at the active site as well the localised-dynamic transition at the C-terminus. Nieslanik *et al*., (2001) have confirmed that the two-step binding mechanism for rat GSTA1-1 is identical to that

observed in the wild-type human class alpha GST. The mechanism includes a very rapid bimolecular docking reaction, followed by the slower isomerisation step. Moreover, k_1 and k_2 are significantly slower in the human GSTA1-1 thus resulting in a lower overall affinity of GS-EA with wild-type hGSTA1-1 (Nieslanik *et al*., 2001).

Although the exact mechanism through which Y8 stabilises the C-terminus is not yet known, it is clear from the present study and another (Nieslanik and Atkins, 2000) that Y8 at the active site controls the dynamics of helix 9 at the C-terminus of GSTA1-1. Y8 in GSTA1-1 presumably modulates the ligand-dependent folding of the C-terminus helix 9 through stabilisation of the transition state for this conformational change, as well as the rates of ligand binding and dissociation (Nieslanik and Atkins, 2000).

Binding energetics of glutathione sulfonate (GSO_3^-) to wild-type and Y8F hGSTA1-1. The crystal structures of two mutant proteins from the rat GSTA1-1 complexed with glutathione sulfonate have recently been determined. The PDB accession codes for these structures are 1ev4.pdb (rGSTA1-1 double mutant W20F/F219Y; our numbering) and 1ev9.pdb (rGSTA1-1 mutant W20F; our numbering) (Adman *et al*., 2001). Glutathione sulfonate is a competitive inhibitor of the GSTs that only binds the G-site of the active site located on each subunit (i.e., one molecule of glutathione sulfonate per subunit).

In the present study, we have successfully used titration calorimetry to measure the energetics of binding of glutathione sulfonate to wild-type and Y8F proteins (Table 6). Inspection of the stoichiometry (N) and binding association constants (K_a) for the wild-type protein reveal that these values are in excellent agreement with the expected values. ITC data reveals a binding stoichiometry of one molecule of $GS0_3^-$ per protein monomer (Reinemer *et al*., 1991; Dirr *et al*., 1994a; Adman *et al*., 2001). Glutathione sulfonate binds tightly to the porcine class pi GSTP1-1 with a K_d = 4μM (Dirr *et al*., 1991). The Y8F mutant also displays a binding stoichiometry of 1:1 of protein:ligand (N value of 1.0 at 5^OC and 25^OC) (Table 6). Both proteins, therefore, bind one molecule of glutathione sulfonate per subunit of protein dimer. Inspection of the binding constants, K_d values, shows that glutathione sulfonate binds about two-fold more tightly to the wild-type than

the mutant protein (Table 6). A comparison between the binding of reduced glutathione and glutathione sulfonate indicates that the wild-type protein binds glutathione sulfonate ~ 100-fold more tightly than it does reduced glutathione. It has also previously been shown that glutathione analogues with a stable anion replacing the uncharged thiol group, e.g., glutathione sulfonate, bind the G-site more tightly than reduced glutathione (Graminski *et al*., 1989a). The ITC results also suggest that the protonated form of the tyrosine 8 side chain is required as the ionised tyrosinate form would destabilise rather than stabilise the interaction between the protein and glutathione sulfonate. Therefore, the presence of the tyrosyl hydroxyl group at the G-site is required for a tighter association with glutathione sulfonate. Removal of the hydroxyl group, as in Y8F, results in diminished binding of the negatively charged glutathione analogue.

The c-values for the wild-type and Y8F proteins were in the required range between 1-1000 as suggested by Wiseman *et al*. (1989). The binding isotherms in this study resemble sigmoidal plots and are useful in gaining accurate binding enthalpy (ΔH^O) and entropy (ΔS^O) values. The binding of glutathione sulfonate to the wild-type and Y8F proteins indicate that the enthalpy of binding (ΔH^O) is the major driving force in the association (i.e., both proteins exhibit large, negative ΔH^O values). The contribution of ΔH^O and ΔS^O to the total free energy of the association (ΔG^O) indicates that the enthalpy of binding is the major contributor. The ΔH^O can be viewed as an indicator of the number of hydrogen bonds broken or formed during the association. On this basis, it is evident that the wild-type protein forms more hydrogen bonds with glutathione sulfonate than the Y8F mutant and that the removal of the tyrosyl hydroxyl group effectively abolishes potential hydrogen bonds from forming.

Both proteins also show very unfavourable entropy values (negative ΔS^O values) except for the binding interaction between the Y8F mutant and glutathione sulfonate at 5^OC (Table 6). However, the overall result is consistent with the view that upon complex formation, the rotational and translational freedom of the glutathione sulfonate is restricted to a larger degree as reflected in the reduced ΔS^O values. The more negative ΔS^O values seen in the wild-type (except at 25^OC) is also an indication that glutathione

sulfonate binds more tightly to the wild-type than the Y8F protein. This result is confirmed by the K_d values. Therefore, the overall result of glutathione sulfonate binding to the wild-type and Y8F protein suggests that this is an enthalpically driven process.

The heat capacity change, ΔC_p, for the dissolution of various non-polar substances (solids, liquids and gases) in water is proportional to their surface area (Privalov and Gill, 1988). The experimentally determined heat capacity change is negative for both proteins upon complex formation with glutathione sulfonate (Table 7). This result, therefore, suggests that there is a substantial burial of non-polar surface area in both proteins. It appears that the Y8F protein has ~ 3-fold more buried surface area than the wild-type protein. The burial of non-polar surface area is not surprising since it is well documented that helix 9 forms a "lid" over the solvent-exposed surface area of domain I in the presence of active site ligands (Sinning *et al*., 1993; Dirr and Wallace, 1999). Studies using hydrostatic pressure (Atkins *et al*., 1997), NMR (Lian, 1998) as well as various active site ligands (Dirr and Wallace, 1999) all suggest that helix 9 may not be completely mobile (dynamic) in the uncomplexed protein. The C-terminal helix may exist as an intact but mobile helix corresponding to a heterogeneous ensemble of dynamic helices. The presence of various isoenergetic conformations is possible since traces of electron density occur in the apo-enzyme at the expected position of the helix backbone (Cameron *et al*., 1995; Dirr and Wallace, 1999).

In order to understand the source of the ionisation energy, the difference in the Gibbs free energy ($\Delta\Delta G$) between glutathione and glutathione sulfonate was calculated. The calculated values were 2.73 kcal/mol and 1.92 kcal/mol for the wild-type and Y8F proteins, respectively. This implies that the wild-type tyrosyl hydroxyl group contributes ~ 1.4 times more energy than the Y8F mutant to the stabilisation of the thiolate anion (GS^-) in the binary complex at the active site of hGSTA1-1. Liu *et al*. (1992) have suggested that the hydroxyl group of tyrosine 6 in the rat isoenzyne 3-3 contributes $\geq$ 1.4 kcal/mol toward the stabilisation of GS^- of the wild-type enzyme.

In the present study, preliminary ITC work was also performed in order to determine the existence of linked protonation effects. The data indicated that the commonly used

buffers (Pipes, Mops and Hepes) were not suitable for the protein system under investigation. From the ITC data, it appears that the hGSTA1-1 is capable of binding to the buffers and, therefore, interacts competitively with the ligands studied. Future studies will have to identify the appropriate buffers in order to determine the contribution by buffers to the binding event.

7. Non-substrate ligand binding to wild-type hGSAT1-1

Apart from their role in catalysis, the GSTs have also been implicated in the binding and sequestration of lipophilic ligands (binding affinity of 10^5-10^7 M^{-1}) and it was for this function that they were initially referred to as "ligandins" (Litwack *et al*., 1971). These ligands included molecules such as hemin, bilirubin, bile salts, steroids, thyroid hormones, fatty acids and drugs (Ketterer *et al*., 1987). GSTs are capable of binding large lipophilic molecules (molecular masses > 400 Dalton) and may, therefore, be involved in the storage and transport of these molecules in the aqueous phase of the cell (Habig *et al*., 1974a; Tipping and Ketterer, 1981; Caccuri *et al*., 1990). It is thought that GSTs serve a transport function and that they direct steroids to their site of action (Hayes and Pulford, 1995). GSTs may also serve a "buffering" role by moderating the effects of transient fluxes in the steroid levels in target organs as well as a role in protection by preventing the accumulation of non-polar molecules at lipophilic sites such as membranes (Listowsky *et al*., 1988). Due to their abundance and water solubility, it is thought that the binding of ligands to GSTs may be the major role of these proteins *in vivo (*McCarthy *et al*., 1996). Previously, it was suggested that the non-substrate ligand-binding site (ligandin or L-site) is distinct from the G- and H-sites since it is capable of haemin binding in the presence of the G-site inhibitor, *S*-methylglutathione (Caccuri *et al*., 1990). However, recent crystallographic evidence suggests that this may not be true since the L-site is also located in the hydrophobic substrate binding site (H-site) (Oakley *et al*., 1999).

Non-substrate ligands are observed to bind in the dimer interface of GSTs from the parasitic helminth *Schistosoma japonica* (McTigue *et al*., 1995) and the squid GST (Ji *et al*., 1997). It has also been suggested that the L-site is located at a buffer-binding site

close to tryptophan 28 in human class pi GST (Ji *et al*., 1997; Prade *et al*., 1997) and tryptophan 20 in the human class alpha GST (Sluis-Cremer *et al*., 1998). The existence of more than one site in the human class pi GST is supported by X-ray crystallographic evidence (Oakley *et al*., 1999) which indicated that the ligandin site is located near the electrophilic substrate H-site. In addition, fluorescence resonance energy transfer experiments have also indicated that the non-substrate ligand binding site in human GSTA1-1 is situated at/near the dimer interface (Sluis-Cremer *et al*., 1996; Sluis-Cremer *et al*., 1998).

In the present study, isothermal titration calorimetry (ITC) was used to dissect the binding energetics of the non-substrate ligands 8-anilino-1-naphthalene sulphonate (ANS) and sulphobromophthalein (BSP) to the wild-type human GSTA1-1 protein.

7.1 Thermodynamics of ANS and BSP binding to hGSTA1-1

7.1.1 Energetics of ANS binding to wild-type hGSTA1-1

A typical calorimetric titration curve of the association of ANS with the wild-type protein is shown in Figure 42 (panel A). The binding isotherm was obtained by titrating ANS into a solution of wild-type hGSTA1-1 in phosphate buffer, pH 6.5 at 10°C. The peaks observed in panel A represent an exothermic interaction with each new addition of ANS. The peak areas diminish with each addition of ligand as the available binding sites on the protein molecules are gradually saturated. The small peaks at the end of the experiment (last ten injections, Figure 42, panel A) represent the post-saturation heats of dilution. The post-saturation heats of dilution were averaged and subtracted from the each experimental point. The integrated area under each corrected peak (corrected for heat of dilution) was divided by the number of moles of ANS injected to obtain the experimental enthalpy, ΔH^{O} (Figure 42, panel B). All experiments were performed as a function of temperature (10-25°C) while keeping all the other conditions constant (i.e., buffer, pH). Under the conditions used in these experiments, each calorimetric titration provided the stoichiometry, binding constant, enthalpy and entropy changes. All the data in each experiment fit well to a single-site binding model. Analysis of the Gibbs free energy change of the interaction (ΔG^{O}) was obtained from the experimentally derived parameters

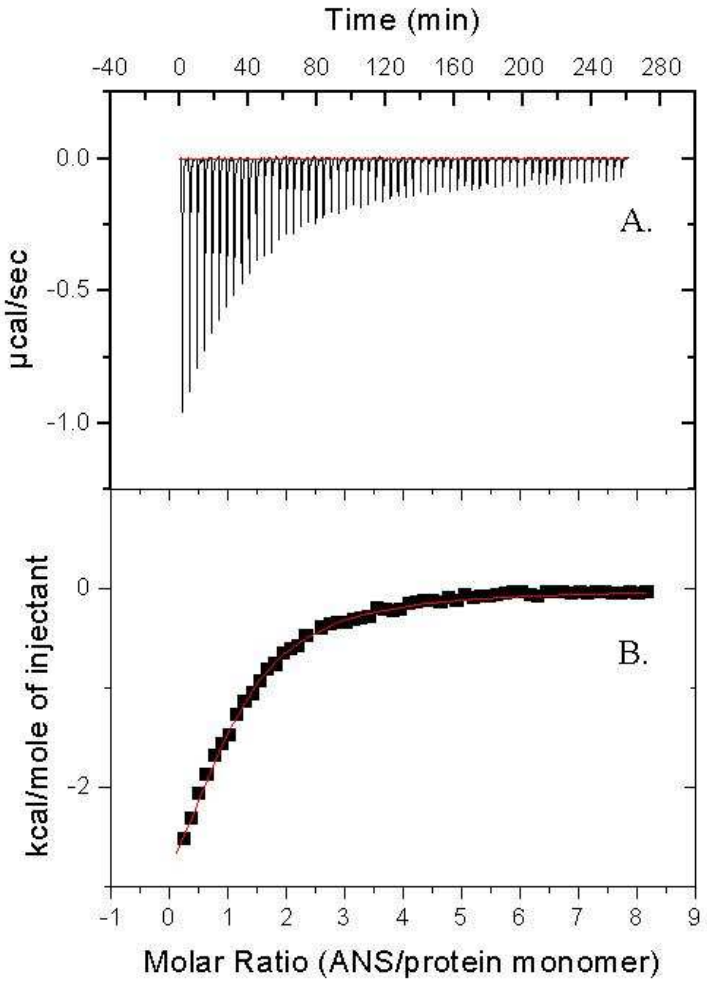

Figure 42. A representative calorimetric titration profile of the binding of the anionic dye ANS to the wild-type hGSTA1-1 protein. The experiment was performed at 10°C. The conditions were: 0.06 mM protein monomer concentration and 3.6 mM ANS in 20 mM sodium phosphate buffer, pH 6.5, containing 0.1 M NaCl, 1 mM EDTA, 0.02% sodium azide and 1 mM *tris*-(carboxyethyl)-phosphine (TCEP). Panel A shows the exothermic heat effects associated with the injection of ANS into the ITC sample cell containing the wild-type protein. Panel B shows the binding isotherm (corrected for heats of dilution) corresponding to the data in panel A. The solid line through the data represents the best fitted curve obtained using the ORIGIN software.

(ΔH^O and ΔS^O) using the equation $\Delta G^O = \Delta H^O - T\Delta S^O$. The results of the binding energetics of ANS to the wild-type protein are presented in Table 8. The stoichiometry of the interaction between ANS and hGSTA1-1 varied between 0.8 (at 25^OC) and 1.0 (at 10^OC). Essentially, the stoichiometry can be described as the binding of one ANS molecule per protein monomer. The binding affinity of the amphipathic dye to the wild-type protein is in agreement with published values obtained from fluorescence studies (Dirr and Wallace, 1999; Sayed *et al*., 2000). The ITC data suggests that the ligand binds tighter at lower temperatures than at higher temperatures. The binding event, which is described by the experimentally observed binding enthalpy, indicates that the enthalpy is more favourable at higher than lower temperatures. The opposite is true for the entropy changes observed. That is, a favourable entropy change is observed at low temperature (positive ΔS^O values) while an unfavourable change is seen at the higher temperatures (negative ΔS^O values).

The linear dependence of the experimentally observed enthalpy (ΔH^O) on temperature is used to determine the heat capacity of the binding interaction, ΔC_p. Under the conditions of this study, the ΔC_p was determined as -0.84 J/mol/K (Figure 43). A negative ΔC_p is the characteristic signature of the burial of solvent-accessible hydrophobic surface area (Luque *et al*., 1998a, 1998b).

7.1.2 Energetics of BSP binding to wild-type hGSTA1-1

Sulphobromophthalein (BSP) is a model compound that has been used quite extensively for probing the ligandin properties of GSTs (Ketterer *et al*., 1987; Mannervik and Danielson; 1988a, 1988b; Sluis-Cremer *et al*., 1998). Oakley and co-workers have recently solved the crystal structure of human class pi GST in complex with BSP (Oakley *et al*., 1999). Structural evidence suggested that BSP binds to a site that is located in part of the H-site. This was the first structural evidence of an additional L-site apart from the L-site already identified in the V-shaped cleft at the dimer interface (McTigue *et al*., 1995; Ji *et al*., 1997).

Table 8. Energetics of the interaction between wild-type GSTA1-1 and the amphipathic dye ANS at different temperature conditions. All the values are based on a single experiment and the errors were obtained by fitting the titration data using the ITC software programme (ORIGIN 5.0).

Temperature (^{O}C)	N	K_d (μM)	ΔH^{O} (kJ/mol)	ΔS^{O} (J/mol/K)	ΔG^{O} (kJ/mol)
10.6	1.0±0.03	35.8±1.6	-18.5±0.7	20.0	-24.2
15.0	0.9±0.1	45.7±3.7	-22.5±1.7	5.0	-23.9
20.0	1.0±0.03	65.4±2.4	-26.4±1.1	-9.8	-23.5
25.0	0.8±0.1	69.0±5.0	-30.7±3.3	-23.3	-23.8

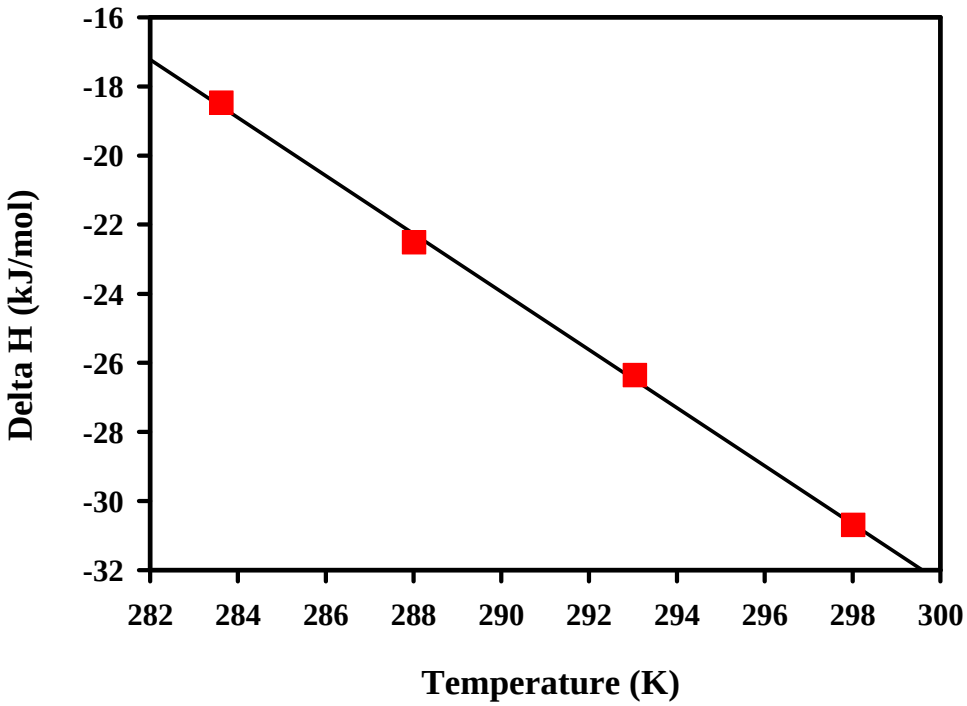

Figure 43. Temperature-dependence of the enthalpy change, ΔH^{O}, upon binding of ANS to the wild-type protein. The data is summarised in Table 10. The solid line through the points is the linear regression fit to the data. The slope of the linear regression yields the change in heat capacity (ΔC_p) upon ligand binding to the protein. The correlation coefficient is 0.998.

A typical calorimetric titration curve of the addition of BSP to the wild-type protein is shown in Figure 44, panel A. Each peak in panel A corresponds to an exothermic interaction. The peak area diminishes with each successive injection of BSP. BSP titration curves, however, differed from all the other ligands (GSH, GSO_3^- and ANS) examined thus far in that no small peaks of constant area were observed at the end of the titration curve. The heat of dilution was determined from a separate experiment under identical conditions (temperature, buffer, pH) except that BSP was injected into buffer without protein. This was then subtracted from the raw data to obtain the heat evolved from each injection. The area under each peak was integrated and the observed enthalpy of binding (ΔH^O) versus the molar ratio of BSP added is shown in Figure 44, panel B. Under these experimental conditions, the post-saturation peaks usually identified in ITC data are not evident (Figure 44, panel B). The data obtained from these titration curves do not fit well to a single-site binding reaction model. The data, however, fits well to a binding model describing two sets of binding sites on the wild-type protein molecule. The thermodynamic parameters describing the association of BSP and hGSTA1-1 are summarised in Table 9.

The data obtained suggests the presence of two BSP-binding sites per monomer. The first site (N1) binds one molecule of BSP per protein monomer with a very high affinity of 0.15 to 0.24 μM BSP in the temperature ranges from 10-25°C. The second binding site on the protein molecule corresponds to a lower affinity site (K_d values range from approximately 6.7 μM to 9.9 μM BSP). The stoichiometry of binding at this site is ~ 3.7 molecules BSP per protein monomer. Figure 44, panel B clearly shows the existence of a biphasic binding isotherm. The first phase is evident from 0-2 (molar ratio) and corresponds to the first binding site on the protein molecule representing the higher affinity binding site. The second phase begins at a molar ratio of ~ 2.5 and continues all the way through to a molar ratio of 7. The second phase represents the lower affinity binding site that is capable of binding ~ 4 molecules of BSP per protein monomer of hGSTA1-1. It is evident that even a molar ratio of ~ four:one of ligand:protein is not sufficient to saturate the second binding site; i.e., no post-saturation peaks are observed in Figure 44, panel B. In addition, BSP appears to bind the higher affinity site ~ 47 times

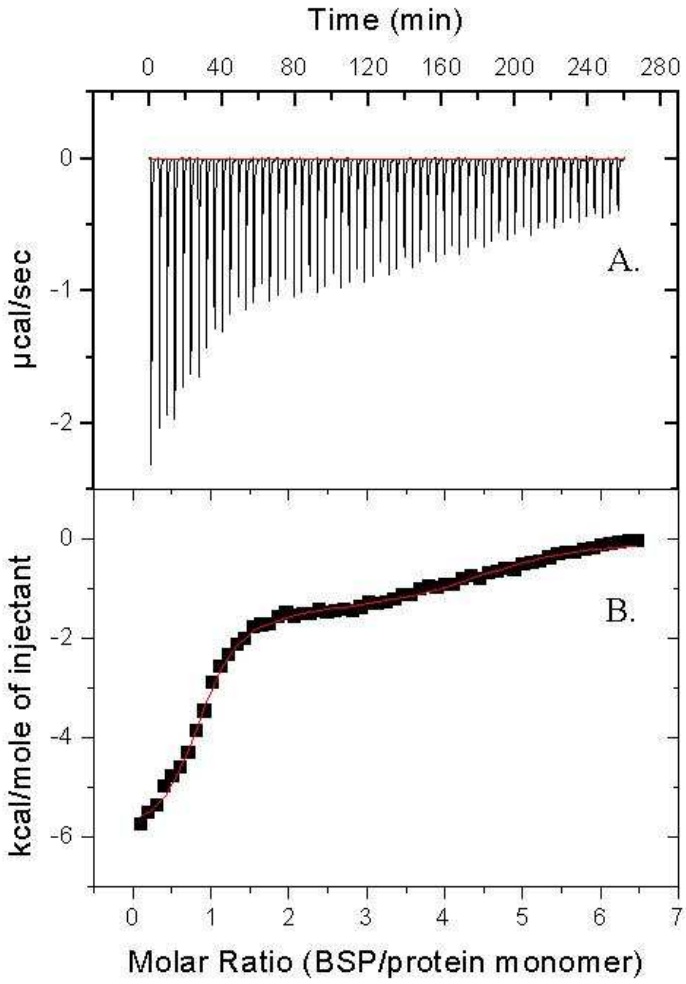

Figure 44. A representative calorimetric titration profile of the binding of BSP to the wild-type hGSTA1-1 protein. The experiment was performed at 20°C.The conditions were: 0.06 mM protein monomer concentration and 3.0 mM BSP in 20 mM sodium phosphate buffer, pH 6.5, containing 0.1 M NaCl, 1 mM EDTA, 0.02% sodium azide and 1 mM *tris*-(carboxyethyl)-phosphine (TCEP). Panel A shows the exothermic heat effects associated with the injection of BSP into the ITC sample cell containing the wild-type protein. Panel B shows the biphasic binding isotherm (corrected for heats of dilution) corresponding to the data in panel A. The solid line through the data represents the best fitted curve obtained using the ORIGIN software.

Table 9. Energetics of the interaction between wild-type GSTA1-1 and BSP at different temperature conditions. The thermodynamic parameters were obtained for the (A) higher and (B) lower affinity binding sites, respectively. All the values are based on a single experiment and the errors were obtained by fitting the titration data using the ITC software programme (ORIGIN 5.0).

A.

Temperature (^{O}C)	N1	K_d1 (μM)	$\Delta H^{O}1$ (kJ/mol)	$\Delta S^{O}1$ (J/mol/K)	$\Delta G^{O}1$ (kJ/mol)
10.0	0.9±0.02	0.15±0.03	-17.4±0.4	68	-36.4
15.0	0.8±0.01	0.21±0.03	-22.6±0.3	49	-36.7
20.0	0.9±0.01	0.18±0.04	-25.4±0.4	42	-37.8
25.0	0.9±0.01	0.24±0.08	-30.4±0.5	25	-37.8

B.

Temperature (^{O}C)	N2	K_d2 (μM)	$\Delta H^{O}2$ (kJ/mol)	$\Delta S^{O}2$ (J/mol/K)	$\Delta G^{O}2$ (kJ/mol)
10.0	3.8±0.1	6.7±1.1	-7.1±0.2	74	-28.0
15.0	3.7±0.1	9.9±1.2	-7.8±0.2	69	-27.7
20.0	3.7±0.1	8.0±1.2	-6.0±0.2	77	-28.6
25.0	3.5±0.1	8.7±2.7	-3.7±0.3	84	-28.7

tighter than the lower affinity site at 15°C.

Occupation of the high and low affinity set of sites on the protein molecule by BSP appears to be enthalpically (ΔH^{O}) and entropically (ΔS^{O}) favourable. The higher affinity site, however, appears to be more enthalpically favourable (ΔH^{O}) and the lower affinity site is more entropically favourable (ΔS^{O}).

The change in heat capacity on binding (ΔC_p) of BSP to the wild-type protein (i.e., the linear dependence of the observed enthalpy of binding (ΔH^{O}) on temperature) is shown in Table 10. The binding of BSP to the higher affinity binding site resulted in a negative ΔC_p (-0.83 kJ/mol/K) whereas the binding of BSP to the lower affinity site corresponded to a positive change in the heat capacity (+0.41 kJ/mol/K) (Figures 45A and B, respectively).

7.2 Discussion

To our knowledge, this study represents the first to describe the energetics of binding of non-substrate ligands to GSTs using ITC. The energetics of non-substrate ligand binding to the wild-type hGSTA1-1 was carried out using ANS and BSP as ligands. The binding of ANS to GSTs has been studied quite extensively by means of techniques such as fluorescence resonance energy transfer (FRET) (Sluis-Cremer *et al*., 1996). ANS is also used as a probe to monitor the appearance/disappearance of structured hydrophobic surface area/patches during protein folding/unfolding experiments (Wallace *et al*., 1998a, 1998b; Wallace and Dirr, 1999; Stevens *et al*., 1998; Hornby *et al*., 2000).

Binding energetics of ANS to wild-type hGSTA1-1. Titration calorimetric experiments were performed under conditions where only the temperature was varied between 10 and 25°C. ITC is extremely effective in that it provides a complete thermodynamic profile of parameters for a protein-ligand interaction.

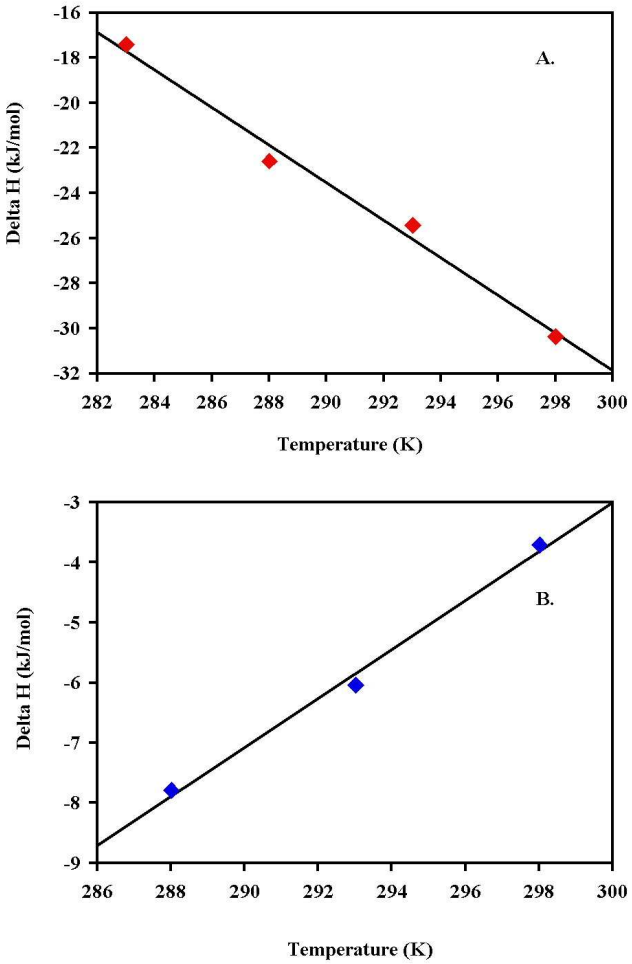

Figure 45. Temperature-dependence of the enthalpy change, ΔH^{O}, upon binding of BSP to the wild-type hGSTA1-1 protein. The data are summarised in Table 10. The change in heat capacity upon BSP binding to the wild-type protein for the (A) higher (filled red diamonds) and (B) lower (filled blue diamonds) affinity binding sites is indicated. The solid line through the points (Figures A and B) is the linear regression fit to the data. The slope of the linear regression yields the change in heat capacity (ΔC_p) upon ligand binding to the wild-type protein. The correlation coefficient for both (A) and (B) is 0.99.

Table 10. The change in heat capacity (ΔC_p) upon binding of non-substrate ligands ANS and BSP to the wild-type hGSTA1-1 protein. The estimated non-polar surface that becomes buried (ΔA_{np} ($Å^2$)) upon protein-ligand interaction is also shown.

Ligand:	**(ΔC_p) (kJ/mol/K)** **Experimental**	**ΔA_{np} ($Å^2$) (monomer) Theoretical**
ANS	-0.84	-800
BSP (higher affinity site)	-0.83	-794
BSP (lower affinity site)	+0.41	+392

Phosphate buffer was used in the study of the binding of ANS to the wild-type hGSTA1-1. This buffer has a very low enthalpy of ionisation (3.77 kJ/mol to 5.12 kJ/mol) (Doyle, 1999; Fukada and Takahashi, 1998). The use of phosphate buffer would, therefore, minimise any artifactual heats of buffer ionisation. Connelly and co-workers have also opted for phosphate (and acetate) buffer as the buffers of choice so that the binding enthalpy does not reflect any contribution due to buffer ionisation (Connelly *et al*., 1992). Eftink and co-workers have also utilised phosphate buffers because they have found that the heat of protonation of the phosphate is approximately zero (Eftink *et al*., 1983). Therefore, the interpretation of the data presented here reflects the $\Delta H^{O}_{binding}$, which consists of the total binding enthalpy for the interaction between ANS and the protein. The $\Delta H^{O}_{binding}$, therefore, includes the enthalpy of buffer ionisation (if any). The first question that needs to be addressed is whether there are any exchanges of protons between the buffer and the protein and/or ligand during the interaction. Future studies involving the characterisation of binding of non-substrate ligands to GSTs should identify the ideal/appropriate buffers system to be used in order to establish the existence of linked protonation events.

Table 8 demonstrates the results obtained from the binding event occurring between hGSTA1-1 and ANS. All the data fit well to a model describing a single set of binding sites. This is taken to mean that one molecule of ANS binds per protein monomer. The data taken at 10°C, describes reasonably well the stoichiometry of the binding event between hGSTA1-1 and ANS. It is not uncommon to observe N values as low as 0.83 being reported as representing a 1:1 binding (Lung-Nan *et al*., 1991). The binding affinities for ANS is good agreement with those already determined in previous studies (Dirr and Wallace, 1999; Sayed *et al*., 2000). The K_d values indicated that the binding constant is dependent on the temperature. ANS binds ~ 2-fold tighter at 10°C than at 25°C. The ΔH^{O} is exothermic at each temperature studied. The enthalpy of binding becomes more favourable as the temperature increases. The large and favourable enthalpic event may be attributed to hydrogen bonding and van der Waals interactions.

Favourable entropic contributions are observed at lower temperatures whereas unfavourable contributions to the entropy of binding are observed at the higher temperatures. The reason for the unfavourable change in the entropy term upon binding of ANS to the wild-type protein may be due to a loss in solvent entropy. ANS probably binds to a site on the protein that does not impose great motional restrictions. The binding of ANS may not favour the burial of a large hydrophobic surface area as well as the expulsion of water molecules. In order for the overall entropy term to contribute favourably to the binding, the liberation of solvent molecules bound to the surface of the ligand and/or binding site of the protein must occur to an extent sufficiently high to over come the entropy changes for the ligand and macromolecule (Sigurskjold *et al*., 1991). Thermodynamic analysis indicates that the binding of ANS is not entropically favoured at higher temperatures and that the favourable contributions to the binding Gibbs energy are of an enthalpic origin. If a binding event is entropically driven, it usually indicates a strong contribution from hydrophobic effects (Jelesarov and Bosshard, 1994). The free energy of binding, ΔG^{O}, changes little with temperature and reflects an enthalpy-entropy compensation in which the favourable enthalpy of hydrogen bond formation and van der Waals interactions provides the major driving force to the overall free energy of the hGSTA1-1-ANS complex. Because ANS contains a charged sulfonate group (SO_3^-), the contribution of electrostatic interactions towards the favourable binding enthalpy cannot be excluded.

The temperature dependence of the ΔH^{O} reveals a negative heat capacity upon ANS binding to the wild-type hGSTA1-1. This is often associated with the removal/burial of hydrophobic groups from contact with solvent. The binding of ANS to the wild-type protein, therefore, corresponds to the reduction of exposed non-polar surface area to solvent. Speculation of the possible ANS binding site may be the solvent-exposed hydrophobic surface area of domain I. The role of F221 in the ligandin function (i.e., ANS binding) of hGSTA1-1 has been demonstrated in Chapter 5. When the wild-type hGSTA1-1 is complexed with active site ligands, the side chain of F221 at the C-terminus of helix 9 contacts the side chain of Val110 from domain II (Figures 18 A and B). Together, the interactions between F221 and Val110 as well as contributions from

residues located in the C-terminal helix 9 (Leu212, Ala215, Arg216 and Phe219) may form a hydrophobic cluster that increases the hydrophobicity of the C-terminus of helix 9.

Inspection of the K_d values indicates that ANS does not bind very tightly (K_d = 69 μM at 25°C) to the site on the protein and that binding at this site may occur without the expulsion of highly ordered water molecules. This may also explain the reduction in solvent entropy observed upon ANS binding. ANS appears to bind a hydrophobic site located at the subunit interface (Sluis-Cremer *et al*., 1996; Dirr and Wallace, 1999). The ANS binding site is also similar to the one that binds estradiol disulfate (Barycki and Colman, 1997) and AEDANS (Wallace *et al*., 1998b). At present, the exact location of the ANS binding site/s is not clear. However, ITC data suggests that a possible site for ANS binding is located near the H-site region (hydrophobic binding site) of the active site. The availability of crystal structure data of wild-type hGSTA1-1 complexed with ANS should provide some insight into the location and number of ANS binding site/s on the hGSTA1-1 protein.

Binding energetics of BSP to wild-type hGSTA1-1. The binding of BSP to the wild-type GST was very different from all the ligands studied thus far. Firstly, analysis of the data indicated that the binding could not be described by a single site reaction model. The data, however, fits well to a model describing two sets of binding sites. The binding isotherm is clearly biphasic over the entire temperature studied. The first phase (0-2 molar ratio) corresponds to a high affinity binding site that is characterised by very tight binding (K_d values range from 0.15 μM to 0.24 μM BSP) and a stoichiometry of one molecule of BSP per protein monomer (N values of 0.8 to 0.9). The second phase (2.5 to 7 molar ratio) is consistent with a lower affinity site that is capable of binding 3.5 to 3.8 molecules of BSP per monomer. It is also evident that the binding of up to 4 molecules of BSP per protein monomer (Figure 44, panels A and B) could not saturate the lower affinity binding site.

Examination of the enthalpies of binding for the higher affinity site indicate that the interaction at this site is highly favourable and could indicate the formation of hydrogen

bonds as well as van der Waals interactions. The binding entropy (ΔS^O) exhibits large positive values indicative of a very favourable interaction. BSP binding to the higher affinity site most likely implicates a site on the protein that involves the expulsion of water molecules and this would result in the high gain in observed solvent entropy (ΔS^O). The contribution of the binding enthalpy (ΔH^O) and entropy (ΔS^O) to the Gibbs free energy of binding (ΔG^O) (Table 9) indicate that both terms serve as the driving force in the association of BSP with the wild-type protein. Based on these results, it may be likely that high affinity BSP binding occurs near the H-site. Crystal structure data of BSP complexed to the human class pi GST has recently implicated the H-site as a novel ligand-binding site (Oakley *et al*., 1999). Recently, it was shown that the binding of BSP does not affect the urea-dependent binding behaviour of ANS to wild-hGSTA1-1 (Dirr and Wallace, 1999). BSP binding to the wild-type protein resulted in ~ 70% quenching of the intrinsic tryptophan 20 fluorescence. This was in agreement with the proximity of the BSP-binding site to the fluorophore (Ji *et al*., 1996; Dirr and Wallace, 1999). Dirr and Wallace (1999) also showed that the binding affinity of BSP for the wild-type protein is enhanced ~ 3.5-fold when the active site is occupied with glutathione. Interestingly, BSP binding studies on the C-terminally truncated mutant (helix 9 deletion mutant) indicated that BSP binds with a two-fold higher affinity and this was accompanied by an almost 100% quenching of tryptophan 20 fluorescence. In light of the fluorescence data of BSP-binding to wild-type and helix 9 deletion proteins, it is quite conceivable that BSP binds a region near the active site located on each subunit. The binding of non-substrate ligands often results in non-competitive inhibition of GST activity (Mannervik and Danielson, 1988; Bico *et al*., 1995). Inhibition of enzyme activity by non-substrate ligand binding would be explained by the proximity of the active site to the non-substrate ligand binding sites (Bico *et al*., 1995; Dirr and Wallace, 1999). The localisation of helix 9 onto domain I has been observed crystallographically with the occupation of the active site using a variety of ligands (Sinning *et al*., 1993; Cameron *et al*., 1995; Gu *et al*., 2000; Adman *et al*., 2001). The reduction of non-polar exposed surface area upon binding of BSP is indicated by the large negative value of the change in heat capacity, ΔC_p (Figure 45A and Table 10).

The second binding site on the protein is referred to as a lower binding affinity site in comparison to the first high affinity site described above. It is clear that ~ four molecules of BSP bind to this site per protein monomer. Overall, BSP appears to bind the first site ~ 40-fold tighter than the second site. The binding of BSP to the second site is enthalpically (negative ΔH^O values) and entropically (positive ΔH^O) favourable in the temperature range studied. However, BSP binding to the second site is entropically favourable (positive ΔS^O values) only at the lower temperatures. Contributions of the binding enthalpy and binding entropy to the Gibbs free energy (ΔG^O) indicate that the major contributor of the binding of BSP to the lower affinity site is the entropic term ($-T\Delta S^O$). This term contributes as much as 75 to 80% of favourable energy to the overall Gibbs free energy of binding (ΔG^O) to the lower affinity site (Table 9). Therefore, the binding of BSP to the lower affinity site is entropically more favourable than the binding enthalpy of the reaction. The binding enthalpy of BSP to the lower affinity site is also reduced with respect to the higher affinity site (Table 9A and B). Speculation of a possible lower affinity binding site could involve the region around helix 2 (see Figure 1A for location of helix 2). There is also evidence to suggest that the sulfonate-containing buffers, Mes and Hepes, bind a similar region in the class mu and pi GSTs (Ji *et al*., 1997; Prade *et al*., 1997). What is clear is that BSP binding to the lower affinity site (Figure 45B, Table 10) does not involve a significant reduction of non-polar surface area when compared to the higher affinity binding site (Figure 45A, Table 10).

7.3 Conclusions

This work is the first to describe the energetics of ligand binding to the active (G- and H-sites) and non-substrate (L-site) ligand binding sites of the human class alpha GSTs using isothermal titration calorimetry. Preliminary work on the binding of glutathione and glutathione sulfonate to the wild-type and Y8F proteins suggests that the Y8F mutant protein binds the physiological tripeptide glutathione tighter than the wild-type protein, whereas the wild-type binds the anionic glutathione analogue, glutathione sulfonate, tighter than the Y8F mutant. The fact that the Y8F mutant displays a larger negative ΔC_p (using glutathione and glutathione sulfonate) may implicate the tyrosyl hydroxyl group, situated at the active site, in modulating the dynamics of the C-terminal helix 9. This

study, however, needs to be extended to include the contribution made by linked-protonation effects to the observed energetic binding parameters in order to know the "true" thermodynamic parameters of the protein-ligand interaction alone. The identification of the most appropriate buffers is, therefore, required to avoid buffer-binding effects because GSTs appear to be buffer-binding proteins. This information would be essential in determining the protonation state of tyrosine 8 at the active. By performing the experiments under conditions of varying pH conditions, it is also possible to determine the pK_a value of this catalytic residue.

The binding of ANS to the wild-type protein indicated that one molecule of ANS binds per protein monomer. The interactions are enthalpically favourable indicating the possibility of hydrogen bond formation. ANS binding also results in a reduction of non-polar surface area exposed to solvent. The proposed binding site is the region around domain I that becomes buried when helix 9 is immobilised.

BSP binding to the wild-type hGSTA1-1 protein involves a high and low affinity set of binding sites. The higher affinity site is capable of binding one molecule of BSP per protein monomer whereas the lower affinity site can accommodate a minimum of four BSP molecules. Binding to the higher affinity site is clearly enthalpically and entropically favourable with both terms contributing to the very favourable Gibbs free energy of binding. Binding to the lower affinity site, however, is not very favourable enthalpically and the major driving force behind the favourable Gibbs free energy of association is the entropic factor ($-T\Delta S$). This interaction is, therefore, entropically driven.

The work presented here has shown that the dissection of the thermodynamics of ligand binding to hGSTA1-1 and the correlation of energetics to structure is crucial towards our understanding of the functioning of this class of enzymes.

CHAPTER 7

REFERENCES

Adman, E.T., Le, T., I, Stenkamp, R.E., Nieslanik, B.S., Dietze, E.C., Tai, G., Ibarra, C. and Atkins, W.M. (2001) Localization of the C-terminus of rat glutathione S-transferase A1-1: crystal structure of mutants W21F and W21F/F220Y. *Proteins* **42**, 192-200

Alberty, R.A. (1994) Biochemical thermodynamics. *Biochim. Biophys. Acta* **1207**, 1-11

Allardyce, C.S., McDonagh, P.D., Lian, L.Y., Wolf, C.R. and Roberts, G.C. (1999) The role of tyrosine-9 and the C-terminal helix in the catalytic mechanism of Alpha-class glutathione S-transferases. *Biochem. J.* **343 Pt 3:525-31.**, 525-531

Anfinsen, C.B. (1973) Principles that govern the folding of protein chains. *Science* **181**, 223-230

Arakawa, T. and Timasheff, S.N. (1984) Protein stabilization and destabilization by guanidinium salts. *Biochemistry* **23**, 5924-5929

Arca, P., Rico, M., Brana, A.F., Villar, C.J., Hardisson, C. and Suarez, J.E. (1988) Formation of an adduct between fosfomycin and glutathione: a new mechanism of antibiotic resistance in bacteria. *Antimicrob. Agents Chemother.* **32**, 1552-1556

Arca, P., Garcia, P., Hardisson, C. and Suarez, J.E. (1990a) Purification and study of a bacterial glutathione S-transferase. *FEBS Lett.* **263**, 77-79

Arca, P., Hardisson, C. and Suarez, J.E. (1990b) Purification of a glutathione S-transferase that mediates fosfomycin resistance in bacteria. *Antimicrob. Agents Chemother.* **34**, 844-848

Armstrong, R.N. (1997) Structure, catalytic mechanism, and evolution of the glutathione transferases. *Chem. Res. Toxicol.* **10**, 2-18

Askelof, P., Guthenberg, C., Jakobson, I. and Mannervik, B. (1975) Purification and characterization of two glutathione S-aryltransferase activities from rat liver. *Biochem. J.* **147**, 513-522

Atkins, W.M., Wang, R.W., Bird, A.W., Newton, D.J. and Lu, A.Y. (1993) The catalytic mechanism of glutathione S-transferase (GST). Spectroscopic determination of the pKa of Tyr-9 in rat alpha 1-1 GST. *J. Biol. Chem.* **268**, 19188-19191

Atkins, W.M., Dietze, E.C. and Ibarra, C. (1997) Pressure-dependent ionization of Tyr 9 in glutathione S-transferase A1-1: contribution of the C-terminal helix to a "soft" active site. *Protein Sci.* **6**, 873-881

Baker, B.M. and Murphy, K.P. (1996) Evaluation of linked protonation effects in protein binding reactions using isothermal titration calorimetry. *Biophys. J.* **71**, 2049-2055

Baker, B.M. and Murphy, K.P. (1997) Dissecting the energetics of a protein-protein interaction: the binding of ovomucoid third domain to elastase. *J. Mol. Biol.* **268**, 557-569

Baker, B.M. and Murphy, K.P. (1998) Prediction of binding energetics from structure using empirical parameterization. *Methods Enzymol.* **295**, 294-315

Baldwin, R.L. (1986) Protein folding: introductory comments. *Methods Enzymol.* **131**, 3-4

Baron, C., Gonzalez, J.F., Mateo, P.L. and Cortijo, M. (1989) Thermodynamic analysis of the activation of glycogen phosphorylase b over a range of temperatures. *J. Biol. Chem.* **264**, 12872-12878

Barycki, J.J. and Colman, R.F. (1997) Identification of the nonsubstrate steroid binding site of rat liver glutathione S-transferase, isozyme 1-1, by the steroid affinity label, 3beta-(iodoacetoxy)dehydroisoandrosterone. *Arch. Biochem. Biophys.* **345**, 16-31

Ben Naim, A., Ting, K.L. and Jernigan, R.L. (1990) Solvent effect on binding thermodynamics of biopolymers. *Biopolymers* **29**, 901-919

Bensimon, D. (1996) Force: a new structural control parameter? *Structure.* **4**, 885-889

Benson, A.M., Talalay, P., Keen, J.H. and Jakoby, W.B. (1977) Relationship between the soluble glutathione-dependent delta 5-3-ketosteroid isomerase and the glutathione S-transferases of the liver. *Proc. Natl. Acad. Sci. U. S. A* **74**, 158-162

Bernat, B.A., Laughlin, L.T. and Armstrong, R.N. (1997) Fosfomycin resistance protein (FosA) is a manganese metalloglutathione transferase related to glyoxalase I and the extradiol dioxygenases. *Biochemistry* **36**, 3050-3055

Bhatnagar, R.S. and Gordon, J.I. (1995) Thermodynamic studies of myristoyl-CoA: protein *N*-myristoyltransferase using isothermal titration calorimetry. *Methods Enzymol.* **35**, 467486

Bico, P., Chen, C.Y., Jones, M., Erhardt, J. and Dirr, H. (1994) Class pi glutathione S-transferase: Meisenheimer complex formation. *Biochem. Mol. Biol. Int.* **33**, 887-892

Birdsall, B., King, R.W., Wheeler, M.R., Lewis, C.A., Godde, S.R., Dunlap, R.B. and Roberts, G.C.K. (1983) Correction for light absorption in fluorescence studies of protein-ligand interactions. *Anal. Biochem.* **132**, 353-361

Bjornestedt, R., Stenberg, G., Widersten, M., Board, P.G., Sinning, I., Jones, T.A. and Mannervik, B. (1995) Functional significance of arginine 15 in the active site of human class alpha glutathione transferase A1-1. *J. Mol. Biol.* **247**, 765-773

Blond, S. and Goldberg, M.E. (1985) Kinetics and importance of the dimerisation step in the folding pathway in the β_2 subunit of *Escherichia coli*. *J.Mol. Biol*. **182**, 587-606

Board, P.G. and Mannervik, B. (1991) The contribution of the C-terminal sequence to the catalytic activity of GST2, a human alpha-class glutathione transferase. *Biochem. J.* **275**, 171-174

Board, P.G., Coggan, M., Wilce, M.C. and Parker, M.W. (1995) Evidence for an essential serine residue in the active site of the Theta class glutathione transferases. *Biochem. J.* **311**, 247-250

Board, P.G., Baker, R.T., Chelvanayagam, G. and Jermiin, L.S. (1997) Zeta, a novel class of glutathione transferases in a range of species from plants to humans. *Biochem. J.* **328**, 929-935

Board, P.G., Coggan, M., Chelvanayagam, G., Easteal, S., Jermiin, L.S., Schulte, G.K., Danley, D.E., Hoth, L.R., Griffor, M.C., Kamath, A.V., Rosner, M.H., Chrunyk, B.A., Perregaux, D.E., Gabel, C.A., Geoghegan, K.F. and Pandit, J. (2000) Identification, characterization, and crystal structure of the Omega class glutathione transferases. *J. Biol. Chem.* **275**, 24798-24806

Booth, J., Boyland, E. and Sims, P. (1961) An enzyme from rat liver catalysing conjugations with glutathione. *Biochem. J.* **79**, 516-524

Bowie, J.U. and Sauer, R.T. (1989) Equilibrium dissociation and unfolding of the Arc repressor dimer. *Biochemistry* **28**, 7139-7143

Bowie, J.U., Clarke, N.D., Pabo, C.O. and Sauer, R.T. (1990) Identification of protein folds: matching hydrophobicity patterns of sequence sets with solvent accessibility patterns of known structures. *Proteins* **7**, 257-264

Boyland, E. and Chasseaud, L.F. (1967) Enzyme-catalysed conjugations of glutathione with unsaturated compounds. *Biochem. J.* **104**, 95-102

Boyland, E. and Chasseaud, L.F. (1969) The role of glutathione and glutathione *S*-transferases in mercapturic acid biosynthesis. *Adv. Enzymol.* **32**, 173-219

Brady, G.P. and Sharp, K.A. (1997) Entropy in protein folding and in protein-protein interactions. *Curr. Opin. Struct. Biol.* **7**, 215-221

Bruns, C.M., Hubatsch, I., Ridderstrom, M., Mannervik, B. and Tainer, J.A. (1999) Human glutathione transferase A4-4 crystal structures and mutagenesis reveal the basis of high catalytic efficiency with toxic lipid peroxidation products. *J. Mol. Biol.* **288**, 427-439

Buetler, T.M. and Eaton, D.L. (1992) Complementary DNA cloning, messenger RNA expression, and induction of alpha-class glutathione S-transferases in mouse tissues. *Cancer Res.* **52** , 314-318

Byrne, M.P., Manuel, R.L., Lowe, L.G. and Stites, W.E. (1995) Energetic contribution of side chain hydrogen bonding to the stability of staphylococcal nuclease. *Biochemistry* **34**, 13949-13960

Caccuri, A.M., Aceto, A., Piemonte, F., Di Ilio, C., Rosato, N. and Federici, G. (1990) Interaction of hemin with placental glutathione transferase. *Eur. J. Biochem.* **189**, 493-497

Cameron, A.D., Sinning, I., L'Hermite, G., Olin, B., Board, P.G., Mannervik, B. and Jones, T.A. (1995) Structural analysis of human alpha-class glutathione transferase A1-1 in the apo-form and in complexes with ethacrynic acid and its glutathione conjugate. *Structure.* **3**, 717-727

Cameron, A.D., Olin, B., Ridderstrom, M., Mannervik, B. and Jones, T.A. (1997) Crystal structure of human glyoxalase I--evidence for gene duplication and 3D domain swapping. *EMBO J.* **16**, 3386-3395

Coles, B. and Ketterer, B. (1990) The role of glutathione and glutathione transferases in chemical carcinogenesis. *Crit Rev. Biochem. Mol. Biol.* **25**, 47-70

Combes, B. and Stakelum, G. (1961) A liver enzyme that conjugates sulfobromophthalein sodium with glutathione. *J. Clin. Invest.* **40**, 981-988

Connelly, P.R. and Thomson, J.A. (1992) Heat capacity changes and hydrophobic interactions in the binding of FK506 and rapamycin to the FK506 binding protein. *Proc. Natl. Acad. Sci. U. S. A* **89**, 4781-4785

Connelly, P.R., Aldape, R.A., Bruzzese, F.J., Chambers, S.P., Fitzgibbon, M.J., Fleming, M.A., Itoh, S., Livingston, D.J., Navia, M.A., Thomson, J.A. and . (1994) Enthalpy of hydrogen bond formation in a protein-ligand binding reaction. *Proc. Natl. Acad. Sci. U. S. A* **91**, 1964-1968

Creighton, T.E. (1984) Pathways and mechanisms of protein folding. *Adv. Biophys.* **18**, 1-20

Crump, M.P., Spyracopoulos, L., Lavigne, P., Kim, K.S., Clark-lewis, I. and Sykes, B.D. (1999) Backbone dynamics of the human CC chemokine eotaxin: fast motions, slow motions, and implications for receptor binding. *Protein Sci.* **8**, 2041-2054

Dammer, U., Popescu, O., Wagner, P., Anselmetti, D., Guntherodt, H.J. and Misevic, G.N. (1995) Binding strength between cell adhesion proteoglycans measured by atomic force microscopy. *Science* **267**, 1173-1175

Danger, D.P., Baldwin, W.S. and LeBlanc, G.A. (1992) Photoaffinity labelling of steroid-hormone-binding glutathione S-transferases with [3H]methyltrienolone. Inhibition of steroid-binding activity by the anticarcinogen indole-3-carbinol. *Biochem. J.* **288**, 361-367

Danielson, U.H. and Mannervik, B. (1985) Kinetic independence of the subunits of cytosolic glutathione transferase from the rat. *Biochem. J.* **231**, 263-267

Dietze, E.C., Ibarra, C., Dabrowski, M.J., Bird, A. and Atkins, W.M. (1996a) Rational modulation of the catalytic activity of A1-1 glutathione S-transferase: evidence for incorporation of an on-face (pi...HO-Ar) hydrogen bond at tyrosine-9. *Biochemistry* **35**, 11938-11944

Dietze, E.C., Wang, R.W., Lu, A.Y. and Atkins, W.M. (1996b) Ligand effects on the fluorescence properties of tyrosine-9 in alpha 1-1 glutathione S-transferase. *Biochemistry* **35**, 6745-6753

Dill, K.A. (1990) Dominant forces in protein folding. *Biochemistry* **29**, 7133-7155

Dirr, H.W. and Reinemer, P. (1991) Equilibrium unfolding of class pi glutathione S-transferase. *Biochem. Biophys. Res. Commun.* **180**, 294-300

Dirr, H., Reinemer, P. and Huber, R. (1994a) Refined crystal structure of porcine class Pi glutathione S-transferase (pGST P1-1) at 2.1 A resolution. *J. Mol. Biol.* **243**, 72-92

Dirr, H., Reinemer, P. and Huber, R. (1994b) X-ray crystal structures of cytosolic glutathione S-transferases. Implications for protein architecture, substrate recognition and catalytic function. *Eur. J. Biochem.* **220**, 645-661

Dirr, H.W. and Wallace, L.A. (1999) Role of the C-terminal helix 9 in the stability and ligandin function of class alpha glutathione transferase A1-1. *Biochemistry* **38**, 15631-15640

Doyle, M.L. (1999) Titration calorimetry. *Current Protocols in Protein Science* 20.4.1-20.4.24

Duggan, B.M., Dyson, H.J. and Wright, P.E. (1999) Inherent flexibility in a potent inhibitor of blood coagulation, recombinant nematode anticoagulant protein c2. *Eur. J. Biochem.* **265**, 539-548

Eftink, M.R., Anusiem, A.C. and Biltonen, R.L. (1983) Enthalpy-entropy compensation and heat capacity changes for protein-ligand interactions: general thermodynamic models and data for the binding of nucleotides to ribonuclease A. *Biochemistry* **22**, 3884-3896

Eklund, H., Ingelman, M., Soderberg, B.O., Uhlin, T., Nordlund, P., Nikkola, M., Sonnerstam, U., Joelson, T. and Petratos, K. (1992) Structure of oxidized bacteriophage T4 glutaredoxin (thioredoxin). Refinement of native and mutant proteins. *J. Mol. Biol.* **228**, 596-618

Epp, O., Ladenstein, R. and Wendel. (1983) The refined structure of the selenoenzyme glutathione peroxidase at 0.2 nm resolution. *Eur. J. Biochem*. **133**, 51-69

Erhardt, J. and Dirr, H. (1995) Native dimer stabilizes the subunit tertiary structure of porcine class pi glutathione S-transferase. *Eur. J. Biochem.* **230**, 614-620

Finer, J.T., Simmons, R.M. and Spudich, J.A. (1994) Single myosin molecule mechanics: piconewton forces and nanometre steps. *Nature* **368**, 113-119

Finkelstein, A.V. and Janin, J. (1989) The price of lost freedom: entropy of bimolecular complex formation. *Protein Eng* **3**, 1-3

Florin, E.L., Moy, V.T. and Gaub, H.E. (1994) Adhesion forces between individual ligand-receptor pairs. *Science* **264**, 415-417

Fukada, H. and Takahashi, K. (1998) Enthalpy and heat capacity changes for the proton dissociation of various buffer components in 0.1 M potassium chloride. *Proteins* **33**, 159-166

Garcia-Saez, I., Parraga, A., Phillips, M.F., Mantle, T.J. and Coll, M. (1994) Molecular structure at 1.8 A of mouse liver class pi glutathione S-transferase complexed with S-(p-nitrobenzyl)glutathione and other inhibitors. *J. Mol. Biol.* **237**, 298-314

Gloss, L.M. and Matthews, C.R. (1998) Mechanism of folding of the dimeric core domain of *Escherichia coli Trp* repressor: A nearly diffusion-limited reaction leads to the formation of an on-pathway dimeric intermediate. *Biochemistry* **37**, 15990-15999

Gokhale, R.S., Ray, S.S., Balaram, H. and Balram, P. (1999) Unfolding of *Plasmodium falciparum* triosephosphate isomerase in urea and guanidinium chloride: Evidence for a novel disulphide exchange reaction in a covalently cross-linked mutant. Biochemistry 38, 423-431

Graminski, G.F., Kubo, Y. and Armstrong, R.N. (1989a) Spectroscopic and kinetic evidence for the thiolate anion of glutathione at the active site of glutathione S-transferase. *Biochemistry* **28**, 3562-3568

Graminski, G.F., Zhang, P.H., Sesay, M.A., Ammon, H.L. and Armstrong, R.N. (1989b) Formation of the 1-(S-glutathionyl)-2,4,6-trinitrocyclohexadienate anion at the active site of glutathione S-transferase: evidence for enzymic stabilization of sigma-complex intermediates in nucleophilic aromatic substitution reactions. *Biochemistry* **28**, 6252-6258

Greenfield, N.J. (1996) Methods to estimate the conformation of proteins and polypeptides from circular dichroism data. *Anal. Biochem.* **235**, 1-10

Grubmuller, H., Heymann, B. and Tavan, P. (1996) Ligand binding: molecular mechanics calculation of the streptavidin-biotin rupture force. *Science* **271**, 997-999

Gu, Y., Singh, S.V. and Ji, X. (2000) Residue R216 and catalytic efficiency of a murine class alpha glutathione S-transferase toward benzo[a]pyrene 7(R),8(S)-diol 9(S), 10(R)-epoxide. *Biochemistry* **39**, 12552-12557

Guex, N. and Peitsch, M.C. (1997) SWISS-MODEL and the Swiss-PdbViewer: an environment for comparative protein modeling. *Electrophoresis* **18**, 2714-2723

Gustafsson, A., Etahadieh, M., Jemth, P. and Mannervik, B. (1999) The C-terminal region of human glutathione transferase A1-1 affects the rate of glutathione binding and the ionization of the active-site Tyr9. *Biochemistry* **38**, 16268-16275

Habermann, S.M. and Murphy, K.P. (1996) Energetics of hydrogen bonding in proteins: a model compound study. *Protein Sci.* **5**, 1229-1239

Habig, W.H., Pabst, M.J., Fleischner, G., Gatmaitan, Z., Arias, I.M. and Jakoby, W.B. (1974a) The identity of glutathione S-transferase B with ligandin, a major binding protein of liver. *Proc. Natl. Acad. Sci. U. S. A* **71**, 3879-3882

Habig, W.H., Pabst, M.J. and Jakoby, W.B. (1974b) Glutathione S-transferases. The first enzymatic step in mercapturic acid formation. *J. Biol. Chem.* **249**, 7130-7139

Habig, W.H. and Jakoby, W.B. (1981) Assays for differentiation of glutathione S-transferases. *Methods Enzymol.* **77**, 398-405

Hayes, J.D. and Pulford, D.J. (1995) The glutathione S-transferase supergene family: regulation of GST and the contribution of the isoenzymes to cancer chemoprotection and drug resistance. *Crit Rev. Biochem. Mol. Biol.* **30**, 445-600

Hoesch, R.M. and Boyer, T.D. (1989) Localization of a portion of the active site of two rat liver glutathione S-transferases using a photoaffinity label. *J. Biol. Chem.* **264**, 17712-17717

Holmgren, A., Soderberg, B.O., Eklund, H. and Branden, C.I. (1975) Three-dimensional structure of Escherichia coli thioredoxin-S2 to 2.8 A resolution. *Proc. Natl. Acad. Sci. U. S. A* **72**, 2305-2309

Honig, B., Sharp, K. and Gilson, M. (1989) Electrostatic interactions in proteins. *Prog. Clin. Biol. Res.* **289**, 65-74

Hornby, J.A., Luo, J.K., Stevens, J.M., Wallace, L.A., Kaplan, W., Armstrong, R.N. and Dirr, H.W. (2000) Equilibrium folding of dimeric class mu glutathione transferases involves a stable monomeric intermediate. *Biochemistry* **39**, 12336-12344

Houry, W.A., Rothwarf, D.M. and Scheraga, H.A. (1996) Circular dichroism evidence for the presence of burst-phase intermediates on the conformational folding pathway of ribonuclease A *Biochemistry* **35**, 10125-10133

Jaenicke, R. and Rudolph, R. (1986) Refolding and association of oligomeric proteins. *Methods Enzymol*. **131**, 218-250

Jackson, S.E. (1998) How do small single-domains proteins fold? *Fold Des*. **3**, R81-R91

Jakoby, W.B. and Ziegler, D.M. (1990) The enzymes of detoxication. *J. Biol. Chem.* **265**, 20715-20718

Janin, J., Miller, S. and Chothia, C. (1988) Surface, subunit interfaces and interior of oligomeric proteins. *J. Mol. Biol.* **204**, 155-164

Janin, J. and Chothia, C. (1990) The structure of protein-protein recognition sites. *J. Biol. Chem.* **265**, 16027-16030

Jelesarov, I. and Bosshard, H.R. (1994) Thermodynamics of ferredoxin binding to ferredoxin:NADP+ reductase and the role of water at the complex interface. *Biochemistry* **33**, 13321-13328

Ji, X., Zhang, P., Armstrong, R.N. and Gilliland, G.L. (1992) The three-dimensional structure of a glutathione S-transferase from the mu gene class. Structural analysis of the binary complex of isoenzyme 3-3 and glutathione at 2.2-A resolution. *Biochemistry* **31**, 10169-10184

Ji, X., Armstrong, R.N. and Gilliland, G.L. (1993) Snapshots along the reaction coordinate of an SNAr reaction catalyzed by glutathione transferase. *Biochemistry* **32**, 12949-12954

Ji, X., von Rosenvinge, E.C., Johnson, W.W., Tomarev, S.I., Piatigorsky, J., Armstrong, R.N. and Gilliland, G.L. (1995) Three-dimensional structure, catalytic properties, and evolution of a sigma class glutathione transferase from squid, a progenitor of the lens S-crystallins of cephalopods. *Biochemistry* **34**, 5317-5328

Ji, X., von Rosenvinge, E.C., Johnson, W.W., Armstrong, R.N. and Gilliland, G.L. (1996) Location of a potential transport binding site in a sigma class glutathione transferase by x-ray crystallography. *Proc. Natl. Acad. Sci. U. S. A* **93**, 8208-8213

Ji, X., Tordova, M., O'Donnell, R., Parsons, J.F., Hayden, J.B., Gilliland, G.L. and Zimniak, P. (1997) Structure and function of the xenobiotic substrate-binding site and location of a potential non-substrate-binding site in a class pi glutathione S-transferase. *Biochemistry* **36**, 9690-9702

Johansson, A.S. and Mannervik, B. (2001) Interindividual variability of glutathione transferase expression in man, in Interindividual variability in drug metabolism in man (Pacifici, G.M. and Pelkonen, O. eds) Taylor and Francis, London, in press

Jones, S. and Thornton, J.M. (1996) Principles of protein-protein interactions. *Proc. Natl. Acad. Sci. U. S. A* **93**, 13-20

Kaplan, W., Husler, P., Klump, H., Erhardt, J., Sluis-Cremer, N. and Dirr, H. (1997) Conformational stability of pGEX-expressed Schistosoma japonicum glutathione S-transferase: a detoxification enzyme and fusion-protein affinity tag. *Protein Sci.* **6**, 399-406

Karshikoff, A., Reinemer, P., Huber, R. and Ladenstein, R. (1993) Electrostatic evidence for the activation of the glutathione thiol by Tyr7 in pi-class glutathione transferases. *Eur. J. Biochem.* **215**, 663-670

Kauzmann, W. (1959) Some factors in the interpretation of protein denaturation. *Adv. Prot. Chem*. **14**, 1-63

Kelly, M.A Liang, H.B., Sytwu I.I., Vlattas, I, Lyons, N.L., Bowen, B.R. and Wennogle, L.P. (1996) Characterisation of SH2-ligand interactions via library affinity selection with mass-spectrometric detection. *Biochemistry* **35**, 11747-11755

Kelly, S.M. and Price, N.C. (1997) The application of circular dichroism to studies of protein folding and unfolding. *Biochim. Biophys. Acta* **1338**, 161-185

Ketley, J.N., Habig, W.H. and Jakoby, W.B. (1975) Binding of nonsubstrate ligands to the glutathione S-transferases. *J. Biol. Chem.* **250**, 8670-8673

Ketterer, B., Srai, K.S. and Christodoulides, L. (1976) Haem-binding proteins of the rat liver cytosol. *Biochim. Biophys. Acta* **428**, 683-689

Ketterer, B., Tan, K.H., Meyer, D.J. and Coles, B. (1987) Glutathione transferases: a possible role in the detoxification of DNA and lipid hydroperoxides, in Glutathione S-transferases and carcinogenesis (Mantle, T.J., Pickett, C.B. and Hayes, J.D. eds.) p149. Taylor and Francis, London.

Kolm, R.H., Sroga, G.E. and Mannervik, B. (1992) Participation of the phenolic hydroxyl group of Tyr-8 in the catalytic mechanism of human glutathione transferase P1-1. *Biochem. J.* **285**, 537-540

Kong, K.H., Takasu, K., Inoue, H. and Takahashi, K. (1992) Tyrosine-7 in human class Pi glutathione S-transferase is important for lowering the pKa of the thiol group of glutathione in the enzyme-glutathione complex. *Biochem. Biophys. Res. Commun.* **184**, 194-197

Kraulis, P.J. (1991) MOLSCRIPT: A program to produce both detailed and schematic plots of protein structures. *J. Appl. Crystallog*. **24**, 946-950

Kuehn, M.J., Ogg, D.J., Kihlberg, J., Slonim, L.N., Flemmer, K., Bergfors, T. and Hultgren, S.J. (1993) Structural basis of pilus subunit recognition by the PapD chaperone. *Science* **262**, 1234-1241

Lacowicz, J.R. (1983) *Principles of fluorescence spectroscopy*. Plenum Press, New York

Laemmli, U.K. (1970) Cleavage of structural proteins during the assembly of the head of bacteriophage T4. *Nature* **227**, 680-685

Lawrence, R.A. and Burk, R.F. (1976) Glutathione peroxidase activity in selenium-deficient rat liver. *Biochem. Biophys. Res. Commun*. **71**, 952-958

Lesk, A.M. and Chothia, C. (1980) Solvent accessibility, protein surfaces, and protein folding. *Biophys. J.* **32**, 35-47

Lehgauer, T. and Rarey, M. (1996) Computational methods for biomolecular docking. *Curr. Opin. Struct. Biol*. **6**, 402-406

Lian, L.Y. (1998) NMR structural studies of glutathione S-transferase. *Cell Mol. Life Sci.* **54**, 359-362

Lim, K., Ho, J.X., Keeling, K., Gilliland, G.L., Ji, X., Ruker, F. and Carter, D.C. (1994) Three-dimensional structure of Schistosoma japonicum glutathione S-transferase fused with a six-amino acid conserved neutralizing epitope of gp41 from HIV. *Protein Sci.* **3**, 2233-2244

Listowsky, I., Abramovitz, M., Homma, H. and Niitsu, Y. (1988) Intracellular binding and transport of hormones and xenobiotics by glutathione-S-transferases. *Drug Metab Rev.* **19**, 305-318

Litwack, G., Ketterer, B. and Arias, I.M. (1971) Ligandin: a hepatic protein which binds steroids, bilirubin, carcinogens and a number of exogenous organic anions. *Nature* **234**, 466-467

Liu, S., Zhang, P., Ji, X., Johnson, W.W., Gilliland, G.L. and Armstrong, R.N. (1992) Contribution of tyrosine 6 to the catalytic mechanism of isoenzyme 3-3 of glutathione S-transferase. *J. Biol. Chem.* **267**, 4296-4299

Livingstone, J.R., Spolar, R.S. and Record, M.T., Jr. (1991) Contribution to the thermodynamics of protein folding from the reduction in water-accessible nonpolar surface area. *Biochemistry* **30**, 4237-4244

Lung-Nan, L., Mason, A.B., Woodworth, R.C. and Brandts, J.F. (1991) Calorimetric studies of the binding of ferric ions to ovotransferrin and interactions between binding sites. *Biochemistry* **30**, 11660-11669

Luque, I. and Freire, E. (1998a) Structure-based prediction of binding affinities and molecular design of peptide ligands. *Methods Enzymol.* **295**, 100-127

Luque, I., Gomez, J., Semo, N. and Freire, E. (1998b) Structure-based thermodynamic design of peptide ligands: application to peptide inhibitors of the aspartic protease endothiapepsin. *Proteins* **30**, 74-85

Luque, I., Todd, M.J., Gomez, J., Semo, N. and Freire, E. (1998c) Molecular basis of resistance to HIV-1 protease inhibition: a plausible hypothesis. *Biochemistry* **37**, 5791-5797

Makhatadze, G.I. and Privalov, P.L. (1990) Heat capacity of proteins. I. Partial molar heat capacity of individual amino acid residues in aqueous solution: hydration effect. *J. Mol. Biol.* **213**, 375-384

Makhatadze, G.I. and Privalov, P.L. (1995) Energetics of protein structure. *Adv. Protein Chem.* **47**, 307-425

Makhatadze, G.I. (1998) Heat capacities of amino acids, peptides and proteins. *Biophys. Chem.* **71**, 133-156

Mannervik, B. and Guthenberg, C. (1981) Glutathione transferase (human placenta). *Methods Enzymol.* **77**, 231-235

Mannervik, B. (1985) The isoenzymes of glutathione transferase. *Adv. Enzymol. Relat Areas Mol. Biol.* **57**, 357-417

Mannervik, B. and Danielson, U.H. (1988a) Glutathione transferases--structure and catalytic activity. *CRC Crit Rev. Biochem.* **23**, 283-337

Mannervik, B. and Danielson, U.H. (1988b) Glutathione transferases--structure and catalytic activity. *CRC Crit Rev. Biochem.* **23**, 283-337

Mannervik, B., Alin, P., Guthenberg, C., Jensson, H., Tahir, M.K., Warholm, M. and Jornvall, H. (1985) Identification of three classes of cytosolic glutathione transferase common to several mammalian species: correlation between structural data and enzymatic properties. *Proc. Natl. Acad. Sci. U. S. A* **82**, 7202-7206

Mannervik, B., Awasthi, Y.C., Board, P.G., Hayes, J.D., Di Ilio, C., Ketterer, B., Listowsky, I., Morgenstern, R., Muramatsu, M., Pearson, W.R. and Pickett, C.B. Sato, K., Widersten, M. and Wolf, C.R. (1992) Nomenclature for human glutathione transferases. *Biochem. J.* **282**, 305-306

Marqusee, S. and Sauer, R.T. (1994) Contributions of a hydrogen bond/salt bridge network to the stability of secondary and tertiary structure in lambda repressor. *Protein Sci.* **3**, 2217-2225

Matthews, B.W. (1995) Studies on protein stability with T4 lysozyme. *Adv. Protein Chem.* **46**, 249-278

McCarthy, D.L., Navarrete, S., Willett, W.S., Babbitt, P.C. and Copley, S.D. (1996) Exploration of the relationship between tetrachlorohydroquinone dehalogenase and the glutathione S-transferase superfamily. *Biochemistry* **35**, 14634-14642

McTigue, M.A., Williams, D.R. and Tainer, J.A. (1995) Crystal structures of a schistosomal drug and vaccine target: glutathione S-transferase from Schistosoma japonica and its complex with the leading antischistosomal drug praziquantel. *J. Mol. Biol.* **246**, 21-27

Meyer, D.J., Coles, B., Pemble, S.E., Gilmore, K.S., Fraser, G.M. and Ketterer, B. (1991) Theta, a new class of glutathione transferases purified from rat and man. *Biochem. J.* **274**, 409-414

Meyer, D.J., Xia, C., Coles, B., Chen, H., Reinemer, P., Huber, R. and Ketterer, B. (1993) Unusual reactivity of Tyr-7 of GSH transferase P1-1. *Biochem. J.* **293**, 351-356

Morgenstern, R., DePierre, J.W. and Ernster, L. (1979) Activation of microsomal glutathione S-transferase activity by sulfhydryl reagents. *Biochem. Biophys. Res. Commun.* **87**, 657-663

Morgenstern, R., Guthenberg, C., Mannervik, B. and DePierre, J.W. (1983) The amount and nature of glutathione transferases in rat liver microsomes determined by immunochemical methods. *FEBS Lett.* **160**, 264-268

Moy, V.T., Florin, E.L. and Gaub, H.E. (1994) Intermolecular forces and energies between ligands and receptors. *Science* **266**, 257-259

Murphy, K.P., Privalov, P.L. and Gill, S.J. (1990) Common features of protein unfolding and dissolution of hydrophobic compounds. *Science* **247**, 559-561

Murphy, K.P. and Gill, S.J. (1991) Solid model compounds and the thermodynamics of protein unfolding. *J. Mol. Biol.* **222**, 699-709

Murphy, K.P., Xie, D., Garcia, K.C., Amzel, L.M. and Freire, E. (1993) Structural energetics of peptide recognition: angiotensin II/antibody binding. *Proteins* **15**, 113-120

Murphy, K.P. (1995) Noncovalent forces important to the conformational stability of protein structures. *Methods Mol. Biol.* **40**, 1-34

Murzin, A.G., Brenner, S.E., Hubbard, T. and Chothia, C. (1995) SCOP: a structural classification of proteins database for the investigation of sequences and structures. *J. Mol. Biol.* **247**, 536-540

Myers, J.K., Pace, C.N. and Scholtz, J.M. (1995) Denaturant m values and heat capacity changes: relation to changes in accessible surface areas of protein unfolding. *Protein Sci.* **4**, 2138-2148

Neet, K.E. and Timm, D.E. (1994) Conformational stability of dimeric proteins: quantitative studies by equilibrium denaturation. *Protein Sci.* **3**, 2167-2174

Nieslanik, B.S. and Atkins, W.M. (2000) The catalytic Tyr-9 of glutathione S-transferase A1-1 controls the dynamics of the C terminus. *J. Biol. Chem.* **275**, 17447-17451

Nieslanik, B., Ibarra, C. and Atkins, W.M. (2001) The C-terminus of glutathione S-transferase A1-1 is required for entropically-driven ligand binding. *Biochemistry* **40**, 3536-3543

Nozaki, Y. and Tanford, C. (1971) The solubility of amino acids and two glycine peptides in aqueous ethanol and dioxane solutions. Establishment of a hydrophobicity scale. *J. Biol. Chem.* **246**, 2211-2217

Oakley, A.J., Bello, M.L., Battistoni, A., Ricci, G., Rossjohn, J., Villar, H.O. and Parker, M.W. (1997a) The structures of human glutathione transferase P1-1 in complex with glutathione and various inhibitors at high resolution. *J. Mol. Biol.* **274**, 84-100

Oakley, A.J., Rossjohn, J., Lo, B.M., Caccuri, A.M., Federici, G. and Parker, M.W. (1997b) The three-dimensional structure of the human Pi class glutathione transferase P1-1 in complex with the inhibitor ethacrynic acid and its glutathione conjugate. *Biochemistry* **36**, 576-585

Oakley, A.J., Lo, B.M., Nuccetelli, M., Mazzetti, A.P. and Parker, M.W. (1999) The ligandin (non-substrate) binding site of human Pi class glutathione transferase is located in the electrophile binding site (H-site). *J. Mol. Biol.* **291**, 913-926

Oliveberg, M. and Fersht, A.R. (1996) Thermodynamics of transient conformations in the folding pathway of barnase: Reorganisation of the folding intermediate at low pH. *Biochemistry* **35**, 2738-2749

Orengo, C.A., Flores, T.P., Taylor, W.R. and Thornton, J.M. (1993) Identification and classification of protein fold families. *Protein Eng* **6**, 485-500

Pace, C.N. (1986) Determination and analysis of urea and guanidine hydrochloride denaturation curves. *Methods Enzymol.* **131**, 266-280

Pace, C.N., Shirley, B.A. and Thomson, J.A. (1989) in *Protein Structure*: a practical approach (Creighton, T.E. ed) 2nd edn, pp 311-330, IRL Press, Oxford University Press, Oxford

Parraga, A., Garcia-Saez, I., Walsh, S.B., Mantle, T.J. and Coll, M. (1998) The three-dimensional structure of a class-Pi glutathione S-transferase complexed with glutathione: the active-site hydration provides insights into the reaction mechanism. *Biochem. J.* **333**, 811-816

Parsons, J.F. and Armstrong, R.N. (1996) Proton configuration in the ground state and transition state of a glutathione transferase-catalysed reaction inferred from the properties of tetradeca-(3-fluorotyrosyl)glutathione transferase. *J. Am. Chem. Soc*. **118**, 2295-2296

Pemble, S.E. and Taylor, J.B. (1992) An evolutionary perspective on glutathione transferases inferred from class-theta glutathione transferase cDNA sequences. *Biochem. J.* **287**, 957-963

Pemble, S.E., Wardle, A.F. and Taylor, J.B. (1996) Glutathione S-transferase class Kappa: characterization by the cloning of rat mitochondrial GST and identification of a human homologue. *Biochem. J.* **319**, 749-754

Perkins, S.J. (1986) Protein volumes and hydration effects. *Eur. J. Biochem*. **157**, 169-180

Pettersson, P.L. and Mannervik, B. (2001) The role of glutathione in the isomerization of delta 5-androstene- 3,17-dione catalyzed by human glutathione transferase a1-1. *J. Biol. Chem.* **276**, 11698-11704

Prade, L., Huber, R., Manoharan, T.H., Fahl, W.E. and Reuter, W. (1997) Structures of class pi glutathione S-transferase from human placenta in complex with substrate, transition-state analogue and inhibitor. *Structure.* **5**, 1287-1295

Privalov, P.L. and Gill, S.J. (1988) Stability of protein structure and hydrophobic interaction. *Adv. Protein Chem.* **39**, 191-234

Privalov, P.L. and Makhatadze, G.I. (1990) Heat capacity of proteins. II. Partial molar heat capacity of the unfolded polypeptide chain of proteins: protein unfolding effects. *J. Mol. Biol.* **213**, 385-391

Privalov, P.L. (1996) Intermediate states in protein folding. *J. Mol. Biol.* **258**, 707-725

Raghunathan, S., Chandross, R.J., Kretsinger, R.H., Allison, T.J., Penington, C.J. and Rule, G.S. (1994) Crystal structure of human class mu glutathione transferase GSTM2-2. Effects of lattice packing on conformational heterogeneity. *J. Mol. Biol.* **238**, 815-832

Reinemer, P., Dirr, H.W., Ladenstein, R., Schaffer, J., Gallay, O. and Huber, R. (1991) The three-dimensional structure of class pi glutathione S-transferase in complex with glutathione sulfonate at 2.3 A resolution. *EMBO J.* **10**, 1997-2005

Reinemer, P., Dirr, H.W., Ladenstein, R., Huber, R., Lo, B.M., Federici, G. and Parker, M.W. (1992) Three-dimensional structure of class pi glutathione S-transferase from human placenta in complex with S-hexylglutathione at 2.8 A resolution. *J. Mol. Biol.* **227**, 214-226

Reinemer, P., Prade, L., Hof, P., Neuefeind, T., Huber, R., Zettl, R., Palme, K., Schell, J., Koelln, I., Bartunik, H.D. and Bieseler, B. (1996) Three-dimensional structure of glutathione S-transferase from Arabidopsis thaliana at 2.2 A resolution: structural characterization of herbicide-conjugating plant glutathione S-transferases and a novel active site architecture. *J. Mol. Biol.* **255**, 289-309

Rose, G.D., Geselowitz, A.R., Lesser, G.J., Lee, R.H. and Zehfus, M.H. (1985) Hydrophobicity of amino acid residues in globular proteins. *Science* **229**, 834-838

Rossjohn, J., Polekhina, G., Feil, S.C., Allocati, N., Masulli, M., De Illio, C. and Parker, M.W. (1998) A mixed disulfide bond in bacterial glutathione transferase: functional and evolutionary implications. *Structure.* **6**, 721-734

Sacchetta, P., Aceto, A., Bucciarelli, T., Dragani, B., Santarone, S., Allocati, N. and Di Ilio, C. (1993) Multiphasic denaturation of glutathione transferase B1-1 by guanidinium chloride. Role of the dimeric structure on the flexibility of the active site. *Eur. J. Biochem.* **215**, 741-745

Sayed, Y., Wallace, L.A. and Dirr, H.W. (2000) The hydrophobic lock-and-key intersubunit motif of glutathione transferase A1-1: implications for catalysis, ligandin function and stability. *FEBS Lett.* **465**, 169-172

Sayle, R. (1994) *Rasmol 2.5: Molecular Graphics Visualisation Tool*, Biomolecular Structures Group, Glaxo Research, Middlesex

Schellman, J.A. (1978) Solvent denaturation. *Biopolymers* **17**, 1305-1322

Schellman, J.A. (1987) The thermodynamic stability of proteins. *Annu. Rev. Biophys. Biophys. Chem.* **16**, 115-137

Sharp, K.A. (1995) Polyelectrolyte electrostatics: salt dependence, entropic and enthalpic contributions to free-energy in the non-linear Poisson-Boltzmann model. *Bioplymers* **36**, 227-243

Sharp, K.A. (2001) Entropy-enthalpy compensation: Fact or artifact? *Protein Sci*. **10**, 661-667

Shastry, M.C., Agashe, V.R. and Udgaonkar, J.B. (1994) Quantitative analysis of the kinetics of denaturation and renaturation of barstar in the folding transition zone. *Protein Sci.* **3**, 1409-1417

Sheinerman, F.B., Norel, R. and Honig, B. (2000) Electrostatic aspects of protein-protein interactions. *Curr. Opin. Struct. Biol.* **10**, 153-159

Shortle, D. (1995) Staphylococcal nuclease: a showcase of m-value effects. *Adv. Protein Chem.* **46**, 217-247

Shortle, D. (1996) The denatured state (the other half of the folding equation) and its role in protein stability. *FASEB J.* **10**, 27-34

Shortle, D., Wang, Y., Gillespie, J.R. and Wrabl, J.O. (1996) Protein folding for realists: a timeless phenomenon. *Protein Sci.* **5**, 991-1000

Sigurskjold, B.W., Altman, E. and Bundle, D.R. (1991) Sensitive titration microcalorimetric study of the binding of Salmonella O-antigenic oligosaccharides by a monoclonal antibody. *Eur. J. Biochem.* **197**, 239-246

Sinning, I., Kleywegt, G.J., Cowan, S.W., Reinemer, P., Dirr, H.W., Huber, R., Gilliland, G.L., Armstrong, R.N., Ji, X., Board, P.G., Olin, B., Mannervik, B. and Jones, T.A. (1993) Structure determination and refinement of human alpha class glutathione transferase A1-1, and a comparison with the Mu and Pi class enzymes. *J. Mol. Biol.* **232**, 192-212

Slagle, S.P., Kozack, R.E. and Subramaniam, S. (1994) Role of electrostatics in antigen-antibody association: anti-hen egg lysozyme/lysozyme complex (HyHEL-5/HEL). *J. Biomol. Struct. Dynam.* **12**, 439-456

Sluis-Cremer, N., Naidoo, N.N., Kaplan, W.H., Manoharan, T.H., Fahl, W.E. and Dirr, H.W. (1996) Determination of a binding site for a non-substrate ligand in mammalian cytosolic glutathione S-transferases by means of fluorescence-resonance energy transfer. *Eur. J. Biochem.* **241**, 484-488

Sluis-Cremer, N., Wallace, L., Burke, J., Stevens, J. and Dirr, H. (1998) Aflatoxin B1 and sulphobromophthalein binding to the dimeric human glutathione S-transferase A1-1: a fluorescence spectroscopic analysis. *Eur. J. Biochem.* **257**, 434-442

Smith, S.B., Finzi, L. and Bustamante, C. (1992) Direct mechanical measurements of the elasticity of single DNA molecules by using magnetic beads. *Science* **258**, 1122-1126

Soulages, J.L. (1998) Chemical denaturation: potential impact of undetected intermediates in the free energy of unfolding and m-values obtained from a two-state assumption. *Biophys. J.* **75**, 484-492

Spolar, R.S., Ha, J.H. and Record, M.T., Jr. (1989) Hydrophobic effect in protein folding and other noncovalent processes involving proteins. *Proc. Natl. Acad. Sci. U. S. A* **86**, 8382-8385

Spolar, R.S., Livingstone, J.R. and Record, M.T., Jr. (1992) Use of liquid hydrocarbon and amide transfer data to estimate contributions to thermodynamic functions of protein folding from the removal of nonpolar and polar surface from water. *Biochemistry* **31**, 3947-3955

Spolar, R.S. and Record, M.T., Jr. (1994) Coupling of local folding to site-specific binding of proteins to DNA. *Science* **263**, 777-784

Stenberg, G., Board, P.G. and Mannervik, B. (1991) Mutation of an evolutionarily conserved tyrosine residue in the active site of a human class Alpha glutathione transferase. *FEBS Lett.* **293**, 153-155

Stenberg, G., Bjornestedt, R. and Mannervik, B. (1992) Heterologous expression of recombinant human glutathione transferase A1-1 from a hepatoma cell line. *Protein Expr. Purif.* **3** , 80-84

Stevens, J.M., Hornby, J.A., Armstrong, R.N. and Dirr, H.W. (1998) Class sigma glutathione transferase unfolds via a dimeric and a monomeric intermediate: impact of subunit interface on conformational stability in the superfamily. *Biochemistry* **37**, 15534-15541

Stevens, J.M., Armstrong, R.N. and Dirr, H.W. (2000) Electrostatic interactions affecting the active site of class sigma glutathione S-transferase. *Biochem. J.* **347 Pt 1**, 193-197

Sturtevant, J.M. (1977) Heat capacity and entropy changes in processes involving proteins. *Proc. Natl. Acad. Sci. U. S. A* **74**, 2236-2240

Tipping, E. and Ketterer, B. (1981) The influence of soluble binding proteins on lipophile transport and metabolism in hepatocytes. *Biochem. J.* **195**, 441-452

Todd, M.J. and Freire, E. (1999) The effect of inhibitor binding on the structural stability and cooperativity of the HIV-1 protease. *Proteins* **36**, 147-156

Tomarev, S.I., Zinovieva, R.D., Guo, K. and Piatigorsky, J. (1993) Squid glutathione S-transferase. Relationships with other glutathione S-transferases and S-crystallins of cephalopods. *J. Biol. Chem.* **268**, 4534-4542

Tsai, C.J., Lin, S.L., Wolfson, H.J. and Nussinov, R. (1997a) Studies of protein-protein interfaces: a statistical analysis of the hydrophobic effect. *Protein Sci.* **6**, 53-64

Tsai, C.J. and Nussinov, R. (1997b) Hydrophobic folding units at protein-protein interfaces: implications to protein folding and to protein-protein association. *Protein Sci.* **6**, 1426-1437

Tsai, C.J., Xu, D. and Nussinov, R. (1997c) Structural motifs at protein-protein interfaces: protein cores versus two-state and three-state model complexes. *Protein Sci.* **6**, 1793-1805

Tsuchida, S., Izumi, T., Shimizu, T., Ishikawa, T., Hatayama, I., Satoh, K. and Sato, K. (1987) Purification of a new acidic glutathione S-transferase, GST-Yn1Yn1, with a high leukotriene-C4 synthase activity from rat brain. *Eur. J. Biochem.* **170**, 159-164

Tsuchida, S. and Sato, K. (1992) Glutathione transferases and cancer. *Crit Rev. Biochem. Mol. Biol.* **27**, 337-384

Vince, R., Daluge, S. and Wadd, W.B. (1971) Studies on the inhibition by glyoxalase by *S*-substituted glutathione. *J. Med. Chem*. **14**, 402-404

Wallace, L.A., Blatch, G.L. and Dirr, H.W. (1998a) A topologically conserved aliphatic residue in alpha-helix 6 stabilizes the hydrophobic core in domain II of glutathione transferases and is a structural determinant for the unfolding pathway. *Biochem. J.* **336**, 413-418

Wallace, L.A., Sluis-Cremer, N. and Dirr, H.W. (1998b) Equilibrium and kinetic unfolding properties of dimeric human glutathione transferase A1-1. *Biochemistry* **37**, 5320-5328

Wallace, L.A. and Dirr, H.W. (1999) Folding and assembly of dimeric human glutathione transferase A1-1. *Biochemistry* **38**, 16686-16694

Wang, R.W., Newton, D.J., Huskey, S.E., McKeever, B.M., Pickett, C.B. and Lu, A.Y. (1992) Site-directed mutagenesis of glutathione S-transferase YaYa. Important roles of tyrosine 9 and aspartic acid 101 in catalysis. *J. Biol. Chem.* **267**, 19866-19871

Waxman, D.J. (1990) Glutathione S-transferases: role in alkylating agent resistance and possible target for modulation chemotherapy--a review. *Cancer Res.* **50**, 6449-6454

Wetlaufer, D.B. (1973) Nucleation, rapid folding, and globular intrachain regions in proteins. *Proc. Natl. Acad. Sci. U. S. A* **70**, 697-701

Widersten, M., Bjornestedt, R. and Mannervik, B. (1996) Involvement of the carboxyl groups of glutathione in the catalytic mechanism of human glutathione transferase A1-1. *Biochemistry* **35**, 7731-7742

Wilce, M.C. and Parker, M.W. (1994) Structure and function of glutathione S-transferases. *Biochim. Biophys. Acta* **1205**, 1-18

Wilce, M.C., Board, P.G., Feil, S.C. and Parker, M.W. (1995) Crystal structure of a theta-class glutathione transferase. *EMBO J.* **14**, 2133-2143

Winder, A.F. and Gent, W.L. (1971) Correction of light-scattering errors in spectrophotometric protein determinations. *Biopolymers* **10**, 1243-1251

Wiseman, T., Williston, S., Brandts, J.F. and Lin, L.N. (1989) Rapid measurement of binding constants and heats of binding using a new titration calorimeter. *Anal. Biochem.* **179**, 131-137

Woody, R.W. (1995) Circular dichroism. *Methods Enzymol.* **246**, 34-71

Xiao, G., Liu, S., Ji, X., Johnson, W.W., Chen, J., Parsons, J.F., Stevens, W.J., Gilliland, G.L. and Armstrong, R.N. (1996) First-sphere and second-sphere electrostatic effects in the active site of a class mu gluthathione transferase. *Biochemistry* **35**, 4753-4765

Xu, D., Lin, S.L. and Nussinov, R. (1997a) Protein binding versus protein folding: the role of hydrophilic bridges in protein associations. *J. Mol. Biol.* **265**, 68-84

Xu, D., Tsai, C.J. and Nussinov, R. (1997b) Hydrogen bonds and salt bridges across protein-protein interfaces. *Protein Eng* **10**, 999-1012

Yang, A.S., Sharp, K.A. and Honig, B. (1992) Analysis of the heat capacity dependence of protein folding. *J. Mol. Biol.* **227**, 889-900

Zhao, Y.M., Muir, T.W., Kent, S., Tischer, E., Scardina, J.M. and Chait, B.T. (1996) Mapping protein-protein interactions by affinity-directed mass spectrometry. *Proc. Natl Acad. Sci USA.* **93**, 4020-4024